Analysis of Differential-Delay Equations for Biology

Ezeofor O. Victory

Thesis submitted to The University of Nottingham

for the degree of Doctor of Philosophy

September, 2016

Acknowledgements

This dissertation is a product of the help and advice from so many people. First and foremost I would like to thank my supervisors Prof. John King and Dr. Rüediger Thul for their support and guidance through out this research years, their patience has been invaluable.

The support from the Department of Mathematical Sciences, University of Nottingham has been particularly wonderful from the information and technology staff to the graduate staff, they have all been awesome.

I would like to appreciate The Tertiary Education Trust fund (TETfund) of Nigeria for its support and funding of this research studies. I am grateful to Nnamdi Azikiwe Univesity, Awka for the opportunity given to me to study at the University of Nottingham.

I cannot forget thank my family especially my lovely wife and kids for always giving me the strength to carry on.

And lastly, I am grateful to God for orchestrating everything to see me through this academic endeavor, for in His time he makes all things beautiful.

Abstract

In this thesis, we investigate the role of time delay in several differential-delay equation focusing on the negative autogenous regulation. We study these models for little or no delay to when the model has a very large delay parameter. We start with the logistic differential-delay equation applying techniques that would be used in subsequent chapters for other models being studied. A key goal of this research is to identify where the structure of the system does change.

First, we investigate these models for critical point and study their behaviour close to these points. Of keen interest is the Hopf bifurcation points where we analyse the parameter associated with the Hopf point. The weakly nonlinear analysis carried out using the method of multiple time scale is used to give more insight to these model. The centre manifold method is shown to support the result derived using the multiple time scale.

Then the second study carried out is the study of the transition from a sine-like wave to a square wave. This is analysed and a scale deduced at which this transition gradually takes place. One of the key areas we focused on in the large delay is to solve for a certain constant a' associated with the period of oscillation.

The effect of the delayed parameter is shown throughout this thesis as a major contributor to the properties of both the logistic delay and the negative

autogenous regulation.

Contents

1 Literature Review **7**

1.1 Overview of research result 15

2 A logistic differential-delay equation **18**

2.1 Introduction 18

2.1.1 Non-dimensionalisation 22

2.2 Stability and Hopf bifurcation 25

2.2.1 Asymptotics of Hopf point 32

2.2.2 Numerics 36

2.3 Weakly nonlinear analysis 39

2.3.1 Multiple time scale (MTS) 40

2.3.2 Comparison of numerical and MTS 46

2.4 Conclusion 52

3 Analysis of a first order negative feedback differential-delay equation **58**

3.1 Introduction 58

3.2 Conclusion 64

4 A more generalised negative autogenous regulation. **65**

4.1 Stability and Hopf bifurcation 65

4.1.1 Asymptotics of the Hopf bifurcation point 68
4.1.2 Numerics 73
4.2 Weakly nonlinear analysis 77
4.2.1 Multiple time scale (MTS) 79
4.2.2 Numerical simulation of the multiple timescale analysis 84
4.3 Normal form and centre-manifold method 85
4.4 Conclusion 94

5 The inclusion of a transcription factor in a negative autoregulation 97
5.0.1 Stability Analysis 100
5.1 Weakly Nonlinear Analysis 106
5.1.1 Numerical simulation of the model 112
5.2 Conclusion 122

6 Large delay in a logistic differential-delay equation 124
6.1 Large Delays 124
6.2 Slow phase for the amplitude of the oscillation 128
6.3 Fast phase-transition layer 130
6.4 Conclusion 141

7 Large delay in negative autogenous differential-delay model 143
7.1 Slow phase of a periodic oscillation 145
7.1.1 Fast phase 147
7.2 Numerical solution 148
7.2.1 Fast phase using a Taylor expanded non-linear terms . 156
7.3 Conclusion 173

8 Conclusion and further work 175

A appendix **179**

A.1 Network Motifs 179

A.2 Delay as bifurcation parameter 180

Bibliography **187**

Chapter 1

Literature Review

The complexity of networks in different fields has continued to gain a lot of attention because of the role they play in our daily lives. The study of these networks is applied to minimize unfavorable properties and maximize the good properties. In the field of biology these networks appear in neuroscience, gene regulation and much more. Understanding these networks and the properties that go along with such networks help in studying diseases, drug delivery and potential cures to ailment. In this work, we shall be investigating different types of networks involved in gene regulation. Genetic information is regulated by the genes hence by understanding the behaviour of this gene regulation we might be able to suppress unwanted properties while promoting beneficial properties.

The transfer of genetic information from DNA to RNA is initiated with the process of gene transcription. This is initiated when the enzyme RNA polymerase (RNAp) recognises a DNA sequence, called the promoter, that enables a gene to be transcribed. This involves the synthesis of messenger RNA (mRNA) and is followed by a process called translation, which converts the mRNA transcripts into proteins. Gene transcription is regulated by special proteins

referred to as transcription factors, which can transit between active and inactive states. Active transcription factors bind to specific sites in a regulatory region of DNA preceding the promoter gene [1, 2].

A gene or protein can be represented as a node and the interaction between this gene and a protein can be called an edge. The collection of connected genes or proteins is called a network. A transcription network is a collective interaction of transcription factor proteins encoded by genes, which in turn can regulate other transcription factors. Examples of transcription network include developmental transcription network [3, 4], neuronal network [5, 6], protein-protein network [7, 8], signal transduction network [9, 10], metabolic network [11, 12] and sensory transcription network [13]. The interaction between nodes (genes) and proteins could be an activation or repression. By gene activation we mean its level of mRNA increases and when it is repressed, its production is said to be slowed or totally terminated.

Transcriptional regulation plays a significant role in determining the behaviour of biological networks but it is not the only type of regulation. Non-transcriptional processes such as phosphorylation and regulated degradation of protein are examples of some of the other processes involved in regulating gene networks. This can happen either extra- or intracellularly [14].
The complexity of network interaction increases from unicellular to multicellular organisms, hence making it difficult to determine the overall behaviour. Therefore they are broken down into constituent sub-networks. Studies by Alon and Milo et al in [2, 15] have shown simple regulatory interconnecting patterns that occur much more frequently in real networks than in randomised networks, these re-occurring patterns are called network motifs. Accuracy of previous modelling approaches was reduced due to over-simplification of the

network by reducing the number of nodes, thus affecting the conclusion drawn. This was investigated by Grochow et al in [16] by applying an improved subgraph isomorphism test. The test produce more functional motifs within larger network motifs and evaluates subgraphs of a given size in less time.
The reviews by Alon [17] and Li at el [1] gives examples different types of network motifs including; autogenous regulation, feed-forward loop (FFL), double feed- backward loop (DFBL), multi-output FFL, single-input module (SIM), dense overlapping regulons (DORs) see appendix A.1 for pictorial representation.

Autogenous regulation (autoregulation) occurs when a gene activates or represses itself, see figure A.2 and A.1. This is usually subdivided into two: negative autoregulation (NAR), where the expression of a gene is repressed by its own gene product and positive autoregulation (PAR) where expression of a gene is activated by its own gene product. Rosenfeld [18] gives the result that NAR reduces the response time of a gene to about one fifth in comparison to simple transcription.

The simplest example of a FFL is the three-node FFL , see figure A.3. This is composed of two input transcription factors, one of which regulates the other, both jointly regulating a target gene, this was investigated experimentally by Alon [19]. The author found the FFL be the most abundant network motif. The FFL was further classified into two categories, the coherent and the incoherent FFL. The Coherent type-1 (C1-FFL) acts as a sign-sensitive delay [20] and the Incoherent type-2 (I1-FFL) as a pulse generator and response accelerator [21]. Another example of FFL is the multi-output FFL which has two target genes. Widder [22] discovered that the evolvability of the FFL was not as a result of parent gene but as a result of the necessity of the function

of such a network motif.

A FBL network is one which the input gene is the target gene. In a three node FBL the input gene say gene 'X' starts the process by triggering a gene, say gene 'Y', gene 'Y' also triggers another gene say 'Z' and gene 'Z' now regulates the production of gene 'X' which started the whole process, this is shown in figure A.4 One of the prominent FBL in developmental transcription is the two-node DFBL which is a network motif, but the three-node FBL is not a network motif [2]. The two node DFBL is made up of two node each repressing or activating the other node. When the nodes are being activated it is called a positive double feedback loop see figure A.5 and when the nodes are being repressed it is known as the negative double feedback loop see figure A.6. The Autogenous regulation could also be called a FBL.
Tiwari et al [23] showed that the structure of a network determines the role been performed by such a network. The authors discovered changes in bistability range and switching times by coupling FBL in autoregulation. Angeli in [24] discovered that functionalities such as multi-stability, faster transient responses, robustness against the fluctuation of parameters and dynamical stability which were observed in small networks also occurred in larger classes of transcriptional networks with feedback loops. Other researchers [1, 17, 15] proposed concepts such as temporal ordering, combination logic, memory and several others to explain why some network motifs occur more frequently than others.

In the book by Alon [2], transcriptional networks were classified to sensory and developmental networks. The author states that all sensory transcription network motifs were found in developmental network motifs but not all developmental networks were found in sensory transcription networks. All

sensory transcription networks are composed of four network motifs, namely, autogenous regulation, FFL, SIM and the DORs. In developmental transcription networks an extra type of network motif, the DFBL, is present which does not occur in the sensory transcription network. These network motifs re-emerge because they perform important functions such multi-stability, robustness against fluctuations of parameters and not necessarily because they arise from the same parent. Certain motifs such as the NAR have the opposite effects to the PAR, where the NAR speeds up interaction and reduces cell-cell variability, the PAR decreases speed and increases cell-cell variation creating bimodal states in the cell. In the SIM the Alon describes the role of hierarchy and temporal ordering to determine the order of gene expression. In the DOR, more insight is required [2]. The DFBL was categorised into positive and negative DFBL. The positive DFBL acts as a memory while the negative DFBL acts as a toggle switch. Both sensory and developmental transcription network motifs act on different timescales with the sensory transcription having a shorter timescale. The changes in gene regulation occur with respect to time and other processes, hence Alon [2] and several others applied differential equations to represent these changes.

The nature of networks can be complex and daunting, hence Thomas et al [25] investigated how such complex networks can be disentangled. The authors applied logical states with feedback loops and concluded that positive FBLs can have three steady states while a negative FBLs, no matter how complex, would not have multistability but can display oscillations [25]. Wang et al in [26] proved that for biological networks composed of cyclic feedback systems there exists a nonempty omega-limit set composed of periodic orbit and equilibria. He showed that using the monotone cyclic system simplified the theoretical analysis and design of cyclic feedback network. Wang also extended

this methodology to large-scale systems using the circadian network to further substantiate the accuracy of his theoretical analysis.

Non-linearities arise in a bid to model these complex networks to capture the properties observed experimentally or in real life. The nonlinear ordinary differential equation differ from the linear differential equation whose solution are easily solvable. Solving nonlinear differential equation bring its challenges and can lead to chaotic or unpredictable solutions.
Since not all reactions commence at the same time it would be key to represent each reaction time in certain reaction from the prior time. In this work, we introduce the use of differential-delay equations to the system of gene regulation which can be applied to processes which begin at different times. This difference in time is being represented by some time lag. The introduction of differential delay equation takes the finite dimensional system and converts it into an infinite dimensional system. Nonlinear differential delay equation present interesting systems to investigate as they could lead to oscillations and chaos.

Some experimental results which were unaccounted for with the ordinary differential equation are now being derived using differential delay equations.
It is obvious that not all processes take place at the same point in time; some occur due to processes occurring at earlier times. This brings about the necessity of using functional differential equations such as delay differential equation (DDE) to model systems in Biology. The inclusion of delays in the transcription of mRNA is frequently adopted in negative feedback systems to produce oscillations, this was investigated by Xia and Zhuang in [27, 28]. The dynamics of gene expression models with time delays confirm that Hopf bifurcations can occur due to changes in the delay parameter. The global existence of the

periodic solutions is established using the stability theory, Bendixson criteria and bifurcation theory [29, 27, 30]. A delay model of gene expression with a positive feedback loop was discovered to maintain robustness and stability in circadian oscillations [31].

The dynamical stability-breaking of the molecular concentration of two generic biochemical reactions were studied by Wang et al [32]. The first is one variable delay model for protein degradation and the second model is a two variable delay feedback. The authors concluded that one can get chaos in a first-order one delay differential-delay equation. They [32] stated the conditions for the existence of a single set positive stationary solution and identified stable and unstable regions of the parameter space.

The complexities involved in network interactions can be linear or nonlinear. Nonlinearities can make the exact solutions of modelled system difficult to solve. It has been experimentally observed that some network motifs display periodic oscillation. These oscillating orbits tend to decay or grow with increase in nonlinearities. One of the methods applied to handle this is the method of asymptotic analysis which is adopted to solve problems of limiting behaviour. The Poincaré-Lindstedt method (PLM) and the method of multiple scale (MMS) are some of the asymptotic methods applied in solving differential equations with periodic orbits. The method multiple scales is effective for finding the limit cycle and analysing the stability of oscillating orbits. These techniques and have been applied to ODE models of the Duffing equation and Van der Pol equations [33, 34]. Wang [35] applied the MMS in analysing the bifurcating of periodic solution for a DDE model of the Duffing equation and he showed that the MMS gave good accuracy locally. Wang in [36] went further to analyse the bifurcations of the DDE equation taking the delay as the bifurcation parameter. A system having two physi-

cal processes acting concurrently can be tackled using the method of matched asymptotic expansion or the method of multiple scales. When these processes that act in different regions the method of matched asymptotic expansion is suitable while the MMS is suitable for processes acting in the same regions, [37]. For the Poincaré-Lindstedt method, the time t is stretched to ωt and for the method of multiple scales, each process is associated with a timescale, $t = \mathcal{O}(1)$ representing the fast time scale and $T = \epsilon t = \mathcal{O}(1)$ representing the slow time scale. The fast time scale accounts for the periodic oscillation and the slow time scale accounts for the change in amplitude and phase shift. The asymptotic approximation for each order of ϵ is then computed while the secular terms are eliminated. Slower scales such as $S = \epsilon^n t; n = 2, 3, 4, ...$ can be introduced for the persistent occurrence of secular terms at higher orders [37], [38].

Previously the method of multiple scales was thought to be effective in analysing delay differential equations only after reduction by using the centre manifold method. Das et al [39] proved that this is not necessary. Das et al showed an analytical method of applying only the MMS and obtaining astounding approximate solutions equivalent to the direct solutions. The author also analysed the behaviour of three delay differential equations near Hopf bifurcation using the method of multiple scales without applying the centre manifold reduction method. Huailei Wang et al. in [35] in the DDE Duffing oscillator observed a paradox at the third approximation. The author suggested the application of slower timescales to solve such a problem. This paradox the also appears in Poincare-Lindsedt method but had no proper suggestion to eliminate this shortcoming. In [36] the method of multiple scales and shooting technique were analysed for the Duffing equation including delays to predict the bifurcation of the periodic motion and their stability. The application of

multiple scales is being extended to large delays in delay differential equations [40] and it is being observed that the first two approximations are accurate enough to match the numerical solutions. Simple DDEs can exhibit certain phenomena such as periodic solutions which simple ordinary differential equations do not exhibit. The method of multiple scales has also been adopted to solve some non-linear DDE problems and it provides very good approximation. Several systems with large delays have been investigated using MMS. Peil et al [41] applied this method to nonlinear broadband bandpass delay electro-optic feedback. Erneux [42] applied the MMS to mechanical systems with very large delay in the Johnson Moon equation for the machine tool vibration and the Minorsky's equation [42].

1.1 Overview of research result

Our work focuses on a detailed study of the negative autogenous regulation with both transcriptional and translational time delays. The critical time delay is analysed for which the stability of the system changes from a stable steady state to an oscillating orbit. We apply the method of asymptotic approximation to find an approximate solution to the model. The perturbation method of multiple scales is applied to study the direction of the bifurcation to the delay differential equation without the centre manifold reduction method applied to the DDE system. The model was analysed to compare the result derived to that studied by Anael et al [43] who applied the Poincaré-Lindstedt Method. We put forth a slow time amplitude equation derived from the method of multiple scales that trace out the envelope equivalent to the damped or growing oscillation. The change oscillation is also investigated as the slowed time tends to infinity. We find solutions at each order of ϵ and apply that solution to the next order to derive a better result that helps to track the

phase shift in the solution. The MMS method produces lengthy equations but the precision and accuracy of these equations are approximately equivalent to the direct numerical method.
Some systems have multiple time lags, in this work we intend to study the effect of each time lag both for the linear part of the equation and the non-linear equation, in general, applying the method of multiple time scale. With this method, we are able to compare each parameter in a given system to get a clear picture of the role it plays in relation to the delay(s) in that modelled system.

We start in chapter 2 with a population model which we use to demonstrate to the concept we shall be using to analyse subsequent models of gene regulation. This model is studied because its nonlinearity could be said to be simple but not necessarily implying that it is less complex.
In Chapter 3 we investigate a negative feedback first order differential- delay equation with a single time lag using the same techniques as in chapter 2. Some of these techniques include the stability and Hopf bifurcation analysis, weakly non-linear analysis applying the method of multiple scales and direct numerical computations. We investigate this equation for the discontinuous system which occurs when the Hill coefficient is large . In chapter 4 we also will analyse the model in chapter 3 for the general Hill coefficient and compare its values with the discontinuous system studied at the beginning of the chapter. In chapter 5 we investigate the NAR as a second order differential-delay equation which includes the protein factor into the model. In this chapter we have two time lags, we will show which of the time delays has more control or which time lag causes a change in stability in the model. Each parameter is studied using the multiple time scale analysis as performed in the previous section. We investigate the time lag from a zero delay to a delay as large as possible.

We will apply methods that are used for solving ordinary differential equation and see how they translate to solving the differential-delay equations.

In chapter 6 we investigate further the population model studied in chapter 2. We will increase the time delay in the model till a square wave arises. In this chapter, we will be studying the square waves arising from large delays. The period of these square waves will be shown to be twice the size of the delay plus some constant. This will be studied for the flat plateaux arising from the slow time scale and the transition layer are as functions of the fast time phase. This is similar to the relaxation oscillation studied in the Van der Pol's equation.

In chapter 7 we investigate the same NAR studied in chapter 2 for large delayed parameter, we will analyse the square waves and make comparisons to the square waves studied in chapter 5. We also try to apply the methods used in chapter 6 and see if it breaks down at some point.

Chapter 2

A logistic differential-delay equation

2.1 Introduction

The rate of change in the population size of an organism or a single species with respect to the available resources has been studied by many authors such as Malthus in 1798 [44], Verhulst in 1836 [45], Hutchinson in 1948 [46], Gopalsamy [47], Idlango [48] and many others. The significance of the information derived from the population dynamics plays important roles in ecology and biomedical sciences in areas such as disease control, resource control and management [49], [50]. Other fields which incorporate this study include agriculture and marine study. Several equations have been adopted to model these changes in population size. These models have extended from single species to multiple species such as predator-prey models. The very basic population growth model took into account the birth and date rate of the species, as shown in equation (2.1)

$$\frac{d}{dt}P(t) = b\,P(t) - \,d\,P(t), \tag{2.1}$$

where $P(t)$ is the population size at time t, b and d are the birth rate and death rate respectively. Equation (2.1) was proposed by Malthus in 1798, [45] but it has several limitations.

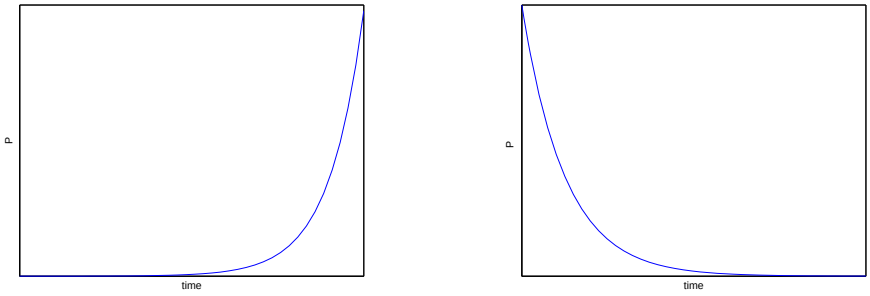


Figure 2.1: The population model of Malthus population model, (a) The $b > d$ and (b) $b < d$.

The solution grows exponentially if the birthrate is greater than the deathrate, $b > d$ and decays to 0 as $t \to \infty$ if $d > b$, see figure 2.1. Such a solution may be valid for a short period of time but as time t gets larger the solution will no longer be a good approximation. All organisms need certain resources for its existence but these resources are not infinite. For $b > d$ as $t \to \infty$, lack of infinite resources can account for the failure of Malthus population model. Resources tend to diminish with increased consumption, the greater the population the greater the rate consumption. An overwhelming increase in population can lead to scarcity which can then lead to a decrease in population. Thus the population size is a function of the available resources. The anomaly of an exponentially growing population was resolved by Verhulst in (1836) when he proposed the logistic model, equation (2.2),

$$\frac{d}{dt}P(t) = R\,P(t)\left(1 - \frac{P(t)}{K}\right), \tag{2.2}$$

where R is the intrinsic growth rate and $K > 0$ is the carrying capacity. The

relation of R to the birth rate b and death rate d is

$$R = b - d. \tag{2.3}$$

The analysis of equation (2.2) gives two steady state $P(t) = 0$ and $P(t) = K$. The later is as a result of the carrying capacity. The solution to equation (2.2) is

$$P(t) = \frac{P_0\, K}{P_0 + (K - P_0)\exp\left(-R\, t\right)}, \tag{2.4}$$

where P_0 is the population size at the initial time t_0. The solution to equation (2.2) gives an increasing population when the population size is less than the carrying capacity, K. If the initial population is greater than the carrying capacity then the population size decays until $P(t) = K$. This model equation is better in comparison to equation (2.1) as it gives a reasonable and logical type of solution to a population dynamics, see figure 2.2.

Equation (2.1) and (2.2) give the impression the change in population size at the present time t does not depend on population at earlier time $t - \tau$. In reality the total number of births depends on the adult population and this has a direct effect on the future population size. An organism has to mature before being able to reproduce. Unfortunately, this time lag, τ was not captured in both models proposed by Malthus and Verhulst. This time delay can be represented in discrete form or as a delay in time in the differential equation. When this equation is in discrete form it is called the logistic map. The inclusion of time lag in the logistic equation was proposed by Hutchinson in (1948) and this gave the following delayed logistic equation

$$\frac{d}{dt}P(t) = \, r\, P(t)\left(1 - \frac{P(t-\tau)}{K}\right), \tag{2.5}$$

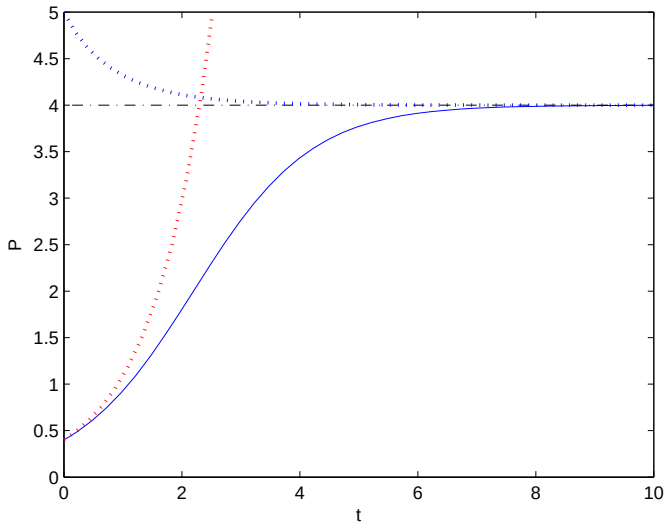


Figure 2.2: The population model of Verhulst population model with $K = 4$ (black dashed line). For $r > 0$ with the two different initial population size, $P_0 = 0.4, 5$. The plots in red are Malthus model equation (2.1) and blue lines are the model proposed by Verhaulst equation (2.2).

where τ is the delayed time, with r and τ both as positive parameters. Equation (2.5) has been studied [51] and Murray [45] showed this model has periodic solutions. This oscillation could be explained in relation to the resources available (K). If there is an increase in population size, this will lead to a shortage in resources and hence a decrease in population. But if there is a decrease in population then more resources will be available, hence an increase in resources leads to and increase in population size. This oscillation cannot exit in a first order ordinary differential equation and this can be shown using the Bendixson's criteria. This delay differential equation and its corresponding discrete equation portray diverse and more complex dynamical behaviour in comparison to its ordinary differential equation [46, 33].

The logistic equation has grown in complexity from its simple form to more

complex forms such as

$$\frac{d}{dt}P(t) = P(t)\,R\{1 - a\,P(t) - g(P([t], P([t-1]), \ldots, P([t-m]))\}, \quad (2.6)$$

studied by Muroya [52].

The logistic equation was rescaled on by Ludwig [53], with the introduction of a harvesting term

$$\frac{d}{dt}P(t) = R\,P(t)\,\left(1 - \frac{P(t)}{K}\right) - G\,P(t), \quad (2.7)$$

where R and K are the same as described in previously and G is the rate at which the species is harvested. The application to equation (2.7) in fishery was discussed in chapter 2 by Bank in [54]. Further to this, other delay differential equations modeling logistic growth have been proposed, one of which was studied by Taylor et al [55], this was given by

$$\frac{d}{dt'}P(t') = -d\,P(t') + bP(t'-\tau')\,(k - bz\,P(t'-\tau'))\,, \quad (2.8)$$

where d is the death rate, τ is time it takes to develop to adult stage, b is the number of birth per adult. $k - bzP(t')$ is the egg to adult survival rate where z is the reduction of survival rate for each additional juvenile and k the maximum egg-adult survival rate [46]. The parameters d, b, k and τ are all positive. The analytical study of (2.8) has not been explicitly solved, we shall in this chapter focus on analysing equation (2.8).

2.1.1 Non-dimensionalisation

The parameters in the logistic models for the ordinary differential equations have been studied by several authors as mentioned and cited in the previous section. We analyse these parameters in the differential-delay equation and investigate how the delay affects the the model and other parameters in the

model. We begin with the conversion of equation (2.8) to its dimensionless form.

Let $p = P/\rho$, $t = \kappa t'$ and $\tau = \kappa\tau'$, substituting into equation (2.8)

$$\kappa\,\rho\,\frac{d}{dt}p(t) = -d\,\rho\,p(t) + \,b\,k\,\rho\,p(t-\tau)\left(1 - \frac{b\,z\,\rho}{k}p(t-\tau)\right). \tag{2.9}$$

Let $d = \kappa$, $\rho = k/bz$ and $r = bk/d$, this will transform equation (2.9) to

$$\frac{d}{dt}p(t) = -p(t) + r\,p(t-\tau)\,(1 - p(t-\tau))\,, \tag{2.10}$$

since the parameters $b > 0$, $d > 0$ and $k > 0$ it implies that the parameter $r > 0$. Selecting a range of arbitrary values for the parameters r and τ, we plot the numeric solutions. Figures 2.3 and 2.4 show that for different values of the two parameters the solution to the system could change drastically and even get to a chaotic state. The choice of these parameters are chosen to display the different possible solutions as shown in both figures. In figure 2.3a we observe a damped oscillation and in figure 2.3b periodic oscillation, this occurs for a fixed delay but and varied parameter r. Further increase in r takes the numerical solution to a chaotic state as shown in figure 2.4a but for fixed r and an increase in the delay we moved from damped oscillation to a periodic oscillation then to a square wave oscillation, see figure 2.4b. Such changes do not occur in a first order ordinary differential equation.

In this chapter we shall be investigating the conditions which makes these changes occur. In the next section we will determine the steady state(s) and investigate the stability of the steady state(s) of equation (2.10), the analysis of the bifurcation points will be studied. The direction of the the Hopf bifurcation with both the intrinsic growth rate and the delayed parameter will be analysed applying the method of weakly nonlinear analysis. The findings of our analysis would be compared with the direct numerics solution of the model in section

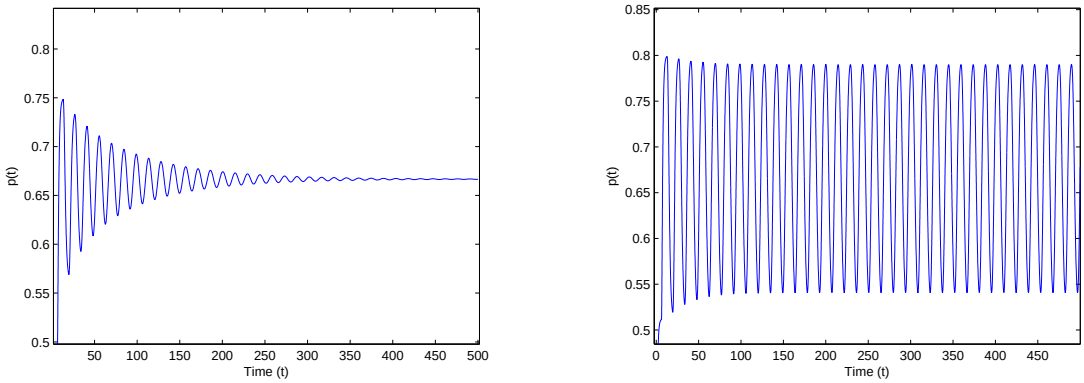


Figure 2.3: The plot of different values of r, (a) $r = 3.0$ and (b) $r = 3.2$, with the same value of $\tau = 6.3$ and initial value $p_0 = 0.2$.

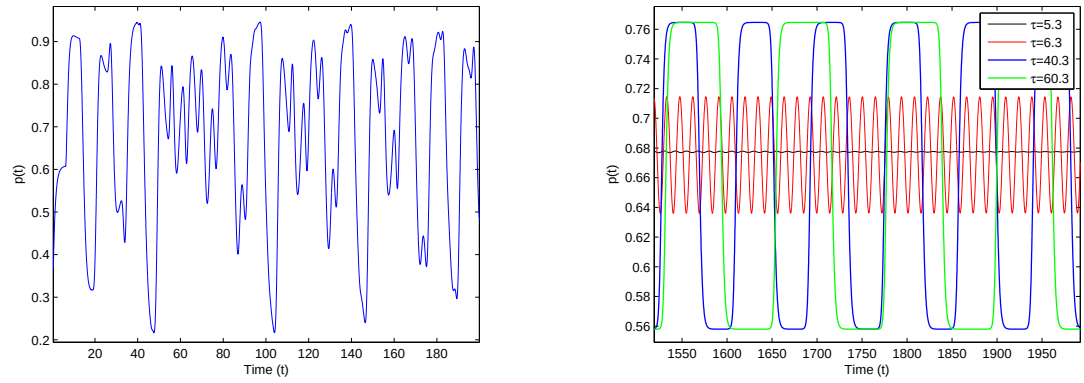


Figure 2.4: (a) The plot for $r = 3.8$ and $\tau = 6.3$ and (b) the plot for same value of $r = 3.1$ but different values of delay; $\tau = 5.3$ (black line), $\tau = 6.3$ (red line), $\tau = 40.3$ (blue line) and $\tau = 60.3$ (green line); with initial value $p_0 = 0.2$.

3. In section 4 we will investigate what happens when the delay get very large ($\tau \to \infty$). With this result more complex model will be analysed in subsequent chapters.

2.2 Stability and Hopf bifurcation

In this section we analyse the stability and distribution of the eigenvalue of equation (2.10).

May in [56] examined the logistic difference equation which is a simplified form equation (2.10). The equation was simplified to the form

$$p_{n+1} = r\, p_n\, (1 - p_n) \tag{2.11}$$

May observed that the maximum value of the RHS of equation (2.11) was attained at $r = 4$ and that the value of p could not exceed 1. Some other results he showed the equation had non-trivial dynamical behaviour if $r < 4$ and that at $a < 1$ equation (2.11) had a steady state at $p = 0$ which was stable. To obtain non-trivial dynamical behaviour $1 < r < 4$. Within the interval of $1 < r < 3$ two steady states which comprised of the first steady state $p = 0$ which now becomes unstable and a new steady state $p = 1 - 1/r$ which is stable is attained. Further increase in the value of r beyond 3 shows a period two-cycle which moves to period-4, 8, 16, $\cdots$ cycle with more increase in r until a chaotic region is seen.

We shall go through our analysis of equation (2.10) as a differential-delay equation comparing the results with [56]. Time lags or delays do not change the number and location of steady states of dynamical system. This implies that at steady state $p(t - \tau) = p(t)$. From equation (2.10)

$$\frac{d}{dt}p(t) + p(t) = rp(t - \tau)(1 - p(t - \tau)). \tag{2.12}$$

To locate the steady state we equate the rate of change to zero, hence from equation (2.12) we get

$$p\,[1 - r(1 - p)] = 0, \tag{2.13}$$

and obtain two steady states

$$p_1^* = 0, \qquad 0 \leq r \leq 1, \tag{2.14a}$$

$$p_2^* = 1 - 1/r, \qquad r > 1, \tag{2.14b}$$

where $p^* = (p_1^*\ , p_2^*)$ are the steady states of the system (2.12). The parameters r and τ are non negative, which implies that at least one of the steady states is positive, $p^* \geq 0$. To study both steady states obtained from equation (2.12) we perturb both steady state by a small quantity $x(t) \ll 1$ and this gives

$$\begin{aligned} p(t) &= p^* + x(t), \\ \frac{d}{dt}p(t) &= \frac{d}{dt}x(t), \end{aligned} \tag{2.15}$$

and substitute this into equation (2.12). This translates the steady states of the equation to the zero origin. We can now rewrite equation (2.12) as

$$\frac{d}{dt}x(t) = -[p^*(t) + x(t)] + r[p^*(t) + x(t-\tau)][1 - (p^*(t) + x(t-\tau))]. \tag{2.16}$$

At $p_1^* = 0$, the steady state p^* in the equation is equivalent to zero. Taking the linear part of equation (2.16) about the steady state gives

$$\frac{d}{dt}x(t) = -\,x(t) + r\,x(t-\tau). \tag{2.17}$$

Let $x(t) = e^{\rho\,t}$ be the solution to equation (2.17). This gives the following transcendental characteristic equation

$$\rho + 1 = re^{-\rho\,\tau}. \tag{2.18}$$

Equation (2.18) has a solution state as shown in figure 2.5 and this equation is satisfied at $r = 1$ when $\rho = 0$ independent of the value of τ. For $\tau = 0$ the eigenvalue, ρ in equation (2.18) is positive for values of $r > 1$ but negative for

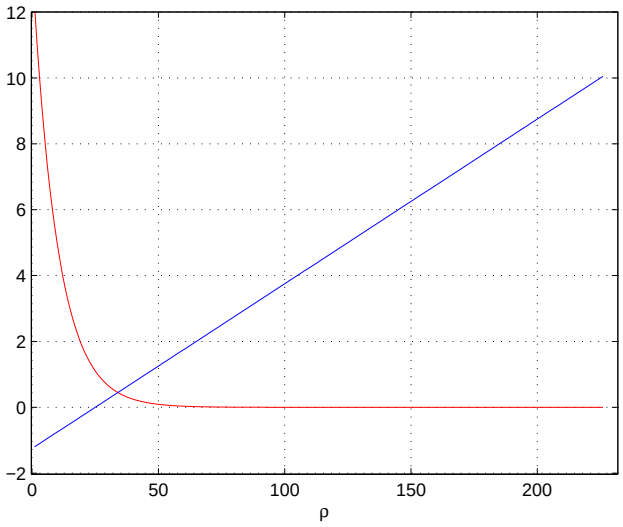


Figure 2.5: A plot of equation (2.18), with $(\rho+1)/r$ in blue and the $\exp(-\rho\,\tau)$ in red, $r = 20$ and $\tau = 0.1$.

$r < 1$ which imply that the steady state at $p_1^* = 0$ is unstable for $r > 1$ and stable for $r < 1$. We will analyse the second steady state p_2^* in a similar way.

For $p_2^* = 1 - 1/r$, $(r > 1)$

$$\begin{aligned} p(t) &= p_2^* + x(t), \\ \frac{d}{dt}x(t) &= -x(t) + (2-r)\,x(t-\tau) - r\,x^2(t-\tau). \end{aligned} \tag{2.19}$$

Let $x(t) = e^{\lambda t}$ be the solution to equation (2.19). The characteristic equation of the equation is

$$\lambda = -1 + (2-r)\,e^{-\lambda\tau} \tag{2.20}$$

We investigate the steady state of equation (2.19) by studying distribution of the eigenvalues applying the linear stability analysis. The linearization of equation (2.20) gives

$$\lambda + 1 - (2-r)\,e^{-\lambda\tau} = 0 \tag{2.21}$$

Equation (2.21) is satisfied at $r = 1$ when $\lambda = 1 - 1/r = 0$ irrespective of the value of the delayed parameter. For $\tau = 0$, when $r > 1$ all real parts of the eigenvalues are negative which implies an asymptotically stable steady state and for $r < 1$ at p_2^* would give negative steady state which is biologically irrelevant since cannot have a negative population. For $\tau > 0$ the preceding statement is only true for r sufficiently close to 1. As we proceed we will keep studying what happens to the model as the parameter r is increased for $\tau > 0$. Comparing equations (2.18) and (2.21) at $\tau = 0$ we have

$$\begin{aligned} \rho &= -1 + r, \\ \lambda &= 1 - r. \end{aligned} \tag{2.22}$$

This borderline case identifies a transcritical bifurcation which is represented in figure 2.6. For the value of $r < 1$, only p_1^* is relevant and this gives a

is negative eigenvalue and for $r > 1$, p_2^* is relevant and gives λ as negative. The switching of stable and unstable points by this steady state identifies the transcritical bifurcation point at $r = 1$, a result that carries over to the case of non-zero delay.

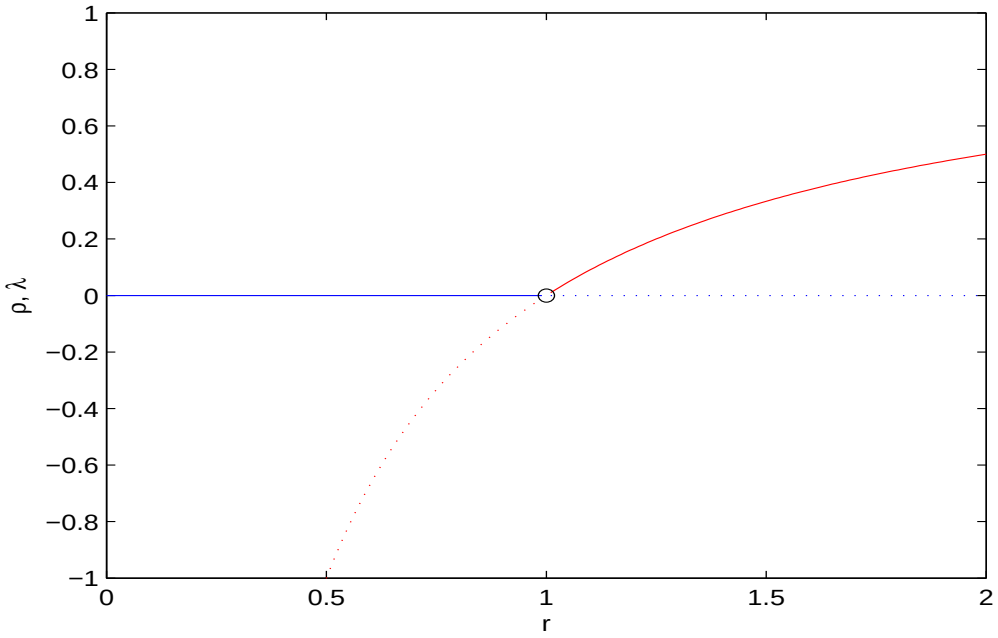


Figure 2.6: Transcritical bifurcation for the steady states of equation (2.22). The fixed point ρ is the blue line and the fixed point λ is in red. The stable fixed points are solid lines while the unstable fixed points are dotted lines.

For equation (2.21) we now study the distribution of eigenvalues for $\tau > 0$. If $\lambda = 0$ this implies that $r = -1$ must be satisfied for the characteristic equation to hold but we know that $r > 0$. To study this transcendental equation let $\lambda \in \mathbb{C}$ such that $\lambda = \sigma + i\,\varpi$ and $\sigma, \varpi \in \mathbb{R}$. Equation (2.21) will be

$$\sigma + i\,\varpi + 1 - (2 - r)\, e^{-(\sigma + i\,\varpi)\tau} = 0, \tag{2.23}$$

which is equivalent to

$$\sigma + i\,\varpi + 1 = (2 - r)\; e^{-\sigma\tau}\left(\cos(\varpi\tau) - i\sin(\varpi\tau)\right). \tag{2.24}$$

Separating the real and imaginary parts of equation (2.24) give

$$\begin{aligned} \sigma + 1 &= -(r-2)\; e^{-\sigma\tau}\left(\cos(\varpi\tau)\right), \\ \varpi &= (r-2)\; e^{-\sigma\tau}\left(\sin(\varpi\tau)\right), \end{aligned} \tag{2.25}$$

as the two equations determine the values of σ and ϖ. From equation (2.25) we can derive the following

$$-\tan(\varpi\tau) = \frac{\varpi}{\sigma+1}, \qquad\qquad (\sigma+1)^2 + \varpi^2 = (r-2)^2 e^{-2\sigma\tau}. \tag{2.26}$$

If there is a bifurcation, σ must change sign from negative to positive or positive to negative, hence σ crosses zero. If $\sigma = 0$ then equations (2.25) and is reduce to the following,

$$1 = -(r_{\text{H}} - 2)\cos(\varpi_{\text{H}}\tau) \qquad\qquad \varpi_{\text{H}} = (r_{\text{H}} - 2)\sin(\varpi_{\text{H}}\tau), \tag{2.27}$$

where r_{H} and ϖ_{H} denote the relevant quantities at the Hopf bifurcation point. With further algebraic computation equation (2.27) can be represented as

$$\begin{aligned} \varpi_{\text{H}} &= \sqrt{(r_{\text{H}} - 2)^2 - 1}, & r_H > 3 \\ \tau &= \frac{1}{\varpi_{\text{H}}}\left(\arccos\left(-\frac{1}{r_{\text{H}} - 2}\right) + 2j\pi\right), & j = 0, 1, 2\cdots. \end{aligned} \tag{2.28}$$

From equation (2.28) a numerical representation of the r-τ curve is shown in figure 2.7 for values of $j = 0$, $j = 1$ and $j = 2$. The smallest value of τ is at $j = 0$ corresponds to the smallest (primary) Hopf bifurcation point of the system. Recall that from equation (2.22b) the system for $r > 1$ but not too large is stable, this stability is retained below the r_{H}-τ curve but changes as

we cross the curve. From figure 2.7 the singular point is identified on the plot, at $r = 3$. We will analyse the singularity at $r = 3$ for large delay in section 2.2.1 and chapter 6.

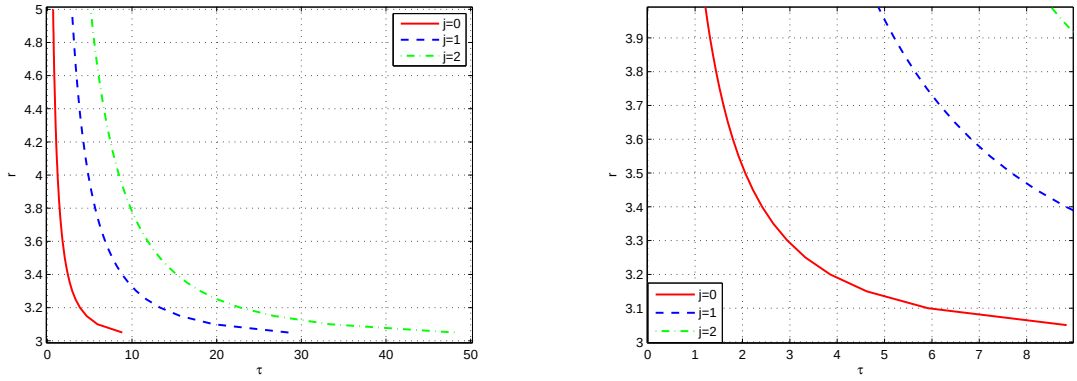


Figure 2.7: Numerical plot of equations (2.27) and (2.28) for $j = 0, 1$ and 2 as as we vary τ.

The implicit differentiation with respect to the parameter τ and r would give us the necessary condition to satisfy the change of the sign of the eigenvalue for $\sigma = 0$ and $\omega \neq 0$. We differentiate equation (2.21) with respect to τ and r,

$$Re\left(\frac{d\lambda}{dr}\right)\Big|_{\sigma=0} = \frac{(1+\tau)+\tau\varpi^2}{\tau^2\varpi^2+(\tau+1)^2} > 0, \tag{2.29}$$

$$Re\left(\frac{d\lambda}{d\tau}\right)\Big|_{\sigma=0} = \frac{\varpi^2(1+2\tau)}{\tau^2\varpi^2+(\tau+1)^2} > 0. \tag{2.30}$$

Equations (2.29) and (2.30) are strictly positive, hence satisfying the transversality condition, which confirms the presence of periodic solution.
From equation (2.21), (2.28) and (2.30) we draw the following conclusion,

1. when $\tau \geq 0$ and $r < 1$, the root derived from equation (2.14a) gives a stable steady state.

2. For $\tau > 0$, if $1 < r < r_{\text{H}}$, the root of equation derived from equation (2.14b) has negative real part, which gives an asymptotically stable steady state.

3. For $\tau > 0$, if $r = r_{\text{H}}$ the steady state has imaginary roots indicating a Hopf bifurcation as attained from equation (2.28).

4. For $\tau > 0$, if $r > r_{\text{H}}$ a periodic solution are attained with the steady state being unstable.

We have made analysis on how the equation (2.12) behaves for $\tau \geq 0$ in the neighborhood of $r = r_{\text{H}}$. We have shown that the analysis carried out gives the same results as obtained in [56]. Further analysis will now be performed using asymptotics expansions.

2.2.1 Asymptotics of Hopf point

The parameters r and τ are investigated in this subsection and their limiting behaviour analysed. The asymptotic approximation to the Hopf bifurcation point is studied and its solution is compared to the numerical solution. There are two possible limit values for τ, the first possibility is that $\tau \to 0$ and the second is that $\tau \to +\infty$. In section 2.2 we analysed the distribution of roots for $\tau > 0$ where we saw that at r_{H} for $\tau > 0$ a Hopf bifurcation point is derived. In this section we will investigate the two limits of τ close the the Hopf bifurcation point. Let $\varpi_{\text{H}}\tau = \omega_{\text{H}}$, substitute into equation (2.27) we derive the following

$$\omega_{\text{H}} = \tau\sqrt{(r_{\text{H}}-2)^2-1} \tag{2.31a}$$

$$\frac{\omega_{\text{H}}}{\tau} = -\tan(\omega_{\text{H}}) \tag{2.31b}$$

$$\tau^2 = \left(\tau^2+\omega_{\text{H}}^2\right)\cos^2(\omega_{\text{H}}) \tag{2.31c}$$

$$r_{\text{H}} = 2-\sec\left(\omega_{\text{H}}\right). \tag{2.31d}$$

From equations (2.31) the value of the ω_{H} should take values between $\pi/2 \leq \omega_{\text{H}} \leq \pi$ giving $\omega_{\text{H}} = \pi$ as $\tau \to \infty$ and $\omega_{\text{H}} = \pi/2$ as $\tau \to 0$, thus we have the following

As $\tau \to \infty$

$$\omega_{\text{H}} \sim k_1\pi\left[1-\frac{1}{\tau}+\frac{1}{\tau^2}+\left(\frac{(k_1\pi)^2}{3}-1\right)\frac{1}{\tau^3}-\left(\frac{(2\,k_1\,\pi)^2}{3}-1\right)\frac{1}{\tau^4}+O(1/\tau^5)\right] \tag{2.32}$$

where $k_1 = 2n+1$ and $n = 0,1,2,3\cdots$ we substitute into equation (2.31d)

$$r_{\text{H}} \sim 3+\frac{(k_1\pi)^2}{2}\frac{1}{\tau^2}-(k_1\pi)^2\frac{1}{\tau^3}-\frac{(k_1\pi)^2}{2}\left(\frac{(k_1\pi)^2}{4}-3\right)\frac{1}{\tau^4}+O(1/\tau^5) \tag{2.33}$$

where $n = 0,1,3,5\cdots$.

As $\tau \to 0$

$$\omega_{\text{H}} \sim \frac{k_2\pi}{2}+\frac{2}{k_2\pi}\tau-\frac{8}{(k_2\pi)^3}\tau^2-\frac{8}{3}\left[\frac{(k_2\pi)^2-24}{(k_2\pi)^5}\right]\tau^3+\frac{128}{3}\left[\frac{(k_2\pi)^2-15}{(k_2\pi)^7}\right]\tau^4+O(\tau^5) \tag{2.34}$$

where $k_2 = 4n+1$

$$r_{\text{H}} \sim \frac{k_2\pi}{2\tau}+2\left(1+\frac{1}{k_2\pi}\right)+\frac{{k_2}^2\pi^2-8}{{k_2}^3\pi^3}\tau-\frac{20\,{k_2}^2\pi^2-192}{3\,{k_2}^5\pi^5}\tau^2 + \frac{9\,{k_2}^4\pi^4-1280\,{k_2}^2\pi^2+17280}{15\,{k_2}^7\pi^7}\tau^3-\frac{188\,{k_2}^2\pi^2-2240}{15\,{k_2}^7\pi^7}\tau^4+O\left(\tau^5\right) \tag{2.35}$$

From the equations derived from the analysis we have that as $\tau \to \infty$, $r_{\text{H}} \to 3$ while as $\tau \to 0$, $r \to k_2\pi/2\tau$ for the leading order term. We compare the curve of $r_{\text{H}}(\tau)$ derived from the analytical study to that of the direct numerical solution

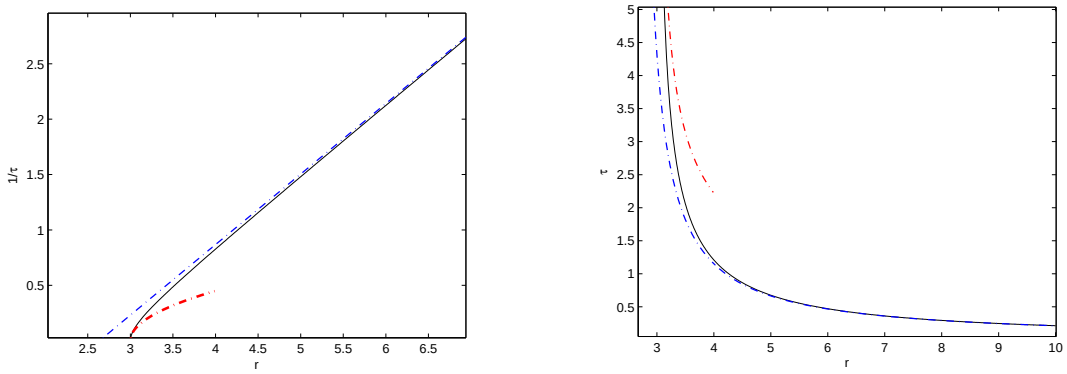


Figure 2.8: The black line is the direct numerical solution from equation (2.28, the cyan dashed line is the asymptotic solution as $\tau \to 0$ from equation (2.35) for values of r_{H} and the red dashed line is the asymptotic solution as $\tau \to \infty$ from equation (2.33) for values of r_{H}. For both asymptotic we plot the first two terms.

Figure 2.8 shows very good approximation for the comparison of the values obtained. For large value r equation (2.35) it shows a very good approximation to the numerical solution which is almost indistinguishable. And as $\tau \to \infty$, we observed that $r_{\text{H}} \to 3$ and the asymptotic become a good representation of the solution. Similarly, we do likewise to $\omega_{\text{H}}(\tau)$,

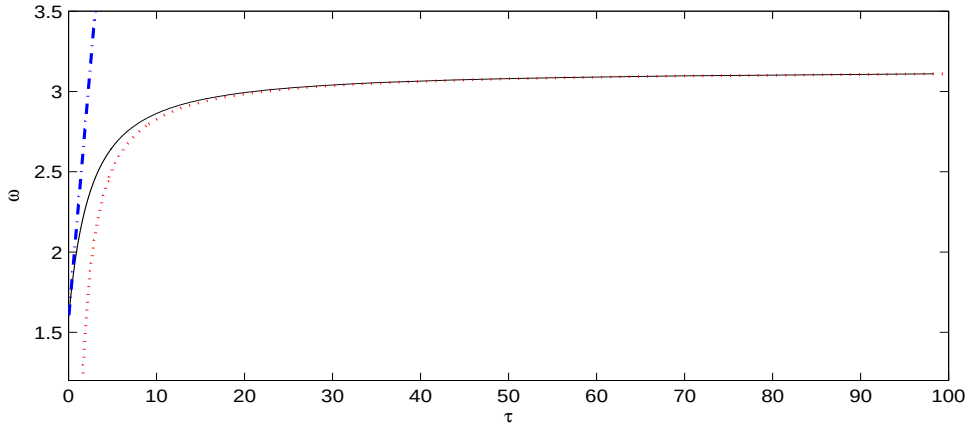


Figure 2.9: Plot of frequency against the delay. The black line is the direct numerical solution from equation (2.28). The red dotted is the asymptotic solution as $\tau \to \infty$ for values of ω_{H} from equation (2.32) and blue dashed-dotted is the asymptotic solution as $\tau \to 0$ from equation (2.34) for values of ω_{H}. For both asymptotic equations (2.32) and (2.34) we plot the first two terms.

Figure 2.9 shows that the analytical solution is a good representation of the numerical solution for both $\tau \to \infty$ and $\tau \to 0$.
Let P be the period of oscillation, from equation (2.32) and (2.34) we derive the period of oscillation for the system

$$P = 2 + \frac{2}{\tau} - \frac{2}{\tau^3} - \frac{2}{\tau^4} + O\left(\frac{1}{\tau^5}\right), \tag{2.36}$$

$$P = 4 - \frac{16}{\pi^2}\tau + \frac{64}{\pi^4}\tau^2 - \frac{256}{\pi^6}\tau^3 + \frac{1024}{\pi^8}\tau^4 + O\left(\tau^5\right). \tag{2.37}$$

Equations (2.36) and (2.37) give the period of 2 as $\tau \to \infty$ and as $\tau \to 0$ we have a period of 4. Figure 2.10 shows how accurate the analytical results are as we tend to the limit under consideration.

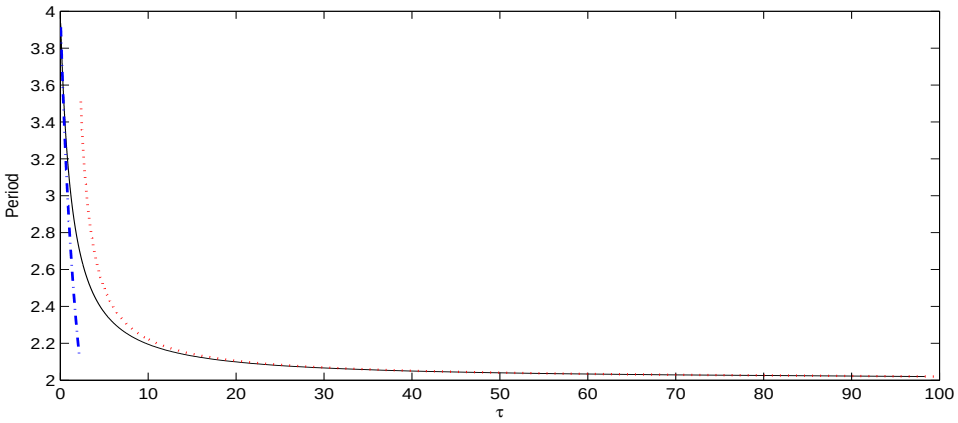


Figure 2.10: Plot of period against the delay, τ. The black line is the direct numerical solution from equation (2.28). The red dotted is the asymptotic solution as $\tau \to \infty$ for values of period from equation (2.36) and blue dashed-dotted is the asymptotic solution as $\tau \to 0$ from equation (2.37) for values of period. For both asymptotic equations (2.36) and (2.37) we plot the first two terms.

From figures 2.8 - 2.10 we have our analytical solutions giving very good approximations to the direct numerics as we get closer to the limit of our analysis. This implies the method applied for this type of model gives a very good results. In subsequent section we will extend our work to include the non-linear part of the model, but for the next section we compare our analysis with the direct numerics.

2.2.2 Numerics

In this section we compare the analytical results derived in section 2.2 with the direct numerical results. For the linearized equation (2.12), we assign a fix value to r_{H}, from which we would obtain τ and ω_{H}. For these numerics let $r_{\text{H}} = 3.1$.

Substituting the value of r_{H} into equation (2.19) gives

$$\frac{d}{dt}x(t) = -x(t) + (2 - 3.1)\, x(t-\tau) - \, 3.1\, x^2(t-\tau). \tag{2.38}$$

The steady state p^* of equation (2.38) is derived from equation (2.14) in section 2.2. For equation (2.38), the steady state $p_1^* = 0$ is the trivial and was discussed in section 2.2. The second steady state $p^* = 0.6774$ is a unique positive steady state. The Hopf bifurcation point for $r_{\text{H}} = 3.1$ is also obtained from equation (2.28) as

$$\begin{aligned} \omega_{\text{H}} &= \sqrt{(r_{\text{H}} - 2)^2 - 1} = 0.4583, \\ \tau &= \frac{1}{\omega_{\text{H}}} \arccos\left(-\frac{1}{r_{\text{H}} - 2}\right) = 5.9178. \end{aligned} \tag{2.39}$$

The plots derived from equation (2.38) for the value of $r_{\text{H}} = 3.1$ is shown in figures 2.11 and 2.12. The linearization of equation (2.12) implies that the steady state p_2 would be shifted to zero line as shown in both figures 2.11 and 2.12 hence the negative values seen in the plot are shifted values.

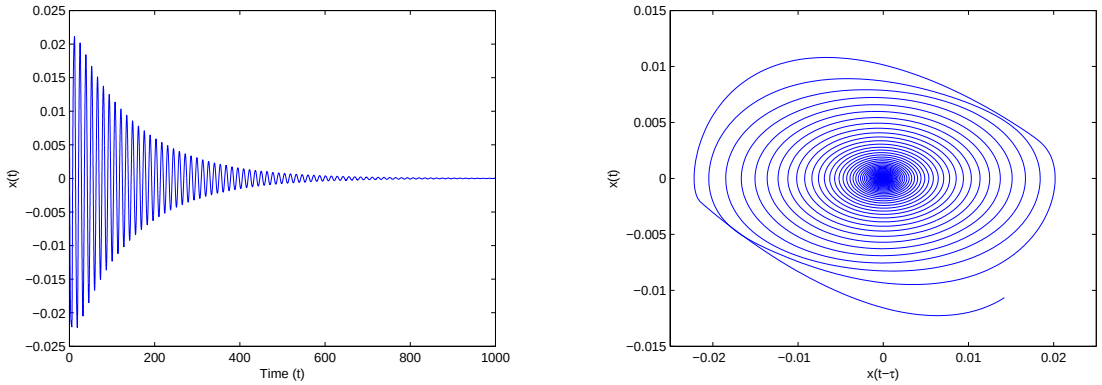


Figure 2.11: Plots of equation (2.38) for $r = 3.05$ and $\tau = 5.9178$, so that $r < r_{\text{H}}$. The steady state of is asymptotically stable. (a) The waveform $x(t)$. (b) A phase portrait of $x(t)$ plotted against $x(t-\tau)$.

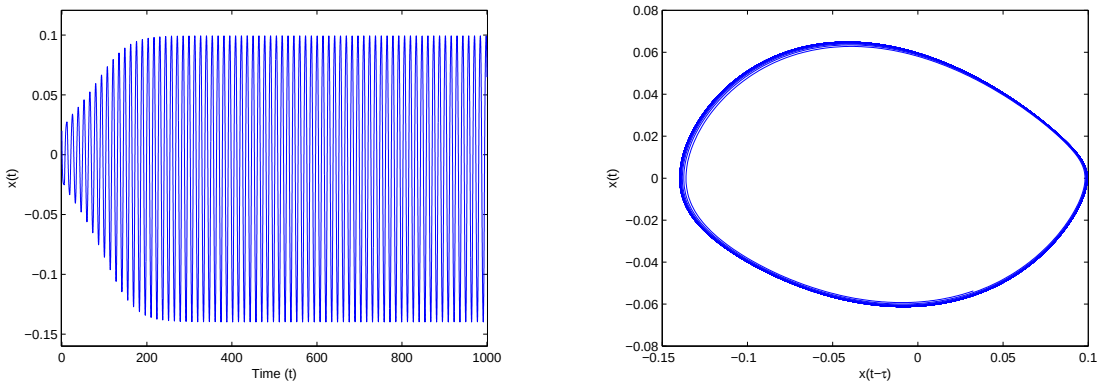


Figure 2.12: Plots of equation (2.38) for $r = 3.2$ and $\tau = 5.9178$, so that $r > r_{\text{H}}$. A periodic solution bifurcates from p^*. (a) The waveform $x(t)$. (b) A phase portrait of $x(t)$ plotted against $x(t-\tau)$.

Figures 2.11 and 2.12 show that for $r < r_{\text{H}}$ the population growth decays but for $r > r_{\text{H}}$ periodic oscillations are derived giving a limit cycle, which implies that at $r = r_{\text{H}}$ a bifurcation occurs. Obtaining a limit cycle from the bifurcation point we can conclude that we have a Hopf Bifurcation. The negative values of x from figures 2.11 and 2.12 are as a result the linearization obtained in equation (2.19). This shifts the steady state to zero and gives negative values of x. With these results, we have shown that the analytical result derived in section 2.2 is accurate and thus represent the solution of the linear part of our modelled equation. In the next section we will analyse the behaviour of the system close to the Hopf bifurcation point when we take the nonlinear part into consideration. We will also analyse the parameters r and τ in the equation.

2.3 Weakly nonlinear analysis

In this section we do extend the work on the logistic model by applying weakly nonlinear analysis to it. The weakly nonlinear analysis is applied in this section to the logistic model (2.19) which has a simple quadratic nonlinearity. This same approach will be used a number of times to subsequent models with greater nonlinearity. Recall that in section 2.2 we studied the stability of the linearised part of the equation (2.19) as shown below,

$$\frac{d}{dt}x(t) = -x(t) + (2-r)\ x(t-\tau) - r\,x^2(t-\tau). \tag{2.40}$$

We derived the critical value for r_{H}, which give rise to Hopf bifurcation as seen below

$$\begin{aligned} \omega_{\text{H}} &= \sqrt{(r_{\text{H}}-2)^2-1}, \\ \tau &= \frac{1}{\omega_{\text{H}}}\arccos\left(\frac{1}{r_{\text{H}}-2}\right). \end{aligned} \tag{2.41}$$

For values of $r < r_{\text{H}}$ the solution decays to zero and for $r > r_{\text{H}}$ we have limit cycles, with r_{H} being the bifurcation point of equation (2.19b). This analysis was based on the linear part of the equation (2.40). In this section we will analyse the direction of the Hopf bifurcation as we introduce the nonlinear term in a systematic way to the linearised equation studied in section 2.2. The inclusion of nonlinear terms to linear dynamical systems could produce secular terms to a well known linear system hence the need for the systematic inclusion of the nonlinear term. With a little nonlinearity added to the linear equation, one might be able to predict or approximate solution of the nonlinear equation (2.40). The inclusion of small nonlinearities makes the problem weakly nonlinear. We begin by rescaling equation (2.40) to take the form of a weakly nonlinear equation. The analysis we are investigating is for r close

to the Hopf point r_{H} thus let $r = r_{\text{H}} + \delta$ where δ is small perturbation from the Hopf point. We can rescale $\delta = \epsilon^2 \Delta$ such that $0 < \epsilon \ll 1$. Also let $x(t) \to \epsilon x(t)$, if we substitute $\epsilon\, x(t)$ into equation (2.40) we get

$$\frac{d}{dt}x(t) + x(t) - (2 - r)\, x(t-\tau) + \epsilon\, r\, x^2(t-\tau) = 0. \tag{2.42}$$

For $\epsilon = 0$, equation (2.42) reduces to the linear equation studied in section 2.2. We also want analyse what happens close to the Hopf bifurcation and derive the direction of the Hopf bifurcation. The weakly nonlinear equation of the logistic model is given by

$$\frac{d}{dt}x(t) + x(t) - x(t-\tau)\, \Big(2 - (r_{\text{H}} + \epsilon^2\Delta)\,(1 + \epsilon\, x(t-\tau))\Big) = 0. \tag{2.43}$$

where r_{H} is a positive constant as described in the previous sections. We have ϵ as the size of our step from the bifurcation point and Δ indicates the direction we decide to move from the bifurcation point. Again at $\epsilon = 0$ we remain on the Hopf bifurcation point of the linear part of equation (2.19b), since we have not taking any step away from it. For $\Delta = 0$ we will be on the Hopf bifurcation point and the equation would be very similar to equation (2.19) but with an ϵ on the nonlinear term. In the next section we would be studying equation (2.43) to analyse the effect of the nonlinear term included.

2.3.1 Multiple time scale (MTS)

There are two well known methods of analyzing weakly nonlinear equations, they are the Poincaré-Lindstedt method and the method of multiple time scales. The method of multiple time scale is also called the method of two timing when studied for two different times. Both methods, are perturbation techniques and we will adopt the method of multiple time scales to analyse

equation (2.40). To do this we begin by expanding $x(t)$ using the perturbation expansion. Hence for this expansion let

$$x(t) = x_0(t,T) + \epsilon x_1(t,T) + \epsilon^2 x_2(t,T) + O(\epsilon^3), \qquad T = \epsilon^2 t. \tag{2.44}$$

$$\frac{d}{dt} = \frac{\partial}{\partial t} + \epsilon^2 \frac{\partial}{\partial T}, \tag{2.45}$$

$$\begin{aligned} x(t-\tau) &= x_0(t-\tau, T-\epsilon^2\tau) + \epsilon x_1(t-\tau, T-\epsilon^2\tau) + \epsilon^2 x_2(t-\tau, T-\epsilon^2\tau) + O(\epsilon^3) \\ &= x_0\left(t-\tau, T\right) + x_1\left(t-\tau, T\right)\epsilon \\ &\quad + \left(x_2\left(t-\tau, T\right) - \frac{\partial}{\partial T} x_0\left(t-\tau, T\right)\tau\right)\epsilon^2 + O\left(\epsilon^3\right). \end{aligned} \tag{2.46}$$

We replace the time by two different times, t and T where t represent the fast timescale and T represent the slow timescale. Substituting equations (2.44)-(2.46) into equation (2.43) gives a perturbation series. Collecting in terms of the order of ϵ we obtain the following

At ϵ^0

$$\frac{\partial}{\partial t} x_0\left(t,T\right) + x_0\left(t,T\right) - x_0\left(t-\tau,T\right)\left(2 - r_{\text{H}}\right) = 0. \tag{2.47}$$

At ϵ^1

$$\frac{\partial}{\partial t} x_1\left(t,T\right) + x_1\left(t,T\right) - x_1\left(t-\tau,T\right)\left(2 - r_{\text{H}}\right) = -r_{\text{H}} x_0\left(t-\tau,T\right)^2. \tag{2.48}$$

At ϵ^2

$$\frac{\partial}{\partial t}x_2\,(t,T) + x_2\,(t,T) - x_2\,(t-\tau,T)\,(2-r_{\text{H}})$$
$$= -\frac{\partial}{\partial T}x_0\,(t,T) - \Delta\,x_0\,(t-\tau,T) - 2\,r_{\text{H}}\,x_1\,(t-\tau,T)\;x_0\,(t-\tau,T) \quad (2.49)$$
$$-\,\tau\;(2-r_{\text{H}})\;\frac{\partial}{\partial T}x_0\,(t-\tau,T)\,.$$

We will solve equation (2.47) - (2.49) and at each stage eliminating any secular term that appears. The solution of these equations without the secular terms give a periodic solution which is the approximate solution we want equation (2.43) to have.

Solving equation (2.47) for $\mathrm{O}(\epsilon^0)$ is equivalent to the linear equation we studied in section 2.2 that was analysed for stability and the distribution of its eigenvalues. At r_{H} we have a Hopf bifurcation which gives rise to a limit cycle. We can therefore represent the solution to equation (2.47) as a periodic solution, dropping the H subscript on ω let

$$x_0(t,T) = A(T)\,\cos(\omega t + \Phi(T)), \quad (2.50)$$

where $A(T)$ is the amplitude and $\Phi(T)$ is the phase both of which are functions of the slow time. There are no secular terms present in the solution to equation (2.47). Having obtained the fast timescales dependence of $x_0(t,T)$ we substitute it into equation (2.48) and solving for $x_1(t,T)$ at $\mathrm{O}(\epsilon)$, this gives

$$x_1\,(t,T) = M(T)\;\cos(2\,\omega t + 2\,\Phi(T)) \;+\; N(T)\;\sin(2\,\omega t \;+ 2\,\Phi(T)) + B(T)\,, \quad (2.51)$$

where

$$M = -\frac{({r_{\text{H}}}^2 - 2\,r_{\text{H}} - 2)\,r_{\text{H}}\,(A\,(T))^2}{2\;(r_{\text{H}}-2)\,(r_{\text{H}}-1)\,(5\,r_{\text{H}}-14)}, \quad (2.52)$$

$$N = \frac{r_{\text{H}}\,(A\,(T))^2\,(r_{\text{H}}-3)\,\sqrt{(r_{\text{H}}-1)\,(r_{\text{H}}-3)}}{(r_{\text{H}}-2)\,(r_{\text{H}}-1)\,(5\,r_{\text{H}}-14)}, \quad (2.53)$$

$$B = -\frac{r_{\text{H}}\left(A\left(T\right)\right)^2}{2\left(r_{\text{H}}-1\right)}. \tag{2.54}$$

Recall from equations (2.27) and (2.28) the values of τ and ω are clearly given so we can substitute them to derive the equations (2.52) - (2.54). The solution to equation (2.48) has no secular terms. Since there are no secular terms thus far, it implies that the solutions $x_0(t,T)$ and $x_1(t,T)$ remain periodic. But our main aim in applying the method of multiple time scale is to locate where secular terms occur and to eliminate them. The two solutions obtained for $x_0(t,T)$ and $x_1(t,T)$ are substituted into equation (2.49) at $\mathrm{O}(\epsilon^2)$. The right hand side (RHS) of equation (2.49) gives

$$\begin{aligned} &J_1(T)\,\cos(\omega t+\Phi(T))\;+\;J_2(T)\,\sin(\omega t\;+\Phi(T)) \\ &+M_2(T)\,\cos(3\,\omega t+3\,\Phi(T))\;+\;N_2(T)\,\sin(3\,\omega t\;+3\,\Phi(T))\,, \end{aligned} \tag{2.55}$$

where

$$\begin{aligned} J_1 = &-\left(\frac{\mathrm{d}}{\mathrm{d}T}A\left(T\right)\right)\left(\tau+1\right)+A\left(T\right)\sqrt{\left(r_{\text{H}}-1\right)\left(r_{\text{H}}-3\right)}\,\tau\,\frac{\mathrm{d}}{\mathrm{d}T}\Phi\left(T\right) \\ &+\frac{\left(2\,{r_{\text{H}}}^5-25\,{r_{\text{H}}}^4+80\,{r_{\text{H}}}^3-72\,{r_{\text{H}}}^2\right)\left(A\left(T\right)\right)^3}{2\,\left(r_{\text{H}}-1\right)\left(5\,r_{\text{H}}-14\right)\left(r_{\text{H}}-2\right)^2} \\ &+\frac{\left(10\,{r_{\text{H}}}^3-58\,{r_{\text{H}}}^2+104\,r_{\text{H}}-56\right)\Delta\,A\left(T\right)}{2\,\left(r_{\text{H}}-1\right)\left(5\,r_{\text{H}}-14\right)\left(r_{\text{H}}-2\right)^2}, \end{aligned} \tag{2.56}$$

$$\begin{aligned} J_2\;=\;&\sqrt{\left(r_{\text{H}}-1\right)\left(r_{\text{H}}-3\right)}\,\tau\,\frac{\mathrm{d}}{\mathrm{d}T}A\left(T\right)+\left(\frac{\mathrm{d}}{\mathrm{d}T}\Phi\left(T\right)\right)\left(\tau+1\right)A\left(T\right) \\ &+\frac{\sqrt{\left(r_{\text{H}}-1\right)\left(r_{\text{H}}-3\right)}r^2\left(11\,{r_{\text{H}}}^2-48\,r_{\text{H}}+48\right)\left(A\left(T\right)\right)^3}{2\,\left(r_{\text{H}}-1\right)\left(5\,r_{\text{H}}-14\right)\left(r_{\text{H}}-2\right)^2} \\ &-\frac{\sqrt{\left(r_{\text{H}}-1\right)\left(r_{\text{H}}-3\right)}\left(5\,{r_{\text{H}}}^3-29\,{r_{\text{H}}}^2+52\,r_{\text{H}}-28\right)\Delta\,A\left(T\right)}{2\,\left(r_{\text{H}}-1\right)\left(5\,r_{\text{H}}-14\right)\left(r_{\text{H}}-2\right)^2}, \end{aligned} \tag{2.57}$$

$$M_2\;=-\frac{\left(2\,{r_{\text{H}}}^5-25\,{r_{\text{H}}}^4+104\,{r_{\text{H}}}^3-164\,{r_{\text{H}}}^2+64\,r_{\text{H}}+16\right){r_{\text{H}}}^2\left(A\left(T\right)\right)^3}{2\,\left(r_{\text{H}}-2\right)^4\left(r_{\text{H}}-1\right)\left(5\,r_{\text{H}}-14\right)}, \tag{2.58}$$

$$N_2 = -\frac{{r_н}^2 \left(A\left(T\right)\right)^3 \sqrt{\left(r_н - 1\right)\left(r_н - 3\right)}\left({r_н}^4 - 36\,{r_н}^2 + 96\,r_н - 48\right)}{2\,\left(r_н - 2\right)^4\left(r_н - 1\right)\left(5\,r_н - 14\right)}. \quad (2.59)$$

We observe that RHS of equation (2.49) contains resonant terms that are equivalent to the homogeneous solution of the equation. This resonant terms would give rise to secular terms as $t \to \infty$. The secular terms in equation (2.55) would be eliminated by equating $J_1 = 0$ and $J_2 = 0$. By equating the secular term to zero we get the following equations

$$\frac{\mathrm{d}}{\mathrm{d}T}A = \kappa\, A\,\left(A^2 - \varrho\,\Delta\right), \quad (2.60a)$$

$$\frac{\mathrm{d}}{\mathrm{d}T}\Phi = \alpha\, A^2 + \beta\,\Delta, \quad (2.60b)$$

where

$\kappa = P_1/P_0$, $\varrho = P_2/P_1$, $\alpha = q_1/p_0$ and $\beta = q_2/P_0$,

$$P_0 = 2\,\left(r_н - 2\right)^2\left(r_н - 1\right)\left(5\,r_н - 14\right)\left({r_н}^2\tau^2 - 4\,r_н\tau^2 + 4\,\tau^2 + 2\,\tau + 1\right), \quad (2.61)$$

$$\begin{aligned} P_1 = -{r_н}^2\,\big(&11\,{r_н}^4\tau - 94\,{r_н}^3\tau - 2\,{r_н}^3 + 298\,{r_н}^2\tau + 25\,{r_н}^2 \\ &-416\,r_н\tau - 80\,r_н + 216\,\tau + 72\big), \end{aligned} \quad (2.62)$$

$$P_2 = -2\,\left(r_н - 2\right)\left(r_н - 1\right)\left(5\,r_н - 14\right)\left(\left(r_н - 2\right)^2\tau + 1\right), \quad (2.63)$$

$$\begin{aligned} q_1 = \sqrt{(r_н - 1)(r_н - 3)}\,\big(&-2\,{r_н}^5\tau + 14\,{r_н}^4\tau - 11\,{r_н}^4 - 32\,{r_н}^3\tau \\ &+48\,{r_н}^3 + 24\,{r_н}^2\tau - 48\,{r_н}^2\big), \end{aligned} \quad (2.64)$$

$$q_2 = \sqrt{(r_н - 1)(r_н - 3)}\,\left(10\,{r_н}^3 - 58\,{r_н}^2 + 104\,r_н - 56\right). \quad (2.65)$$

In an effort to eliminate the secular terms we have derived two equations, equation (2.60a) for the rate of change in amplitude and equation (2.60b) for the rate of change in phase. We will now study the effect of the nonlinear term on the amplitude and the phase from equation (2.60) as we vary r close to the Hopf bifurcation point. When the rate of change of the amplitude is zero we should have reached a steady state amplitude for $\Delta > 0$ and this steady state is a limit cycle. From equation (2.60a)

$$A^2 = \frac{P_2}{P_1}\Delta, \tag{2.66}$$

where P_1 and P_2 are as described above.

If the rate of change of the amplitude is not zero then the solution to equation (2.60a) is

$$A\left(T\right) = \frac{\sqrt{\Delta\, P_2}}{\sqrt{\Delta\, A\left(0\right) \mathrm{e}^{-2\,\frac{\Delta\, P_2 T}{P_0}}\, P_2 + P_1}}, \tag{2.67}$$

where $A(0)$ is the initial value of the amplitude at $t = 0$. From equation (2.44) we know that $T = \epsilon^2\, t$. Applying this to equation (2.67) to analyse what happens to the amplitude of the equation as $t \to \pm\infty$. From equation (2.67), for $\Delta > 0$ as $t \to -\infty$, the amplitude, $A(T) \to 0$ and as $t \to \infty$ the amplitude $A(T)$ tends to the steady amplitude in equation (2.66) for any arbitrary initial value of $A(0)$. This implies that the limit cycle would have a maximum amplitude of $\sqrt{\Delta\, P_2/P_1}$. To complete the solution to equation (2.43), we need to find the value of $\Phi(T)$ which describes any possible shift in the oscillating solution. We substitute the value of the amplitude into equation (2.60b) and solve for the phase constant, $\Phi(T)$. With these two parameters, the value of $x(t)$ in equation (2.44) is

$$x(t) = \frac{\sqrt{\Delta\, P_2}}{\sqrt{\Delta\, A\,(0)\, \mathrm{e}^{-2\,(\Delta\, P_2)/(P_0)T} P_2 + P_1}} \cos(\omega t + \Phi(T)). \tag{2.68}$$

From equation (2.68), a periodic solution occurs if and only if $\Delta\, A(0)\, \exp(-2\,\Delta\, P_2\, T/P_0) P_2 = 0$. From equation (2.60a) if $\Delta > 0$ the equation has three real roots $A(T) = 0$ and the other two represented by equation (2.66). For $A(T) = 0$ we do have an unstable steady state while the other two roots represent the limit cycle. For $\Delta < 0$ there is only one steady state and that is $A(T) = 0$ which is stable. From this we draw the conclusion that we have a supercritical Hopf bifurcation. Applying the method of multiple time scale we have solved the weakly nonlinear equation (2.43) and have also derived the Hopf bifurcation to be supercritical without initially reducing the equation to an operator differential equation as is the case with the center manifold reduction method.

In the next section we will numerically solve equation (2.43) and compare the result with our analysis from this section.

2.3.2 Comparison of numerical and MTS

In this section we will be comparing the direct numerical solution of equation (2.43) with the analytical results we got from multiple timescale (MTS). We will maintain our previous value of r_{H} as 3.1 from which we derive τ as 5.92. For any shift in r close to the Hopf bifurcation point it will be done with parameters ϵ and Δ. We start by comparing the amplitude of the MTS from equation (2.67), this is plotted in figure (2.13) and (2.14).

Figure 2.13 has a positive value for Δ while figure 2.14 has a negative Δ. Form both figures we clearly see the amplitude of the oscillation from the MTS (green lines) tracing out the amplitude from the direct numerical solution (blue

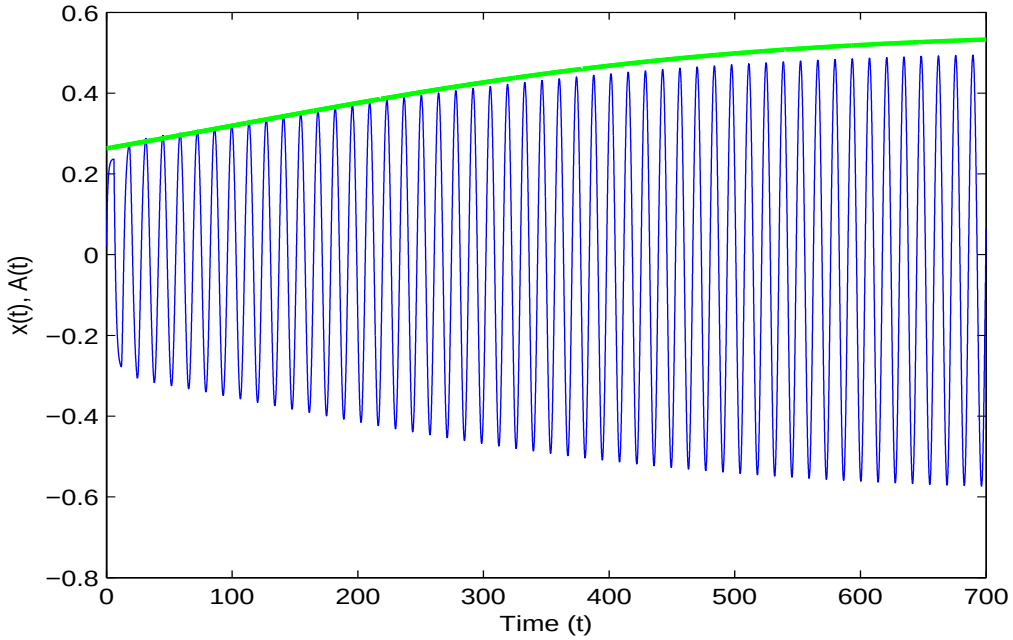


Figure 2.13: The blue solid line is the direct plot of equation (2.43) with initial condition $x(0) = 0.318\ \sin(-2.42)$, while the green line is the multiple time scale plot from the equation (2.60a) with initial condition $A(0) = 0.26$, for $r_{\text{H}} = 3.1$, $\epsilon = 0.1$, $\tau = 5.92$ and $\Delta = 2$.

lines) approximately accurately. For more accuracy in the weakly nonlinear analysis, there are two ways with the method of multiple timescale. One is to get solutions higher order of epsilon and secondly to introduce a slower time scale. For $\Delta > 0$ periodic oscillations are derived but for $\Delta < 0$ we have a damped oscillation taking the amplitude to zero giving more credibility to our conclusion from the analysis that the Hopf bifurcation is supercritical. Comparing figures 2.13 - 2.16 it is obvious that the MTS solution is symmetric while the direct numerical plot is not symmetric to the time axis. The leading order solution of the MTS is the linear and this accounts for this symmetry (the envelope determining the amplitude of the oscillations is symmetric under

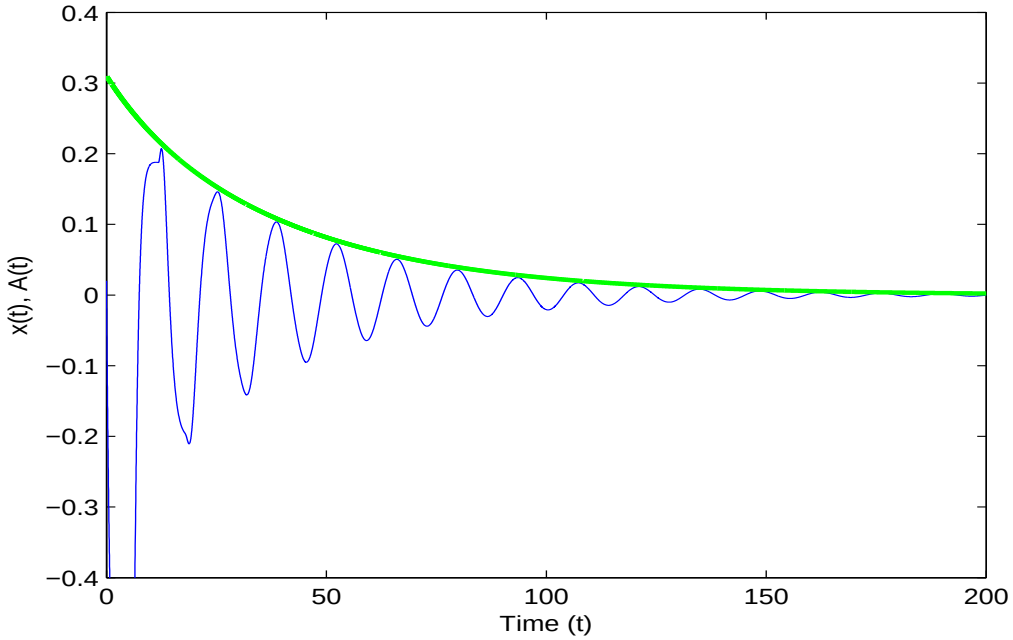


Figure 2.14: The blue solid line is the direct plot of equation (2.43) with initial condition $x(0) = 0.318\ \sin(-2.42)$, while the green line is the multiple time scale plot from the equation (2.60b) with initial condition $A(0) = 0.315$, for $r_{\text{H}} = 3.1$, $\epsilon = 0.1$, $\tau = 5.92$ and $\Delta = -2$.

$x \to -x$, giving the same values for x and $-x$) as shown in figure 2.19.

This lack of symmetry in the direct numerical method is as a result of the nonlinear term being large. This problem can be regulated by reducing the size of the nonlinear term and to do this we decrease the size of ϵ. With a reduced ϵ the amplitude of the multiple time scale solution will match the direct numerical method solution. See figures 2.17 and 2.18 display such symmetry of the MTS method.

In figures 2.17 and 2.18 we have set the phase shift to zero, so that both plot are clearly visible. As $t \to \infty$ the value of the phase shift becomes a constant. We will later show that with the appropriate $\Phi(T)$ the MTS and direct numerical

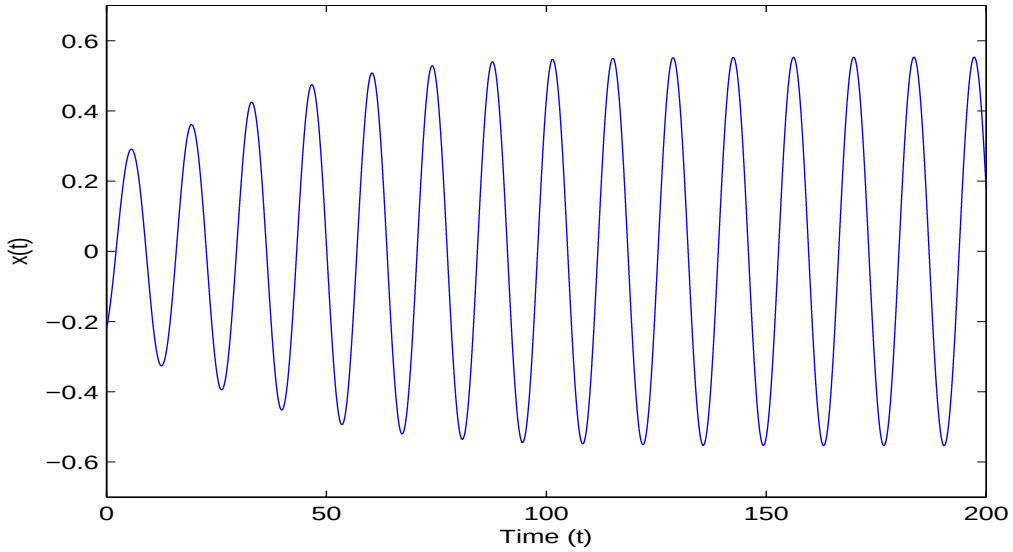


Figure 2.15: Plot of solution (2.43) showing oscillation in population size over time for values of $r_{\text{H}} = 3.1$, $\epsilon = 0.3$, $\tau = 5.92$ and $\Delta = 2$, using the method of multiple scales.

solution are almost indistinguishable. For increased accuracy we can reduced value of epsilon but this will mean that the solution takes much longer time to get to its steady state. Another way we can increase the accuracy of the MTS is to include higher order solutions to the leading other term.

The amplitude of both solutions in figures 2.17 and 2.18 are approximately matched the direct numerical solution for $\pm\Delta$.

The plots for a longer time interval shows clearly the amplitude of the periodic solution, as seen in figures 2.19.

Figure 2.19 best describes the analysis made in equation (2.66) about the amplitude. For $\Delta > 0$ a steady state is reached for the amplitude thus describing equation (2.66). For $\Delta < 0$ we observe a change in amplitude which is described by equation (2.67) for which a decaying amplitude occurs. The solution of the system with $\Phi(t) = 0$ is plotted in figure 2.17 and 2.18, this

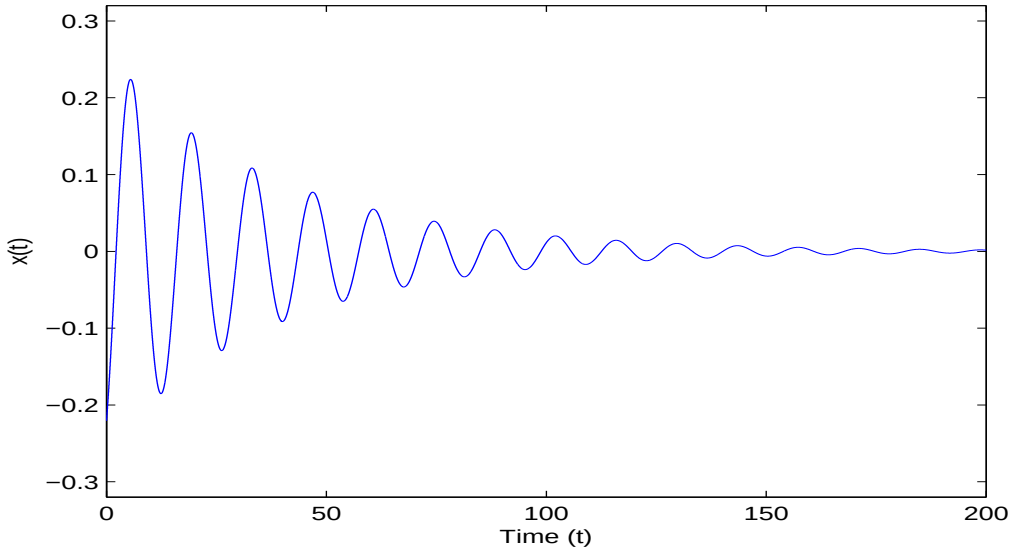


Figure 2.16: Plots of solution (2.43) showing decaying oscillation in population size over time for values of $r_{\text{H}} = 3.1$, $\epsilon = 0.3$, $\tau = 5.92$ and $\Delta = -2$ using the method of multiple scales.

shows a constant shift in the phase. With the appropriate initial value for $\Phi(T)$ we get a very good approximation to the direct numerical solution as seen in figures 2.20-2.25.

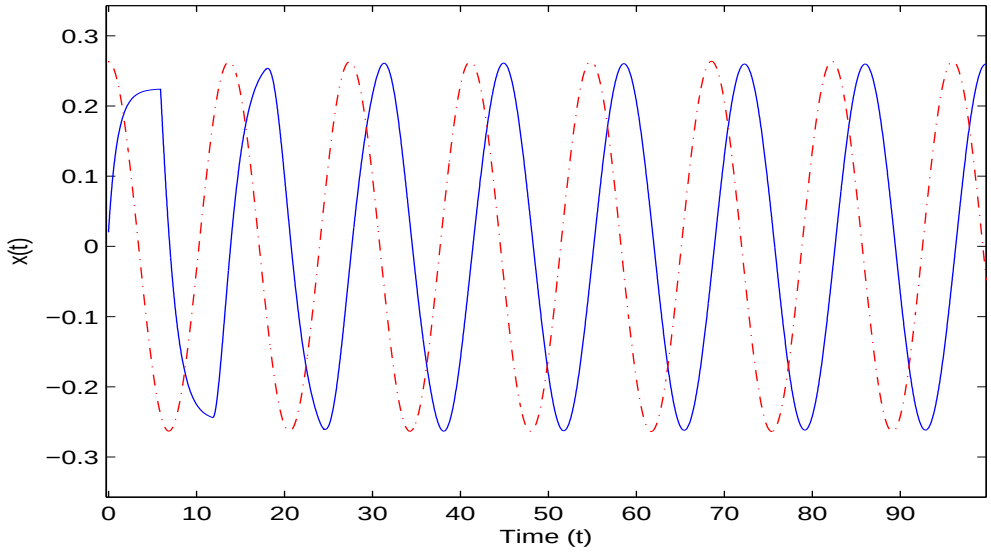


Figure 2.17: For $r_{\text{H}} = 3.1$, $\epsilon = 0.01$, $\tau = 5.92$ and $\Delta = 3$. The blue solid line is the direct plot of equation (2.43) with initial condition $x(0) = 0.3180\sin(-2.42)$, while the red dash-dotted line is the plot from the equation (2.60a) with initial condition, $A(0) = 0.26$ and $\Phi(0) = 0$.

Figures 2.20-2.25 show the accuracy of the MTS method in comparison to the direct numerical method. The time taken to plot MTS solution is by far shorter than that of the direct numerical method. For points before the bifurcation point we get decay and for points after the Hopf bifurcation point we get periodic oscillation. This implies that using r as the bifurcation parameter we obtain supercritical Hopf bifurcation. For other values of r we can apply the general solutions given here to solve and make comparison between the direct numerical method and the multiple time scale method.

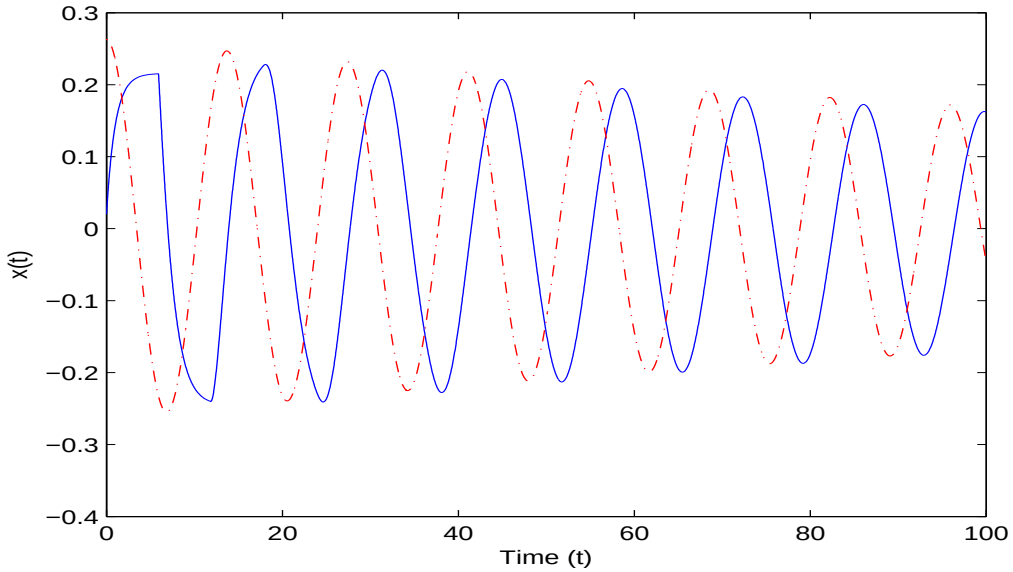


Figure 2.18: For $r_{\text{H}} = 3.1$, $\epsilon = 0.01$, $\tau = 5.92$ and $\Delta = -3$. The blue solid line is the direct plot of equation (2.43) with initial condition $x(0) = 0.3180\sin(-2.42)$, while the red dash-dotted line is the plot from the equation (2.60b) with initial condition, $A(0) = 0.26$ and $\Phi(0) = 0$,

2.4 Conclusion

In this chapter we have seen that the logistic model (2.10) could display a range solutions as shown in equation (2.14) of section 2.2 depending on the value of r. From equation (2.28) the condition for a Hopf bifurcation was derived and we were able to get periodic solution for the logistic model (2.10). The production of periodic oscillation is an interesting phenomenon with first order differential-delay equation which is not obtainable with first order ordinary differential equation periodic solutions do not occur. The introduction τ does not automatically imply the birth of periodic solution, but when the model satisfy certain condition as in equation (2.28) then a Hopf bifurcation is produced. We then applied the multiple time scale in the form of weakly non-

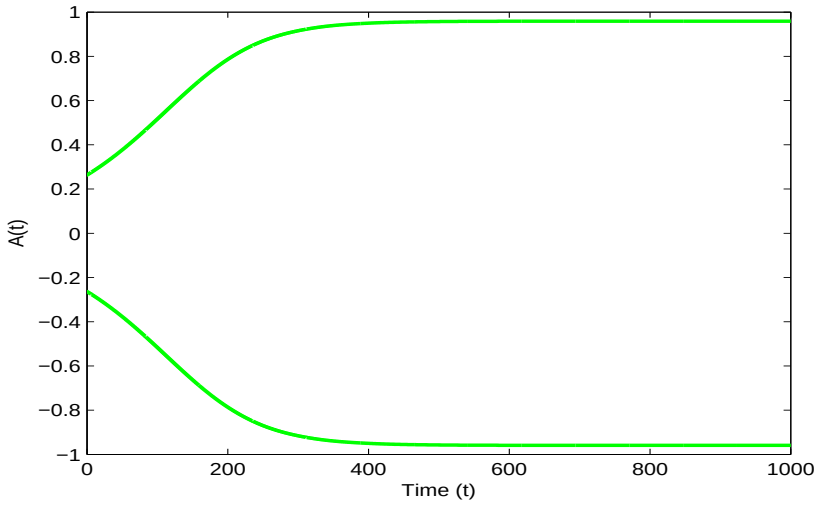


Figure 2.19: Plots of solution (2.43) showing amplitude of the MTS over time for values of $r_{\text{H}} = 3.1$, $\epsilon = 0.1$, $\tau = 5.92$ and $\Delta = 6$.

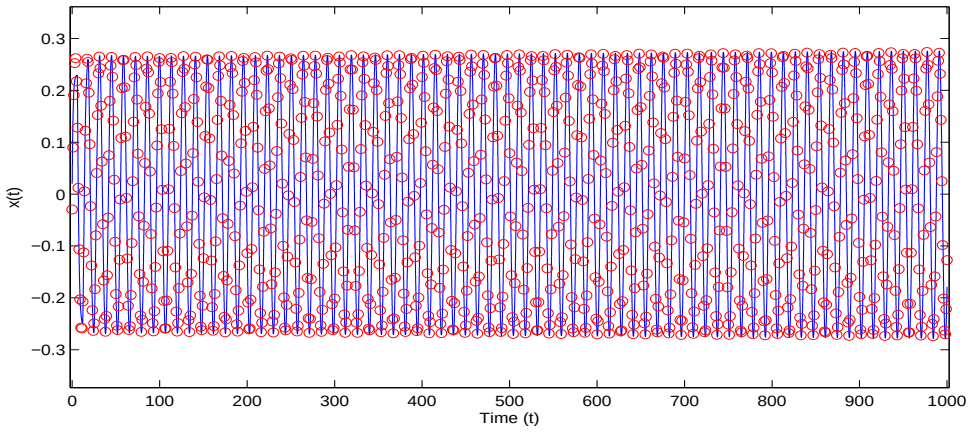


Figure 2.20: For $r_{\text{H}} = 3.1$, $\epsilon = 0.01$, $\tau = 5.92$ and $\Delta = 3$. The blue solid line is the direct plot of equation (2.43) with initial condition $x(0) = 0.3180\sin(-2.42)$, while the red dash-circle line is the plot from the equation (2.60) with initial condition, $A(0) = 0.26$ and $\Phi(0) = 4.5$.

linear analysis to study the Hopf bifurcation point and derived a supercritical Hopf bifurcation. This differential-delay logistic model (2.10) gave a better

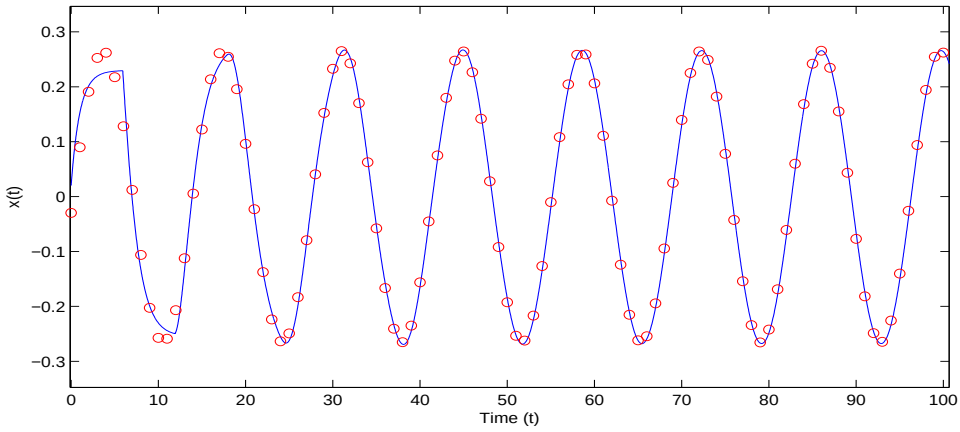


Figure 2.21: This is the same plot as figure (2.20) for time from 0 to 100, where $r_{\text{H}} = 3.1$, $\epsilon = 0.01$, $\tau = 5.92$ and $\Delta = 3$. The blue solid line is the direct plot of equation (2.43) with initial condition $x(0) = 0.3180\sin(-2.42)$, while the red dash-circle line is the plot from the equation (2.60) with initial condition, $A(0) = 0.26$ and $\Phi(0) = 4.5$.

dynamical behaviour of what happens in a population growth circle which has a certain carrying capacity. When a population size is small relative to the available resources a growth in the population is more feasible but if the resources are scare then the populace struggle for these resources for survival and this phenomenon continues over time.

The introduction of τ gave a better perspective to the logistic model, we shall be applying similar methodology to investigate other models and study them close to certain critical points.

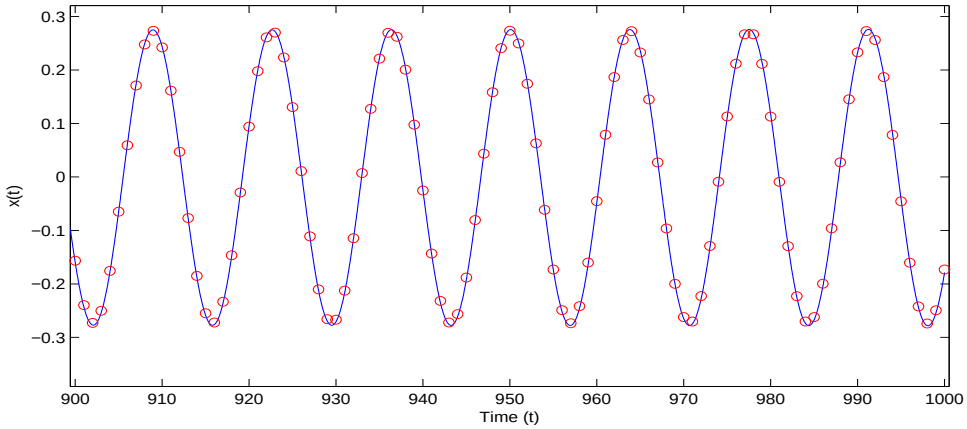


Figure 2.22: This is the same plot as figure (2.20) for time from 900 to 1000, where $r_{\text{H}} = 3.1$, $\epsilon = 0.01$, $\tau = 5.92$ and $\Delta = 3$. The blue solid line is the direct plot of equation (2.43) with initial condition $x(0) = 0.3180\sin(-2.42)$, while the red dash-circle line is the plot from the equation (2.60) with initial condition, $A(0) = 0.26$ and $\Phi(0) = 4.5$.

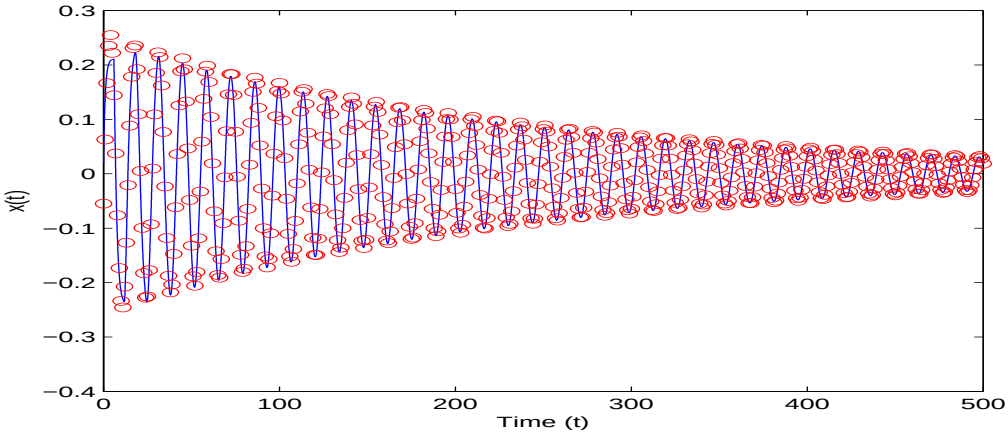


Figure 2.23: For $r_{\text{H}} = 3.1$, $\epsilon = 0.1$, $\tau = 5.92$ and $\Delta = -3$. The blue solid line is the direct plot of equation (2.43) with initial condition $x(0) = 0.3180\sin(-2.42)$, while the red dash-circle line is the plot from the equation (2.60) with initial condition, $A(0) = 0.26$ and $\Phi(0) = 4.5$.

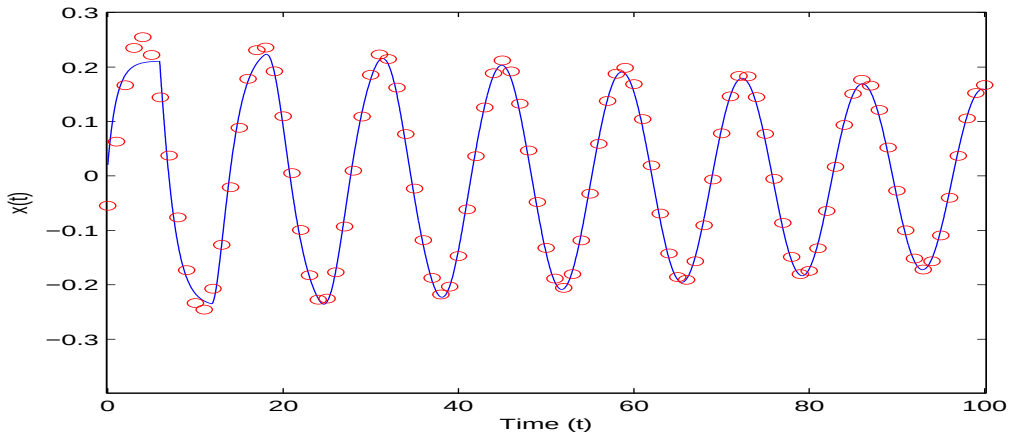


Figure 2.24: This is the same plot as (2.23) for time from 0 to 100, with the same values for $r_{\text{H}} = 3.1$, $\epsilon = 0.1$, $\tau = 5.92$ and $\Delta = -3$. The blue solid line is the direct plot of equation (2.43) with initial condition $x(0) = 0.3180\sin(-2.42)$, while the red dash-circle line is the plot from the equation (2.60) with initial condition, $A(0) = 0.26$ and $\Phi(0) = 4.5$.

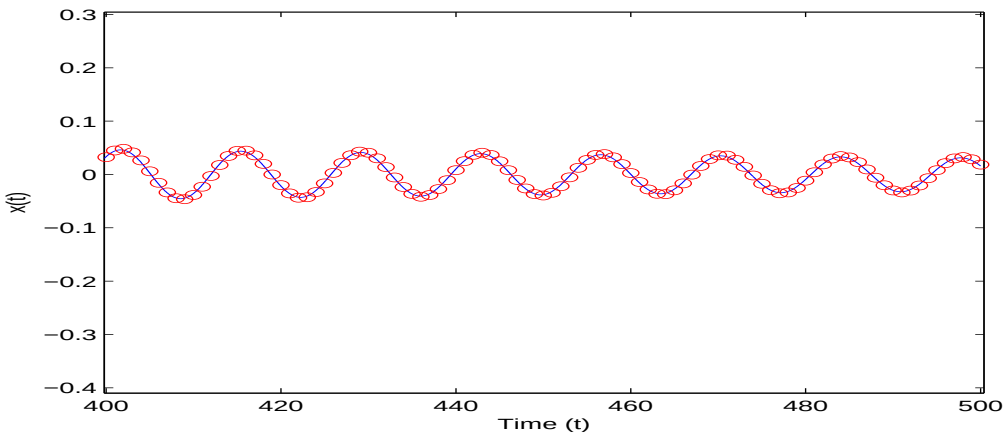


Figure 2.25: This is the same plot as (2.23) for time from 400 to 500, with the same values for $r_{\text{H}} = 3.1$, $\epsilon = 0.1$, $\tau = 5.92$ and $\Delta = -3$. The blue solid line is the direct plot of equation (2.43) with initial condition $x(0) = 0.3180\sin(-2.42)$, while the red dash-circle line is the plot from the equation (2.60) with initial condition, $A(0) = 0.26$ and $\Phi(0) = 4.5$.

Chapter 3

Analysis of a first order negative feedback differential-delay equation

3.1 Introduction

In this chapter we will be investigating the behaviour of a first order differential delay equation with negative feedback. This equation forms the building block for so many models that have been investigated and in the next chapter we will be looking at a higher order equation that is composed of this type of equation. Alon in [2] described the role and properties that arise with a gene having negative feedback using a first order ordinary differential equation. This class of ordinary differential equation has been extended to include time delays by authors such as [57, 58, 59, 60] in various models. The popularity of this type of differential-delay equation has grown following the studies by Mackey and Glass [57] in 1977. These models range from population model which includes harvesting studied by Berezansky et al in [58] to those investigated

by Mackey et al [59, 60] to analyse the periodic oscillations of blood cell in chronic myelogenous leukemia and long period of oscillation in a modelled of hematopoietic stem cell. As we study our model we will be analysing the effect of each parameter and how it affects the model.

The Mackey-Glass equation is mathematically represented as

$$\frac{\mathrm{d}}{\mathrm{dt}}\tilde{x}(t) = \frac{k}{1+\tilde{x}^n(t-\tau)} - \tilde{x}(t) \tag{3.1}$$

where t is the time, τ is the time delay, k is the maximal production rate and n the Hill coefficient. The right hand side of equation (3.1) is made up of two terms, the first being the negative feedback term. From figure 3.1, at $x = 1$ the value of the Hill function is the same irrespective of the value of n. This value corresponds to half the value of k and this is achieved when $x(t)$ is equal to the value of the first term in the denominator of the first term. This term is referred to as the activation coefficient.

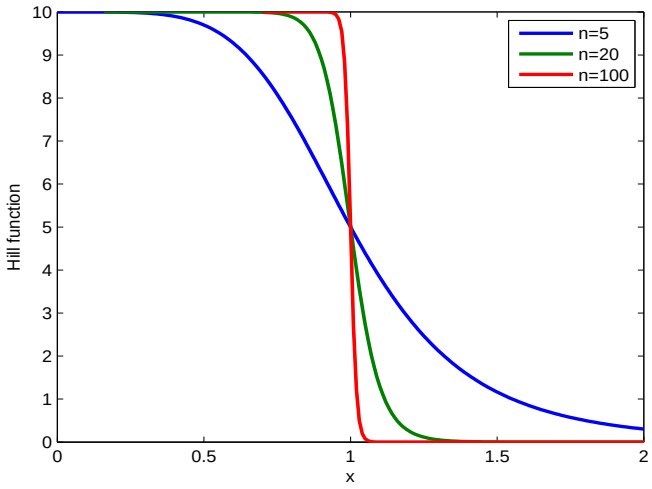


Figure 3.1: Representation of the Hill function for different values of the Hill coefficient, n and a fixed value of $k = 10$.

From equation (3.1) we have that that the nonlinear part of the equation is

negative feedback Hill function whose steepness depends on the value of n as shown in figure 3.1. Equation 3.1 approaches a Heaviside (step) function as $n \rightarrow \infty$, when this happens the system can be approximated by a pair of linear ordinary differential equations as follows

$$\frac{\mathrm{d}}{\mathrm{dt}}\tilde{x}(t) = -\tilde{x}(t) + \begin{cases} 0 & \tilde{x}(t-\tau) > 1 \\ & \\ k, & \tilde{x}(t-\tau) < 1. \end{cases} \tag{3.2}$$

These two differential equations are valid in different time intervals which we denote as t_n, where $n = 1, 2, 3, \cdots$. We study each of these equations, analyse its solution within its respective time interval and investigate how it transits to the next ordinary differential equation. From the first differential equation

$$\frac{\mathrm{d}}{\mathrm{dt}}\tilde{x}(t) = -\tilde{x}(t), \qquad \tilde{x}(0) = \tilde{x}_0 \tag{3.3}$$

let $\tilde{x}_0$ be an initial value at the time $t = 0$ and recall that $\tilde{x}(t-\tau) > 1$. The solution is given as

$$\tilde{x}(t) = \tilde{x}_0\, e^{-t} \tag{3.4}$$

This solution is valid until we get to a time t_1, at time t_1 we know that the value of $\tilde{x}(t_1 - \tau) = 1$ since it is the point were we transit from this solution but yet to operate within the next solution. Substituting into equation (3.4) we have

$$\tilde{x}(t_1 - \tau) = 1 = \tilde{x}_0\, e^{-(t_1-\tau)}. \tag{3.5}$$

From this equation we derive the value of t_1 as

$$t_1 = \ln(\tilde{x}_0) + \ln(e^{\tau}) \;=\; \ln(\tilde{x}_0\, e^{\tau}) \tag{3.6}$$

Now that the value of t_1 is known, we can solve for $\tilde{x}(t_1)$ by substituting into equation (3.4),

$$\begin{aligned}\tilde{x}_1 &= \tilde{x}_0\, e^{-t_1} = \tilde{x}_0\, e^{-(\ln \tilde{x}_0\, e^{\tau})} \\ &= e^{-\tau}\end{aligned}$$

The solution of equation (3.3) between the interval of $0 < t < t_1$ shows an exponentially decaying solution as $\tau \to \infty$. Next we solve for the equation which is valid for the second ordinary differential equation on the time interval $t_1 < t < t_2$,

$$\frac{\mathrm{d}}{\mathrm{dt}}\tilde{x}(t) = -\tilde{x}(t) + k, \qquad \tilde{x}(t_1) = \tilde{x}_1 \tag{3.7}$$

the solution derived to the equation is

$$\tilde{x}(t) = \tilde{x}_1\, e^{-(t-t_1)} + k\,(1 - e^{-(t-t_1)}), \tag{3.8}$$

Similarly at a certain time t_2 this solution would not be valid, hence this point we use $\tilde{x}(t_2 - \tau) = 1$, substituting this into the equation (3.8)

$$\tilde{x}(t_2 - \tau) = 1 = \tilde{x}_1\, e^{-(t_2-\tau-t_1)} + k\,(1 - e^{-(t_2-\tau-t_1)}). \tag{3.9}$$

From the equation (3.9) we solve to derive the value of t_2, which we get as

$$t_2 = \ln\left(\tilde{x}_0 \left(\frac{\tilde{x}_1 - k}{1 - k}\right) e^{2\tau}\right) \tag{3.10}$$

we substitute this value of t_2 into equation (3.8), which is then applied to obtain the value of $\tilde{x}_2$. This is given as

$$\tilde{x}_2 = (1 - k)\, e^{-\tau} + k. \tag{3.11}$$

This solution (3.11) shows an exponential increasing value to solution of equation (3.7).

We now solve for the next time interval, $t_2 < t < t_3$ where a possible change is solution occurs. If a change occurs then the equation would would also change to the first differential equation

$$\frac{d}{dt}\tilde{x}(t) = -\tilde{x}(t) \qquad \tilde{x}(t_2) = \tilde{x}_2, \tag{3.12}$$

the solution to the equation is

$$\tilde{x}(t) = \tilde{x}_2\, e^{-(t-t_2)}, \tag{3.13}$$

just like in earlier calculations this solution is valid until t_3 where we apply the condition $\tilde{x}(t_3 - \tau) = 1$ which is given as

$$\tilde{x}(t_3 - \tau) = 1 = \tilde{x}_2\, e^{-(t_3-\tau-t_2)}. \tag{3.14}$$

From this equation we solve for t_3 which we derive as

$$t_3 = \ln\left(\tilde{x}_0\, \tilde{x}_2 \left(\frac{\tilde{x}_1 - k}{1-k}\right) e^{3\tau}\right). \tag{3.15}$$

Substituting the values of t_2 and t_3 into the equation (3.13) the value of $\tilde{x}_3$ is given as

$$\tilde{x}_3 = e^{-\tau}. \tag{3.16}$$

The value of $\tilde{x}_3$ is the same as the value of $\tilde{x}_1$ and has the same conclusion of being an exponentially decaying solution. Next we repeat the same process for the value of $\tilde{x}_4$ on the interval of $t_3 < t < t_4$ and so on. We discover that alternating values are equal, from which we conclude that the system oscillate between certain points. With the values oscillating between two point we derive the amplitude of oscillation from equations (3.11) and (3.16) as

$$Amp = k\, \left(1 - e^{-\tau}\right), \tag{3.17}$$

where Amp is the amplitude of oscillation.

Likewise we now compute the period of oscillation. Let P be the period of oscillation, from t_0 to t_2 is one period and t_1 to t_3 is another period and so on. By subtracting equation (3.6) from equation (3.15) or by subtraction t_0 from equation (3.10) we get

$$P = \ln\left(\tilde{x}_0\left(\frac{\tilde{x}_1 - k}{1-k}\right)e^{2\tau}\right) - 0 \qquad or \qquad P = \ln\left(\tilde{x}_0\,\tilde{x}_2\left(\frac{\tilde{x}_1 - k}{1-k}\right)e^{3\tau}\right) - \ln(\tilde{x}_0\,e^{\tau}) \tag{3.18}$$

$$P = \ln\left(\tilde{x}_0\left(\frac{\tilde{x}_1 - k}{1-k}\right)e^{2\tau}\right) \qquad or \qquad P = \ln\left(\tilde{x}_2\left(\frac{\tilde{x}_1 - k}{1-k}\right)e^{2\tau}\right). \tag{3.19}$$

Since the solution to our equation is periodic it implies the value of $\tilde{x}_0$ is equivalent to the value of $\tilde{x}_2$ implying that both equations in equation (3.19) are the same. Substituting the values of $\tilde{x}_1$ and $\tilde{x}_2$ into the equation (3.19) gives

$$P = \ln\left((1 - k\,e^{\tau})\left(1 + \frac{k}{1-k}\,e^{\tau}\right)\right). \tag{3.20}$$

This is further simplified to the asymptotic limits of the delay as $\tau \to \infty$ or as $\tau \to 0$

$$P = 2\,\tau + \ln\left(\frac{k^2}{k-1}\right) - \mathrm{e}^{-\tau} + O\left(\mathrm{e}^{-2\,\tau}\right), \qquad \tau \to \infty \tag{3.21}$$

$$P = \frac{k^2}{k-1}\tau - \frac{k^2\,(k^2 - 3\,k + 3)}{2\,(k-1)^2}\tau^2 + O\left(\tau^3\right), \qquad \tau \to 0. \tag{3.22}$$

From equation (3.21) the period of oscillation tend to 2τ as $\tau \to \infty$ and from equation (3.22) the period of oscillation tends to $\frac{k^2}{k-1}\,\tau$ as $\tau \to 0$. It is clear that as $\tau \to \infty$ from equation (3.21) that the value of the delay is

very important to deriving the period of oscillation. The first term is $2\,\tau$ while the second term is k and from equation (3.1) we know that k is a constant. This implies that the second term of the period of oscillation as $\tau \to \infty$ is a constant. Hence equation (3.21) shows that Period $\sim 2\tau +$ a constant where the constant is a function of k. In later chapters we shall be investigating this constant using numerical approach to find its value.

3.2 Conclusion

Our analysis in this chapter shows the possibility of a single Hopf bifurcation point for the parameters k and τ. One of our key finding from the analysis carried out here is that the centre manifold analysis gives the same result with the multiple time scale, we shall continue with the method of multiple time scale. The multiple time scale method even though it produces more more computational data it is less intensive in comparison to the centre manifold analysis. We also found that for large delay the period of oscillation is just greater than twice the delay.

Chapter 4

A more generalised negative autogenous regulation.

In this chapter we progress by investigating the negative autogenous regulation studied in chapter 3 for the general case of the Hill coefficient, n. We shall be comparing some of the results derived in this chapter to that in the the previous chapter. More numerical computation would be given to give the pictorial perspective of how both model differ or how both are similar. Now returning to the general n equation (3.1) which is

$$\frac{d}{dt}\tilde{x}(t) = \frac{k}{1+\tilde{x}^n(t-\tau)} - \tilde{x}(t) \tag{4.1}$$

where the parameter remain the same as in the previous chapter. In the next section we analyse the stability of the model equation (4.1).

4.1 Stability and Hopf bifurcation

In this section we investigate the steady state of the equation (3.1) for the general value of n. Equation (3.1) can have only one steady state solution

as shown in figure 4.1 which shows only one cut across the Hill function. At steady state the rate of change is zero, let $\tilde{x}^*$ be the steady of equation (3.1), this gives a steady state solution as

$$k = \tilde{x}^*(1 + \tilde{x}^{*n}) \tag{4.2}$$

To study the distribution of eigenvalues and the steady state we linearise and analyse equation (3.1).

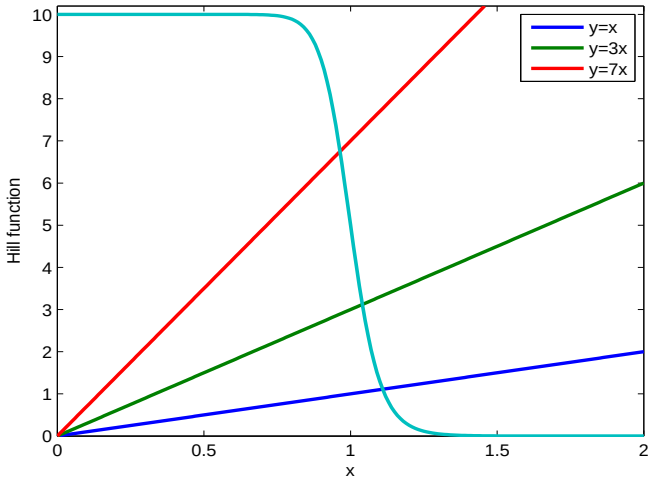


Figure 4.1: A plot showing that the decay rate cuts the Hill function once, $k = 10$ and $n = 20$.

Let $\tilde{x} = \tilde{x}^* + x$ where x is a small perturbation from the steady state. Substituting this into equation (3.1) and linearising it we get

$$\frac{d}{dt}x(t) = -x(t) + K\, x(t - \tau) \tag{4.3}$$

where

$$K = -\frac{n\, \tilde{x}^{*n} k}{\tilde{x}^*(1 + \tilde{x}^{*n})^2} \tag{4.4}$$

from which we derive its corresponding characteristic equation,

$$\Delta(\lambda) \equiv \lambda + 1 - K\, e^{-\lambda\tau} = 0. \tag{4.5}$$

If $\tau = 0$ then equation (4.5) has the root

$$\lambda = -1 + K \tag{4.6}$$

which is a similar result to the stability analysis of equation (3.1) as an ordinary differential equation studied by Alon [2]. The root of the equation is stable when $K < 1$ and unstable when $K > 1$. The inclusion of τ does not increase or decrease the number of steady state, but the solution to such equation give rise to transcendental eigenvalues which can influence the stability of the steady state. Let $\lambda = \alpha + i\varpi$ where $\alpha, \varpi \in \mathbb{R}$, from equation (4.5) we derive

$$\alpha + i\,\varpi + 1 = Ke^{(\alpha + i\,\varpi)\tau} \tag{4.7}$$

separating the real part from the imaginary part

$$\begin{aligned} \alpha + 1 &= K\, e^{-\alpha\,\tau}\, \cos(\varpi\tau) \\ \varpi &= -K\, e^{-\alpha\,\tau}\, \sin(\varpi\tau). \end{aligned} \tag{4.8}$$

If there is a change in stability of the model then the roots cross from negative to positive or vice versa, let $\alpha = 0$ be substituted into equation (4.8) and is reduced to

$$\begin{aligned} 1 &= K\, \cos(\varpi\tau), \\ \varpi &= -K\, \sin(\varpi\tau). \end{aligned} \tag{4.9}$$

From equation (4.9) we have

$$\varpi = \pm\sqrt{K^2 - 1}, \tag{4.10a}$$

$$\tau_j = \frac{\cos^{-1}(1/K) + 2\,j\pi}{\sqrt{K^2 - 1}}, \tag{4.10b}$$

where $j = 0, 1, 2, \cdots$. The primary Hopf bifurcation τ_{H} occurs at $j = 0$. For equation (4.10) to hold $K^2 > 1$ is a necessary condition. Equation (4.10a) is derived by squaring and adding equation (4.9). When equation (4.10) is satisfied a Hopf bifurcation occurs. Hence for $\tau < \tau_{\text{H}}$ there is only one real root which is a stable steady state solution for equation (4.3). At $\tau = \tau_{\text{H}}$ a Hopf bifurcation emerges and for $\tau > \tau_{\text{H}}$ there is periodic oscillation. As τ passes through τ_{H} we have a change in the steady state from the stable steady state to a periodic oscillation which corresponds to what we stated previously, that delays could result in a change of steady state not a change in the number of steady states.

These oscillation would not occur in this equation if it where a first order ordinary differential equation even if the value of $K^2 > 1$. Hence with the introduction of delays periodic oscillations are possible and the effect of the parameter K can also vary from that obtained with the first order ordinary differential equation.

In the next section we analyse the parameters k, n, and τ in equation (3.1) and the limit of K and ω as $\tau \to 0, \infty$.

4.1.1 Asymptotics of the Hopf bifurcation point

The parameters K and τ from equations (4.4) and (4.10b) respectively are investigated in this subsection and their limiting behaviour analysed. The asymptotic approximation to the Hopf bifurcation point is studied and the results are compared to the direct numerical solution. There are two possible

limit values for τ, the first possibility is that $\tau \to 0$ and the second is that $\tau \to +\infty$. In this section we investigate these two limits of τ close to the Hopf bifurcation point $|\omega - \omega_H| \ll 1$. Let $\varpi_{\text{H}}\tau = \omega_{\text{H}}$, substitute into equation (4.9) we derive the following

$$\omega_{\text{H}} = \tau\sqrt{K^2 - 1} \tag{4.11a}$$

$$\frac{\omega_{\text{H}}}{\tau} = -\tan(\omega_{\text{H}}) \tag{4.11b}$$

$$\tau^2 = \left(\tau^2 + \omega_{\text{H}}^2\right)\cos^2(\omega_{\text{H}}) \tag{4.11c}$$

$$K = \sec\left(\omega_{\text{H}}\right) \tag{4.11d}$$

From equations (4.11b) the value of the ω_{H} should take values between $\pi/2 \leq \omega_{\text{H}} \leq \pi$ giving $\omega_{\text{H}} = \pi$ as $\tau \to \infty$ and $\omega_{\text{H}} = \pi/2$ as $\tau \to 0$, thus we have the following

As $\tau \to \infty$

$$\omega_{\text{H}} \sim n_1\pi\left[1 - \frac{1}{\tau} + \frac{1}{\tau^2} + \left(\frac{(n_1\pi)^2}{3} - 1\right)\frac{1}{\tau^3} - \left(\frac{(2\,n_1\,\pi)^2}{3} - 1\right)\frac{1}{\tau^4} + O(1/\tau^5)\right] \tag{4.12}$$

where $n_1 = 2n_0 + 1$ and $n_0 = 0, 1, 2, 3\cdots$. We substitute this value of ω into equation (4.11d) to derive the corresponding value of K

$$K \sim 1 + \frac{(n_1\pi)^2}{2}\frac{1}{\tau^2} - (n_1\pi)^2\frac{1}{\tau^3} - \frac{(n_1\pi)^2}{2}\left(\frac{(n_1\pi)^2}{4} - 3\right)\frac{1}{\tau^4} + O(1/\tau^5). \tag{4.13}$$

And as $\tau \to 0$ we apply equation (4.11c) which gives

$$\omega_{\text{H}} \sim \frac{n_2\pi}{2} + \frac{2}{n_2\pi}\tau - \frac{8}{(n_2\pi)^3}\tau^2 - \frac{8}{3}\left[\frac{(n_2\pi)^2 - 24}{(n_2\pi)^5}\right]\tau^3 + \frac{128}{3}\left[\frac{(n_2\pi)^2 - 15}{(n_2\pi)^7}\right]\tau^4 + O(\tau^5), \tag{4.14}$$

deriving its corresponding value of K by substituting this value into equation (4.11d) gives

$$K \sim \frac{n_2\pi}{2\tau} + \frac{2}{n_2\pi} + \frac{{n_2}^2\pi^2 - 8}{{n_2}^3\pi^3}\tau - \frac{20\,{n_2}^2\pi^2 - 192}{3\,{n_2}^5\pi^5}\tau^2 + \frac{9\,{n_2}^4\pi^4 - 1280\,{n_2}^2\pi^2 + 17280}{15\,{n_2}^7\pi^7}\tau^3 - \frac{188\,{n_2}^2\pi^2 - 2240}{15\,{n_2}^7\pi^7}\tau^4 + O\left(\tau^5\right) \tag{4.15}$$

where $n_2 = 4n_0 + 1$ and n_0 is as described previously.

From the analytical solutions to the equations derived we have that as $\tau \to \infty$, $K \to 1$ while as $\tau \to 0$, $K \to \infty$ from the first two terms of each equation. We compare the curve of $K(\tau)$ derived from the analytical study to that of the direct numerical solution

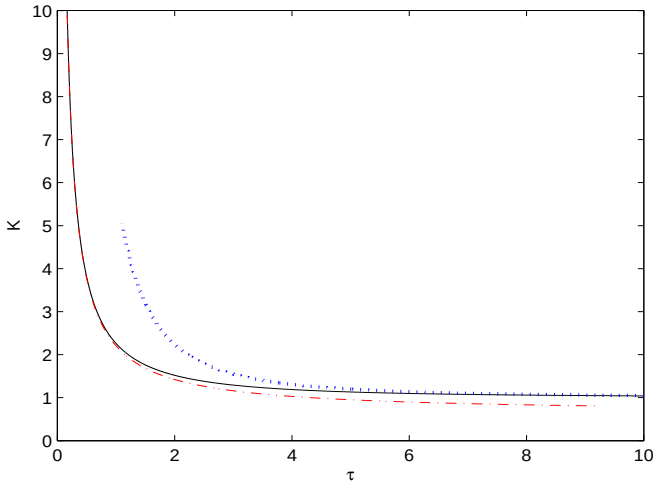


Figure 4.2: The black line is the direct numerical solution of equation (4.10b), the cyan dashed line is the asymptotic solution as $\tau \to \infty$ of K for the first two terms of equation (4.15) and the red dashed line is the asymptotic solution as $\tau \to 0$ of K for the first two terms of equation (4.13).

Figure 4.2 shows is good approximation for the comparison of the values obtained at certain intervals. As $\tau \to 0$ the result derived from equation (4.15), is a good approximation to the numerical solution which is almost indistinguishable is derived, the smaller the value of τ the better the approximation.

As $\tau \to \infty$, the analytical solution is extremely indistinguishable and is a good representation of the solution for large values of τ. From these two equations and figure 4.2 we have that τ and K are inversely proportional quantities. This accuracy is also replicated in the plot of the frequency.

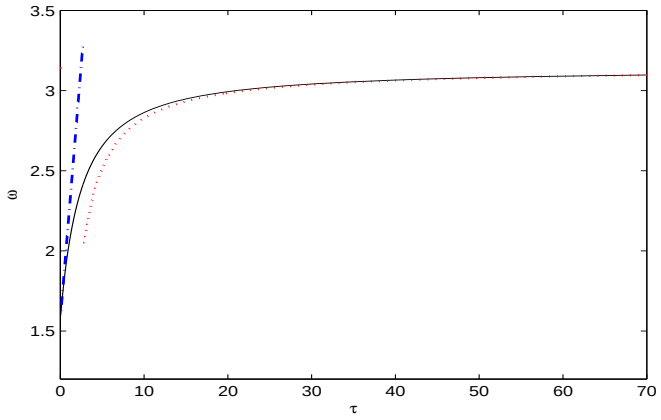


Figure 4.3: This the plot of the frequency against the delay. The black line is the direct numerical solution of equation (4.9). The red dotted line is the asymptotic solution as $\tau \to \infty$ for values of ω_{H} for the first two terms of equation (4.12) and blue dashed-dotted is the asymptotic solution as $\tau \to 0$ for values of ω_{H} for the first two terms of equation (4.14).

Similarly we plot the values of both frequencies against the value of the delayed time parameter $\omega_{\text{H}}(\tau)$. Figure 4.3 shows that the analytical solution is a very good representation of the direct numerical solution as $\tau \to \infty$ and $\tau \to 0$, with the corresponding frequencies as $\omega \to \pi$ and $\omega \to \pi/2$ respectively. We further extend the analytical solution of the two limits of τ to derive the period of oscillation. Let P be the period of oscillation, from equation (4.12) and (4.14) we derive the period of oscillation for the system

$$P = 2 + \frac{2}{\tau} - \frac{2}{\tau^3} - \frac{2}{\tau^4} + O\left(\frac{1}{\tau^5}\right), \tag{4.16}$$

$$P = 4 - \frac{16}{\pi^2}\tau + \frac{64}{\pi^4}\tau^2 - \frac{256}{\pi^6}\tau^3 + \frac{1024}{\pi^8}\tau^4 + O\left(\tau^5\right). \tag{4.17}$$

Equation (4.16) gives the period of the differential delay equation as $P \to 2$ as $\tau \to \infty$ while equation (4.17) gives the period of oscillation as $\tau \to 0$ as $P \to 4$. Figure 4.4 is a comparison of the direct numerics with both asymptotic limit of τ. As $\tau \to \infty$ we see the red dotted line becomes indistinguishable from the direct numerical plot in black but as $\tau \to 0$ it is the blue dashed-dotted line that is a good approximation to the direct numerics. Hence the period of oscillation ranges between 2 and 4.

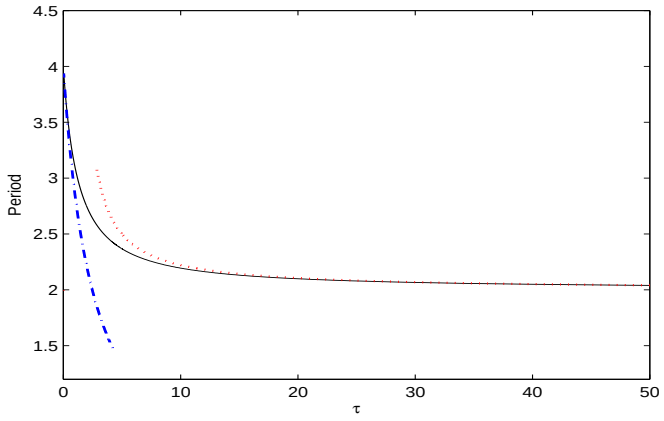


Figure 4.4: This the plot of the period against the delay. The black line is the direct numerical solution of equation (4.10). The red dotted line is the asymptotic solution as $\tau \to \infty$ for the first two terms of equation (4.16) and blue dashed-dotted is the asymptotic solution as $\tau \to 0$ for the first two terms of equation (4.17).

Recall that the frequency in section 4.1.1 was rescaled in the statement just before we obtained equation (4.11). If this frequency is rescaled back to the original one by substituting $\omega = \varpi\tau$ then the value of period for both limits

of the delay would be

$$P = 2\tau + 2 - \mathcal{O}\left(\tau^{-2}\right), \tag{4.18a}$$

$$P = 4\tau - \frac{16\,\tau^2}{\pi^2} + \mathcal{O}\left(\tau^3\right), \tag{4.18b}$$

with equation (4.18a) as the period for $\tau \to \infty$ and equation (4.18b) as the period for $\tau \to 0$. Comparing the result derived for the general n with our result from section 3.1 we have that the period as $\tau \to \infty$ tends to the same value of 2τ but as $\tau \to 0$ we would apply a direct numeric simulation to compare with equation (4.18b).

From the analytic results derived we have seen that as we approach the limit as $\tau \to 0,\ \infty$ the period of oscillation plotted in figure 4.4 shows the results derived are indistinguishable approximation of the direct numerical solution of the equation under study. Likewise the frequency of periodic oscillation figure 4.3 are accurate as we tend to the limit of the delay parameter.

In the next section we will look at simulated computation to illustrate the result derived from sections 1 and 2, comparing all our analysis and the direct numerics.

4.1.2 Numerics

In this section we illustrate the analytical results derived for various values and compare them to direct numerical solution. One of the first results derived was that of oscillations after a Hopf bifurcation point and that this applied to both parameters k and τ.

When $k = 0.8$ and $n = 5$, from equation (4.4) $K^2 = 0.464$ which is less than one and hence there is no periodic oscillation an shown in figure 4.5 by the black line. But when the value of $K^2 > 1$ we get periodic oscillation and the

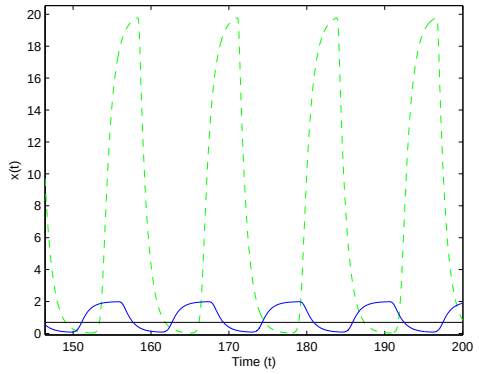


Figure 4.5: For a fixed value of $n = 5$ and $\tau = 5$, the comparison for different values of k, ($k = 0.8$ black line, $k = 2$ blue line, $k = 20$ green dashed lines).

larger the value of k the greater the amplitude. From this it implies that as k increases the amplitude of oscillation also increases for values of $K^2 < 1$. Now we carry out similar plot using the delay as the independent parameter,

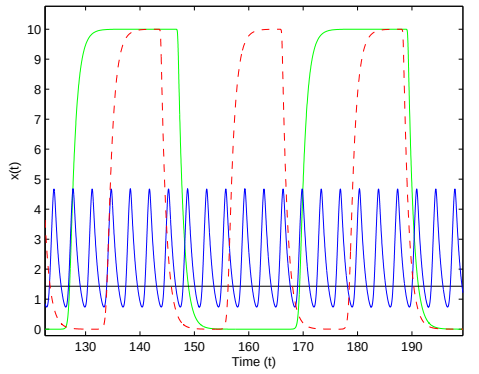


Figure 4.6: For $n = 5$ and $k = 10$, the comparison for different values of τ ($\tau = 0.2$ black line, $\tau = 1$ blue line, $\tau = 10$ red dashed line and $\tau = 20$ green line).

From figure 4.6 we once again have correspondence with the analytical result derived, for $\tau < \tau_{\text{H}}$ we have no periodic solution but for $\tau > \tau_{\text{H}}$ we get periodic oscillatory solution. From the numerics we can see the nature of the periodic

oscillation, in figure 4.5 we have sinusoidal oscillations irrespective of how large the value of k is but in figure 4.6 as $\tau \to \infty$ the oscillation take the form of a square wave and the growth of the amplitude is terminated after a certain value of τ. A bifurcation plot of these two parameters would give more insight to the equation in focus. With this we would also locate the Hopf bifurcation point and compare our analytical result with the direct numerics.

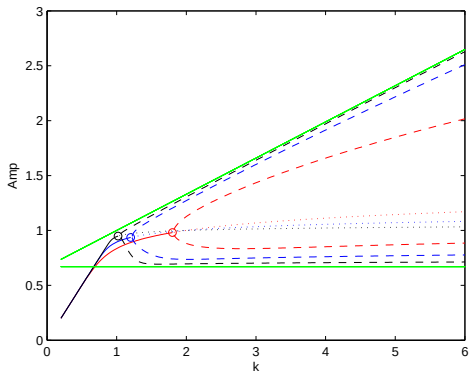


Figure 4.7: A bifurcation diagram of the amplitude of oscillation plotted against the parameter k for $\tau = 0.4$ and $n = 10$ red, $n = 20$ blue, $n = 50$ black and the green lines are the results from equations (3.11) and (3.16) of the piecewise linear model.

In figure 4.7 we see that as $k \to \infty$ the amplitude also tends to infinity but in figure 4.8 as $\tau \to \infty$ the amplitude of the oscillation initially increases until it gets to the value of the parameter k after which there is no further increases in the amplitude. Another very important detail provided by the bifurcation plots is the role of the parameter n. In figures 4.7 and 4.8 as $n \to \infty$ the amplitude of the oscillation of the continuous function tends to the amplitude of the discontinuous function studied in the first section. This accuracy between the discontinuous function and the continuous function gets better as $n \to \infty$, even close to the Hopf bifurcation point there is an increases

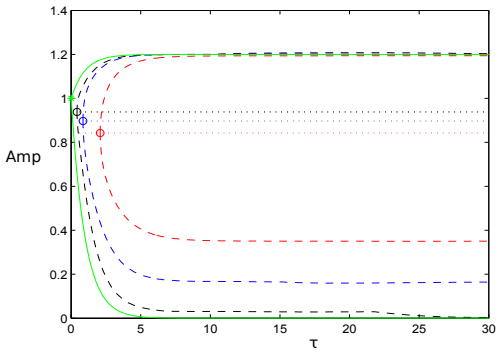


Figure 4.8: A bifurcation diagram of the amplitude of oscillation plotted against the parameter τ for $k = 1.2$ and $n = 10$ red, $n = 20$ blue, $n = 50$ black and the green lines are the results from equations (3.11) and (3.16) of the piecewise linear model.

in accuracy as $n \to \infty$. Hence as $n \to \infty$ the analytical solution of the discontinuous function is a good approximation of direct numerics.

At this point we also compare the period of oscillation of the discontinuous function and the analytical solution for the general n as $\tau \to \infty$.

From figures 4.9a and 4.9b we can see a good approximation. The accuracy is indistinguishable in figure 4.9a and only slightly differentiable in figure 4.9b. As $\tau \to \infty$ there is no distinction but for values of $\tau \to 0$ slight differences are observed.

With these numerical simulation we can see that the analytical result derived are very good approximations to the direct numeric. Most of the results derived are for the linear part of the equation in the next section we would be considering the nonlinear terms and analyse the behaviour of the periodic solution close to the Hopf bifurcation point.

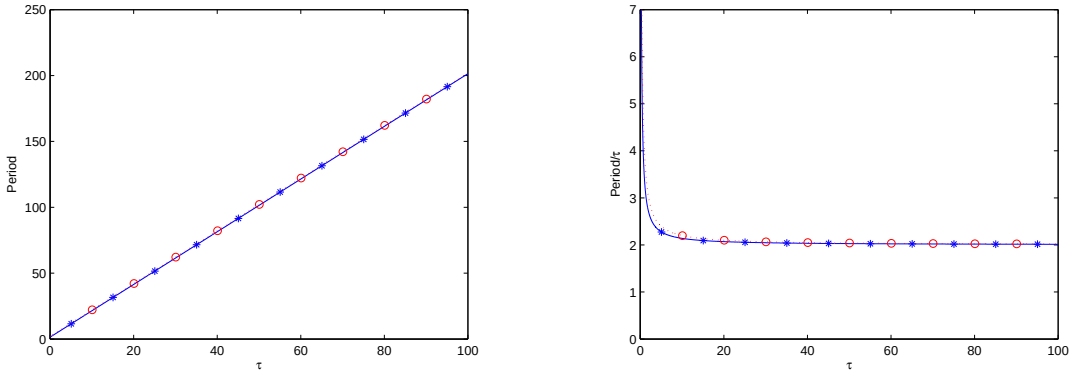


Figure 4.9: (a) Plot comparing the period of oscillation of the piecewise linear model, equation (3.21) in chapter 3 and the general model equation (4.18a) in chapter 4 as $\tau \to \infty$ for a fixed value of $k = 1.8$. (b) Plot of period/τ plotted against τ for the same values as (a). The red (-o-) line is the piecewise linear model period while the blue solid asterisk line is the period of the general model.

4.2 Weakly nonlinear analysis

In the previous section we showed that for values of $\tau < \tau_{\text{H}}$ the equation decays to the stable steady state and for $\tau > \tau_{\text{H}}$ we have limit cycles, with τ_{H} being the bifurcation point of equation (3.1). This analysis was based on the linear part of the linearised equation. In this section we will analyse the direction of the Hopf bifurcation as we introduce the nonlinear terms in a systematic way to the linear equation studied in section 4.1. The inclusion of nonlinear terms to linear dynamical systems could give an unpredicted or chaotic solution to a well known linear system hence the need for the systematic inclusion of the nonlinear term. The study of this nonlinear equation is called weakly nonlinear analysis and we apply the method of multiple timescale to solve this nonlinear system. We begin by rescaling equation (3.1) to take the form of a weakly nonlinear oscillations. Let $0 < \epsilon \ll 1$ and $x(t) \to \epsilon x(t)$, we substitute into

equation (3.1) to give

$$\frac{d}{dt}x(t) + \tau x(t) - \tau\, K\, x(t-1) \; + \epsilon\, \tau\, L\, x^2(t-1) + \epsilon^2\, \tau\, H\, x^3(t-1) = 0, \quad (4.19)$$

where

$$\begin{aligned} K &= \frac{k\, n\tilde{x}^{*n}}{\tilde{x}^{*n}\,(1+\tilde{x}^{*n})^2}, \\ L &= \frac{k\, n\tilde{x}^{*n}(n\tilde{x}^{*n} - n + \tilde{x}^{*n} + 1)}{\left(\tilde{x}^{*n}+1\right)^3\; \tilde{x}^{*2n}}, \\ H &= \frac{k\, n\tilde{x}^{*n}}{6\,(\tilde{x}^{*n}+1)^4\,\tilde{x}^{*3n}}\,(6n\tilde{x}^{*n}(1+\tilde{x}^{*n})(n-1) \\ &\quad -(n-1)(n-2)(1+\tilde{x}^{*n})^2 - 6\,(n\tilde{x}^{*n})^2\big)\,. \end{aligned} \quad (4.20)$$

At $\epsilon = 0$, equation (4.19) reduces to a linear equation, the linear part is a rescaled equation to that studied in section (4.1). We also want analyse what happens close to the Hopf bifurcation and derive the direction of the Hopf bifurcation. Taking τ as the bifurcating parameter, we add a small shift $0 < \delta \ll 1$ to τ_{H}, hence our new $\tau = \tau_{\text{H}} + \delta$ i.e. $\delta = \tau - \tau_{\text{H}}$. We rescale $\delta = \epsilon^2\Delta$ and our new weakly nonlinear equation is

$$\begin{aligned} \frac{d}{dt}x(t) + (\tau_{\text{H}} + \epsilon^2\Delta)x(t) - (\tau_{\text{H}} + \epsilon^2\Delta)\, K\, x(t-1) \; + \epsilon\,(\tau_{\text{H}} + \epsilon^2\Delta)\, L\, x^2(t-1) \\ + \epsilon^2\,(\tau_{\text{H}} + \epsilon^2\Delta)\, H\, x^3(t-1) = 0. \end{aligned} \quad (4.21)$$

where τ_{H} is a positive constant as described in the previous sections. We have ϵ as the step size from the Hopf bifurcation point and Δ indicates the direction and number of steps we decide to move from the bifurcation point. For $\Delta = 0$ we will be on the Hopf bifurcation point studying just the nonlinear term.

4.2.1 Multiple time scale (MTS)

The method of multiple time scales is effective in studying oscillatory systems, it also reveals the stability of the periodic solution being studied. We adopt the method of multiple time scales to analyse equation (4.21). In applying the method of multiple scales we assume that $x(t)$ is a function of two times, $x(t,T)$ such that t is the fast time scale and T is the slow time scale. Hence let the asymptotic expansion of $x(t)$ be

$$x(t) \approx x_0(t,T) + \epsilon x_1(t,T) + \epsilon^2 x_2(t,T) + O(\epsilon^3), \qquad T = \epsilon^2 t. \tag{4.22}$$

$$\frac{d}{dt} \approx \frac{\partial}{\partial t} + \epsilon^2 \frac{\partial}{\partial T}, \tag{4.23}$$

$$\begin{aligned} x(t-\tau) &\approx x_0(t-\tau, T-\epsilon^2\tau) + \epsilon x_1(t-\tau, T-\epsilon^2\tau) + \epsilon^2 x_2(t-\tau, T-\epsilon^2\tau) + O(\epsilon^3) \\ &= x_0\left(t-\tau, T\right) + x_1\left(t-\tau, T\right)\epsilon \\ &\quad + \left(x_2\left(t-\tau, T\right) - \frac{\partial}{\partial T} x_0\left(t-\tau, T\right)\tau\right)\epsilon^2 + O\left(\epsilon^3\right)). \end{aligned} \tag{4.24}$$

Substituting equations (4.22)-(4.24) into equation (4.19) gives a perturbation series. Collecting terms of equal powers of ϵ we obtain the following

at ϵ^0

$$\frac{\partial}{\partial t} x_0\left(t,T\right) + \tau_{\text{H}}\, x_0\left(t,T\right) + \tau_{\text{H}}\, K x_0\left(t-1,T\right) = 0, \tag{4.25}$$

at ϵ^1

$$\frac{\partial}{\partial t} x_1\left(t,T\right) + \tau_{\text{H}}\, x_1\left(t,T\right) + \tau_{\text{H}}\, K x_1\left(t-1,T\right) = \tau_{\text{H}}\, L\left(x_0\left(t-1,T\right)\right)^2, \tag{4.26}$$

at ϵ^2

$$\frac{\partial}{\partial t}x_2\left(t,T\right)+\tau_{\text{H}}\,x_2\left(t,T\right)+\tau_{\text{H}}\,K x_2\left(t-1,T\right)=-\frac{\partial}{\partial T}x_0\left(t,T\right)-\Delta\,x_0\left(t,T\right)$$
$$+\,\tau_{\text{H}}\,K\,\frac{\partial}{\partial T}x_0\left(t-1,T\right)-\Delta\,K x_0\left(t-1,T\right)+2\,\tau_{\text{H}}\,L x_0\left(t-1,T\right)x_1\left(t-1,T\right)$$
$$+\,\tau_{\text{H}}\,H\left(x_0\left(t-1,T\right)\right)^3. \tag{4.27}$$

We solve equation (4.25) - (4.27), substituting the previous into the next while eliminating the secular terms. Equation (4.25) has no nonlinearity and is similar to the linear equation studied in previous sections, let the solution to equation (4.25) be

$$x_0\left(t,T\right)=A\left(T\right)\cos\left(\omega\,t+\Phi\left(T\right)\right) \tag{4.28}$$

where $A(T)$ is the amplitude and $\Phi(T)$ is the phase. There are no secular terms present in the solution to equation (4.28). Having obtained the fast timescale dependence of $x_0(t,T)$ we substitute this into equation (4.26) and solving for $x_1(t,T)$ at $\mathrm{O}(\epsilon)$, this gives

$$x_1\left(t,T\right)=M(T)\,\cos(2\,\omega t+2\,\Phi(T))\;+\;N(T)\,\sin(2\,\omega t\;+2\,\Phi(T))\;+B(T), \tag{4.29}$$

where

$$\begin{aligned}M&=\frac{\left(A\left(T\right)\right)^2L\left(K^2+2\,K-2\right)}{2\,K\left(5\,K^2+K-4\right)},\\ N&=-\frac{\left(K-1\right)\sqrt{K^2-1}\left(A\left(T\right)\right)^2L}{K\left(5\,K^2+K-4\right)},\\ B&=\frac{\left(A\left(T\right)\right)^2L}{2(K+1)}.\end{aligned} \tag{4.30}$$

The solution to equation (4.26) has no secular terms as well. Since there are no secular terms thus far, it implies that the solutions $x_0(t,T)$ and $x_1(t,T)$

remain periodic. But our major aim in applying the method of multiple time scale is to locate where secular terms occur and to eliminate them. The two solutions obtained for $x_0(t,T)$ and $x_1(t,T)$ are substituted into equation (4.27) at $\mathrm{O}(\epsilon^2)$. The right hand side (RHS) of equation (4.27) then gives

$$\begin{aligned} &J_1(T)\,\cos(\omega t+\Phi(T))\;+\;J_2(T)\,\sin(\omega t\;+\Phi(T)) \\ &+M_2(T)\,\cos(3\,\omega t+3\,\Phi(T))\;+\;N_2(T)\,\sin(3\,\omega t\;+3\,\Phi(T))\,, \end{aligned} \tag{4.31}$$

where

$$\begin{aligned} J_1 =& -\left(\tau_{\mathrm{H}}+1\right)\frac{\mathrm{d}}{\mathrm{d}T}A\left(T\right)+\tau_{\mathrm{H}}\sqrt{K^2-1}A\left(T\right)\frac{\mathrm{d}}{\mathrm{d}T}\Phi\left(T\right)+\frac{3H\tau_H\,KA\left(T\right)^3}{4} \\ &+\frac{\left(2\,K^3-13\,K^2+4\,K+4\,\right)A\left(T\right)^3L^2\tau_{\mathrm{H}}}{2\,K^2\left(K+1\right)\left(5\,K-4\right)}, \\ J_2 =&\sqrt{K^2-1}\frac{\mathrm{d}}{\mathrm{d}T}A\left(T\right)-\sqrt{K^2-1}\left(\tau_{\mathrm{H}}+1\right)A\left(T\right)\frac{\mathrm{d}}{\mathrm{d}T}\Phi\left(T\right) \\ &\left(\Delta\;-\;\frac{3\,H\tau_{\mathrm{H}}\,KA\left(T\right)^2}{4}+\frac{\left(-11\,K^2+4K+4\right)A\left(T\right)^2L^2\tau_{\mathrm{H}}}{2\,K^2\left(K+1\right)\left(5\,K-4\right)}\right), \\ M_2 =&-\frac{\left(2\,K^5-5\,K^4-16\,K^3+20\,K^2+16\,K-16\right)\left(A\left(T\right)\right)^3L^2\tau_{\mathrm{H}}}{2\,K^4\left(K+1\right)\left(5\,K-4\right)} \\ &+\frac{\left(15\,K^4+3\,K^5-32\,K^2-4\,K+16\,K\right)H\tau_{\mathrm{H}}A\left(T\right)^3}{4K^3\left(K+1\right)\left(5\,K-4\right)}, \\ N_2 =&-\frac{\left(A\left(T\right)\right)^3\tau_{\mathrm{H}}\sqrt{K^2-1}}{4K^4\left(K+1\right)\left(5\,K-4\right)}\;\left(5\,HK^5+(2\,L^2+H)K^4+8\,K^3(2L^2-3\,H)\right. \\ &\left.-4\,K^2\left(6\,L^2+\;H\right)-16\,K(2\,L^2-\;H)+32\,L^2\right). \end{aligned} \tag{4.32}$$

Equation (4.31) contains secular terms which could change the periodic solution of the system, hence we equate $J_1=0$ and $J_2=0$. The following two equations arise in the process which are both functions of the slow time,

$$\frac{\mathrm{d}}{\mathrm{d}T}A = \kappa\, A\, \left(A^2 - \varrho\, \Delta\right), \tag{4.33a}$$

$$\frac{\mathrm{d}}{\mathrm{d}T}\Phi = \alpha\, A^2 + \beta\, \Delta, \tag{4.33b}$$

the first of which is the Ginzburg-Landau equation. In equation (4.33) we have $\kappa = P_1/P_0$, $\varrho = P_2/P_1$, $\alpha = q_1/p_0$ and $\beta = q_2/P_0$,

$$P_0 = 4\, K^2\, (K+1)\, (5\, K-4)\left(K^2 {\tau_{\text{H}}}^2 + 2\, \tau_{\text{H}} + 1\right), \tag{4.34}$$

$$\begin{aligned} P_1 = {} & \left(15\, HK^5 + 22\, K^4 L^2 + 3\, HK^4 - 12\, K^3 L^2 - 12\, HK^3 - 4\, K^2 L^2\right) \tau_{\text{H}} \\ & - \left(4\, K^3 L^2 + 15\, HK^3 + 26\, K^2 L^2 + 3\, HK^2 - 8\, KL^2 - 12\, KH - 8\, L^2\right) \end{aligned}$$

$$P_2 = 4\, K^2 \left(5\, K^4 + K^3 - 9\, K^2 - K + 4\right) \Delta \tag{4.35}$$

$$\begin{aligned} q_1 = {} & -\tau_{\text{H}} \sqrt{(K^2-1)}\, \left(4\, K^3 L^2 \tau_{\text{H}} - 4\, K^2 L^2 \tau_{\text{H}} + 15\, HK^3 + 22\, K^2 L^2\right. \\ & \left. + 3\, HK^2 - 8\, KL^2 - 12\, KH - 8\, L^2\right), \end{aligned} \tag{4.36}$$

$$q_2 = 4\, K^2\, (K+1)\, (5\, K-4)\, (\tau+1)\, \sqrt{(K^2-1)}\Delta. \tag{4.37}$$

Equation (4.33a) represents the rate of change in amplitude while equation (4.33b) represents the rate of change in phase. For the linear case, the solution is periodic but with the introduction of the nonlinear terms secularity is obtained in the solution. The change in the amplitude is investigated from the Ginzburg-Landau equation derived in equation (4.33a). We now analyse the effect of the nonlinear term on the amplitude as we vary the delay close to the Hopf bifurcation point. When the rate of change of the amplitude is zero we should have reached a steady state for the amplitude and this steady state is a limit cycle. From equation (4.33a) this is given as

$$A^2 = \varrho\Delta, \tag{4.38}$$

where ϱ is as described above. We now solve for $\Phi(T)$ at the point where the rate of change of the amplitude $A(T)$ is zero by substituting equation (4.38) into equation (4.33b), this gives

$$\Phi(T) = (\alpha\varrho + \beta)\Delta\, T + \Phi_0, \tag{4.39}$$

where Φ_0 is the constant of integration. If the rate of change of the amplitude is not zero then the solution to equation (4.33a) is

$$A\,(T) = \frac{\sqrt{\Delta\,\varrho}}{\sqrt{\Delta\, A_0\,\varrho\,\mathrm{e}^{-2\,\Delta\,\varrho\,T} + 1}}, \tag{4.40}$$

where A_0 is the initial value of the amplitude at $t = 0$. From equation (4.22) we know that $T = \epsilon^2\, t$. Substituting $T = \epsilon^2\, t$ into equation (4.40) to analyse what happens to the amplitude of the equation as $t \to \pm\infty$. From equation (4.40), as $t \to -\infty$, the amplitude, $A(T) \to 0$ and as $t \to \infty$ the amplitude $A(T)$ tends to the steady amplitude derived in equation (4.38) for any arbitrary initial value of A_0. This implies that the limit cycle would have a maximum amplitude of $\sqrt{\varrho\,\Delta}$. To complete the solution to equation (4.19), we need to find the value of $\Phi(T)$ which describes the possible shift in the phase of the oscillating solution. We substitute the value of the amplitude into equation (4.33b) and solve for the phase constant, $\Phi(T)$

$$\Phi(T) = \frac{\ln\left(\Delta\, C\varrho\,\mathrm{e}^{-2\,\Delta\,\kappa\,\varrho\,T} + 1\right)\alpha}{2\,\kappa} + (\alpha\,\varrho + \beta)\,\Delta\,T + \Phi_0 \tag{4.41}$$

where Φ_0 is the integrating constant. With these two parameters, the amplitude $A(T)$ and phase $\Phi(T)$, the value of $x(t)$ in equation (4.22) to order $O(\epsilon^0)$ is

$$x(t) = \frac{\sqrt{\Delta\,\varrho}}{\sqrt{\Delta\,A_0\,\varrho\,\mathrm{e}^{-2\,\Delta\,\varrho\,\epsilon^2\,t}+1}}\,\cos(\omega t + \Phi(\epsilon^2\,t)). \tag{4.42}$$

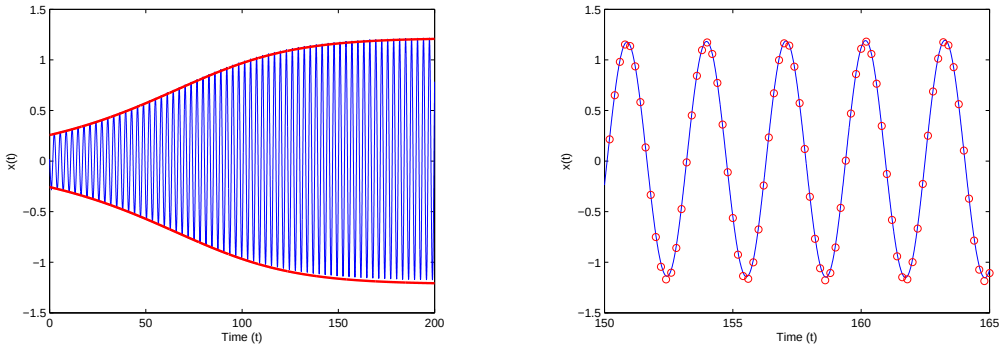
From equation (4.42), a periodic solution occurs if and only if $A_0\,\Delta\,\varrho\exp(-2\,\Delta\,\varrho\,T) = 0$. From equation (4.33a), if $\Delta > 0$ the amplitude of the oscillation has three real roots and $A(T) = 0$ would be an unstable steady state while the other two roots of would represent the amplitude of limit cycle as in equation (4.38). For $\Delta < 0$ there is only one real root and that is $A(T) = 0$ which is a stable steady state. With this we have that the Hopf bifurcation is supercritical.

4.2.2 Numerical simulation of the multiple timescale analysis

From the analytical solution derived from equations (4.33) and (4.42) we compare this with direct numerical simulation.

Figure 4.10a shows the amplitude of oscillation from the analysis carried out from equation (4.33a) in red solid lines while the blue lines represent the direct numerical solution, we have an initial growth in amplitude to the limit of periodic steady state amplitude for a positive Δ. We see that the multiple time scale analysis is a good representation of the amplitude for the period oscillation. The complete analytic solution from equation (4.42) is shown in the figure 4.10b. Figure 4.10b shows both analytical and numerical solutions. The analytical result in red is not a perfect approximation to the direct numerics in blue. To get a higher accuracy of the amplitude and phase shift of the periodic oscillation it would be required finding higher order terms of the multiple timescale solution or having more slow time.

The change in phase $\Phi(T)$ is also plotted to conclude the analytical simulation to our calculation in figure 4.11.



(a) (b)

Figure 4.10: A diagram comparing MTS and direct numerics for values of $k = 1.8$, $n = 5$, $\epsilon = 0.1$, $\Delta = 3.4$ and $\tau_H = 0.9671$ the blue line is the direct numerics with initial condition $x(0) = 0.2$. (a)The red line is the amplitude derived from the MTS of equation (4.33a) with initial condition $A(0) = 0.27$. (b) The red circle is the complete solution from the MTS from equation (4.33) with initial conditions $A(0) = 0.27$ and $\Phi(0) = 8$.

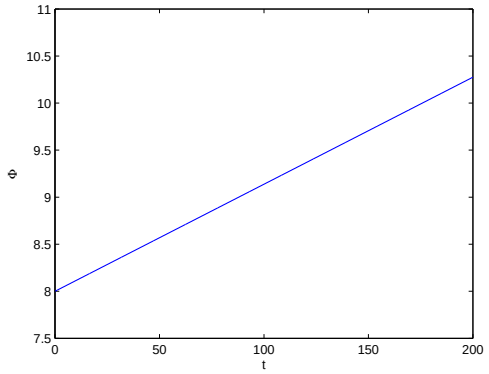


Figure 4.11: Plot of phase shift $\Phi(T)$ for values of $k = 1.8$, $n = 5$, $\epsilon = 0.1$, $\Delta = 3.4$ and $\tau_H = 0.9671$ with initial condition $\Phi(0) = 8$ from equation (4.41).

4.3 Normal form and centre-manifold method

In this section we apply a different approach to analyse the stability and direction of the Hopf bifurcation. In section 4.2 the method of multiple time scale

was used to study the property in the neighborhood of the Hopf bifurcation point but in this section we apply the normal form and center manifold theorem [61, 62, 63]. To do this, we perturb the Hopf bifurcation point such that $\tau = \tau_H + \gamma$ where $\gamma \in \mathbb{R}$ just like in section 4.2. With this equation (4.19) takes the form of equation

$$\frac{d}{dt}x(t)+(\tau_{\text{H}}+\gamma)\,x(t)-(\tau_{\text{H}}+\gamma)\,K\,x(t-1)+(\tau_{\text{H}}+\gamma)\,L\,x^2(t-1)+(\tau_{\text{H}}+\gamma)\,H\,x^3(t-1)=0, \tag{4.43}$$

which implies that if $\gamma = 0$ the solution to equation (4.43) would return to the Hopf bifurcation point. Let the phase space be $C = C([-1, 0], \mathbb{R})$ which is the space of continuous mapping from $[-1, 0]$ into $\mathbb{R}$. With the center manifold method we start by representing equation (4.43) as an operator differential equation. To do this let a linear operator L_γ be given as

$$L_\gamma(\varphi) = -(\tau_{\text{H}} + \gamma)\,\varphi(0) + (\tau_{\text{H}} + \gamma)\,K\,\varphi(-1), \tag{4.44}$$

where $\varphi \in C$ and let the function F be given as

$$F(\gamma, \varphi) = (\tau_{\text{H}} + \gamma)\,\left(L\,\varphi^2(-1) + H\,\varphi^3(-1) + O(\varphi^4)\right). \tag{4.45}$$

We also let

$$\eta(\theta, \gamma) = -(\tau_{\text{H}} + \gamma)\delta(\theta) + (\tau_{\text{H}} + \gamma)\,K\delta(\theta + 1), \tag{4.46}$$

where δ represents the Dirac's δ function. Now from the Riesz representation theorem, where $\eta(\theta, \gamma)$ with $\theta \in [-1, 0]$ is a bounded variation function such that

$$L_\gamma\varphi = \int_{-1}^{0} d\eta(\theta, \gamma)\varphi(\theta) \quad \forall\,\varphi \in C. \tag{4.47}$$

Now for $\varphi(\theta) \in C$ we define

$$A(\gamma)\varphi = \begin{cases} \frac{d\varphi(\theta)}{d\theta}, & -1 \leq \theta < 0, \\ \int_{-1}^{0} d\eta(t,\gamma)\varphi(t) & \theta = 0, \end{cases}$$
$$R(\gamma)\varphi = \begin{cases} 0, & -1 \leq \theta < 0, \\ F(\gamma,\varphi) & \theta = 0. \end{cases} \tag{4.48}$$

Thus we can represent equation (4.19) as

$$\frac{dx_t}{dt} = A(\gamma)x_t + R(\gamma)x_t \tag{4.49}$$

where $x_t = x(t+\theta)$ and let the adjoint operator A^* of A be defined as follows

$$A^*(\gamma)\psi(s) = \begin{cases} -\frac{d\psi(s)}{ds}, & 0 < s \leq 1, \\ \int_{-1}^{0} d\eta(t,0)\psi(-t) & s = 0, \end{cases} \tag{4.50}$$

where $\psi \in C^1 = C^1([0,1],\mathbb{R})$. We then define a bilinear inner product by

$$\langle \psi, \varphi \rangle = \bar{\psi}(0)\varphi(0) - \int_{-1}^{0}\int_{0}^{\theta} \bar{\psi}(\zeta-\theta)\, d\eta(\theta,0)\varphi(\zeta)d\zeta, \tag{4.51}$$

where $\bar{\psi}$ is the complex conjugate of ψ. In section (3.3) we derived the eigenvalues $\pm\, i\omega$ for $A(0)$ and $A^*(0)$. Now let $q(\theta)$ be the eigenvector of $A(0)$ and let the eigenvector of $A^*(0)$ be $q^*(s)$. Thus we have $A(0)q(\theta) = i\omega\, q(\theta)$ and $A^*(0)q^*(\theta) = -i\omega\, q^*(\theta)$. For $\langle q^*, q\rangle = 1$ and $\langle q^*, \bar{q}\rangle = 0$ we apply the normalization condition. Direct computation gives the following

$$\begin{aligned} q(\theta) &= e^{i\,\omega\theta} \quad \theta \in [-1,0], \\ q(s) &= B\, e^{i\,\omega\, s} \quad s \in [0,s], \end{aligned} \tag{4.52}$$

where B is a constant. To obtain the value of this constant we apply the normalisation condition $\langle q, p\rangle = 1$ in equation (4.51) which gives

$$\bar{B} = \frac{1}{1 + \tau_H K\, e^{-i\omega\tau_H}}. \tag{4.53}$$

From equation (4.49), at the point where $\gamma = 0$ we have $x_t(0) = x_t$, the center manifold C_0 given without any perturbation, that is $\gamma = 0$. Let $z = \langle q^*, x_t\rangle$ and

$$W(t,\theta) = x_t(\theta) - 2\,\Re\{z\, q(\theta)\}, \tag{4.54}$$

where $\Re$ is the real part of the function. On the center manifold C_0, $W(t,\theta) = W(z,\bar{z},\theta)$ such that

$$W(z,\bar{z},\theta) = W_{20}(\theta)\frac{z^2}{2} + W_{11}(\theta)\, z\,\bar{z} + W_{02}(\theta)\frac{\bar{z}^2}{2} + \cdots, \tag{4.55}$$

where z,$\bar{z}$ are local coordinates for C_0 in the direction of q^* and $\bar{q}^*$ respectively and $\theta \in [-1, 0]$. For any x_t on the center manifold we consider only real solutions of equation (4.49), we have

$$\begin{aligned}
\frac{dz}{dt} &= \langle q^*, \frac{dx_t}{dt}\rangle = \langle q^*, A(\gamma)\, x_t + R(\gamma)\, x_t\rangle \\
&= i\omega\tau_H\, z + q^*(\theta)F(W + 2\,\Re\{z, q(\theta)\}) \\
&= i\omega\tau_H\, z + \bar{q}^*(0)F(W(z,\bar{z},0) + 2\,\Re\{z, q(0)\}) \\
&= i\omega\tau_H\, z + \bar{q}^*(0)F_0(z,\bar{z}) \\
&= i\omega\tau_H\, z + g(z,\bar{z})
\end{aligned} \tag{4.56}$$

We have $F_0(z,\bar{z}) = F(0, x_t)$ and from equation (4.52) and (4.56) $g(z,\bar{z}) = \bar{B}F_0(z,\bar{z})$.

$$F_0(z,\bar{z}) = F_{z^2}\frac{z^2}{2} + F_{z\bar{z}}\, z\bar{z} + F_{\bar{z}^2}\frac{\bar{z}^2}{2} + F_{z^2\bar{z}}\frac{z^2\bar{z}}{2} + \cdots \tag{4.57}$$

From equations (4.49), (4.54) and (4.56) we have

$$\begin{aligned}\frac{dW}{dt} &= \frac{dx_t}{dt} - \frac{dz}{dt}q - \frac{d\bar{z}}{dt}\bar{q} \\ &= \begin{cases} AW - 2\Re\{\bar{B}F_0\, q(\theta)\} & \theta \in [-1, 0) \\ AW - 2\Re\{\bar{B}F_0\, q(\theta)\} + F_0 & \theta = 0 \end{cases} \\ &= AW + H(z, \bar{z}, \theta)\end{aligned} \tag{4.58}$$

where $F_0 = F_0(z, \bar{z})$ and we define

$$H(z, \bar{z}, \theta) = H_{20}\frac{z^2}{2} + H_{11}\, z\bar{z} + H_{02}\frac{\bar{z}^2}{2} + \cdots. \tag{4.59}$$

From the above equations we now derive

$$\begin{aligned}H(z, \bar{z}, \theta) &= -2\Re\{\bar{B}F_0\, q(\theta)\} \\ &= -q^*(0)F_0\, q(\theta) - q^*(0)\bar{F}_0\bar{q}(\theta) \\ &= \left(g_{20}\frac{z^2}{2} + g_{11}\, z\bar{z} + g_{02}\frac{\bar{z}^2}{2} + g_{21}\frac{z^2\bar{z}}{2} + \cdots\right) q(\theta) \\ &\quad - \left(g_{20}\frac{z^2}{2} + g_{11}\, z\bar{z} + g_{02}\frac{\bar{z}^2}{2} + g_{21}\frac{z^2\bar{z}}{2} + \cdots\right) \bar{q}(\theta).\end{aligned} \tag{4.60}$$

If we compare the coefficients from the expanded form of equation (4.58) gives

$$\begin{aligned}\frac{d}{dt}W_{20}(\theta) &= 2i\omega\, W_{20}(\theta) - H_{20}(\theta), \\ AW_{11}(\theta) &= -H_{11}(\theta).\end{aligned} \tag{4.61}$$

With the fact that

$$x_t(\theta) = W(z, \bar{z}, \theta) + z\, q(\theta) + \bar{z}\bar{q}(\theta), \tag{4.62}$$

together with equation (4.54) we have

$$\begin{aligned}g(z, \bar{z}) &= -L\bar{B}\tau_H e^{-2i\omega\tau_H} z^2 - L\bar{B}z\bar{z} - L\bar{B}\tau_H e^{-2i\omega\tau_H}\bar{z}^2 \\ &\quad - L\bar{B}\left(\left[2W_{11}(-1)e^{-i\omega\tau H} + W_{20}(-1)e^{i\omega\tau_H}\right] z^2\bar{z}\right. \\ &\quad \left. + \left[2W_{11}(-1)e^{i\omega\tau_H} + W_{02}(-1)e^{-i\omega\tau_H}\right] z\bar{z}^2\right).\end{aligned} \tag{4.63}$$

The expanded form of $g(z,\bar{z})$ from equation (4.57) we have

$$g(z,\bar{z}) = g_{20}\frac{z^2}{2} + g_{11}\, z\bar{z} + g_{02}\frac{\bar{z}^2}{2} + g_{21}\frac{z^2\bar{z}}{2} + \cdots. \tag{4.64}$$

We compare the coefficients of equations (4.63) and (4.64) in terms of z and $\bar{z}$, this gives us

$$\begin{aligned} g_{20} &= -2\tau\, L\, \bar{B} e^{-2\, i\omega\tau_{\mathrm{H}}}, \\ g_{11} &= -2\tau\, L\, \bar{B}, \\ g_{02} &= -2\tau\, L\, \bar{B} e^{2\, i\omega\tau_{\mathrm{H}}}, \\ g_{21} &= -2\tau\, L\, \bar{B}[2W_{11}(-1)e^{-\, i\omega\tau_{\mathrm{H}}} + 2W_{20}(-1)e^{i\omega\tau_{\mathrm{H}}}]. \end{aligned} \tag{4.65}$$

From equations (4.59) and (4.60) it implies that a comparison of the coefficients gives

$$\begin{aligned} H_{20}(\theta) &= -g_{20}q(\theta) - \bar{g}_{02}\bar{q}(\theta), \\ H_{11}(\theta) &= -g_{11}q(\theta) - \bar{g}_{11}\bar{q}(\theta), \end{aligned} \tag{4.66}$$

hence we can express equation (4.61) as

$$\frac{d}{dt}W_{20}(\theta) = 2i\omega W_{20}(\theta) + g_{20}q(\theta) + \bar{g}_{02}\bar{q}(\theta). \tag{4.67}$$

The solution to $W_{20}(\theta)$ gives

$$W_{20}(-1) = -\frac{g_{20}}{i\omega}e^{i\omega\theta} - \frac{\bar{g}_{02}}{3i\omega}e^{-i\omega\theta} + E_1 e^{2\, i\omega\theta}. \tag{4.68}$$

We carry out the same procedure for W_{11}

$$\frac{d}{dt}W_{11}(\theta) = g_{11}q(\theta) + \bar{g}_{11}\bar{q}(\theta), \tag{4.69}$$

and this gives

$$W_{11}(-1) = \frac{g_{11}}{i\omega}e^{i\omega\theta} - \frac{\bar{g}_{02}}{i\omega}e^{-i\omega\theta} + E_2, \tag{4.70}$$

where E_1 and E_2 are constants which we shall determine to in order to totally solve for $W_{20}(\theta)$ and $W_{11}(\theta)$. Now we take into consideration that $\theta = 0$,

$$H(z, \bar{z}, 0) = -2\Re\{\bar{B}F_0 q(0)\} + F_0 \tag{4.71}$$

which gives

$$\begin{aligned} H_{20}(0) &= -g_{20} - \bar{g}_{20}\bar{B} - 2\,Le^{-2i\omega\tau_{\mathrm{H}}}, \\ H_{11}(0) &= -g_{11} - \bar{g}_{11}\bar{B} - 2L. \end{aligned} \tag{4.72}$$

We substitute $\theta = 0$ into equation (4.61), this gives

$$\begin{aligned} (A - 2i\omega)\, W_{20}(0) &= -H_{20}(0), \\ AW_{11}(0) &= -H_{11}(0). \end{aligned} \tag{4.73}$$

We now have

$$\begin{aligned} AW_{20}(0) &= -(\tau_H + \gamma)W_{20}(0) + (\tau_H + \gamma)KW_{20}(-1), \\ AW_{11}(0) &= -(\tau_H + \gamma)W_{11}(0) + (\tau_H + \gamma)KW_{11}(-1). \end{aligned} \tag{4.74}$$

Combining equations (4.74)and (4.72) it gives

$$\begin{aligned} -(\tau_H)W_{20}(0) + (\tau_H)KW_{20}(-1) - 2i\omega W_{20}(0) &= g_{20}q(0) + \bar{g}_{20}\bar{q}(0) + 2\,Le^{-2i\omega\tau_H}, \\ -(\tau_H)W_{11}(0) + (\tau_H)KW_{11}(-1) &= g_{11}q(0) + \bar{g}_{11}\bar{q}(0) + 2\,L. \end{aligned} \tag{4.75}$$

With this we are able to evaluate E_1 and E_2

$$\begin{aligned} E_1 &= \frac{F_1}{\tau_H + \tau_H K e^{-2i\omega\tau_H} - 2i\omega}, \\ E_2 &= \frac{F_2}{-\tau_H + \tau_H K}, \end{aligned} \tag{4.76}$$

where

$$\begin{aligned} F_1 &= 2\tau_H\, Le^{-2\,i\omega\tau_H}, \\ F_2 &= 2\tau_H\, L. \end{aligned} \tag{4.77}$$

From these results we have drawn the following conclusion

$$\begin{aligned} C_1(0) &= \frac{i}{2\omega\tau_H}\left(g_{11}g_{20} - 2|g_{11}|^2 - \frac{|g_{02}|^2}{3}\right) + \frac{g_{21}}{2}, \\ \mu_2 &= -\frac{\Re[C_1(0)]}{\Re\{\lambda'(\tau_H)\}}, \\ \beta_2 &= 2\Re[C_1(0)], \\ T_2 &= -\frac{\Im[C_1(0)] + \mu_2[\lambda'(\tau_H)}{\omega}. \end{aligned} \tag{4.78}$$

From our earlier analysis we know that the $\Re\lambda'(\tau_H)$ is positive. This implies that the steady state of the Hopf bifurcation is asymptotically stable if $\Re C_1(0)$ is positive and it is unstable if it is negative. Since μ_2 shows the direction of the Hopf bifurcation, we can say that for $\Re C_1(0) > 0$ we have a supercritical bifurcation. For a subcritical bifurcation $\Re C_1(0)$ will have to be negative.

The centre manifold analysis confirms the analysis carried out using the multiple time scale analysis. Both of which confirm that a supercritical Hopf bifurcation occurs for our model. The type of Hopf bifurcation derived from the method of multiple time scale and the center manifold analysis can be checked with the numerical bifurcation plot. This is shown in figures 4.12 and 4.13, which are simulated using the DDE-Biftool [64]. Both figures agree with the analytical results derived using the multiple time scale and the center manifold analysis.

From figure 4.12 we see that for any increase in the delay parameter τ we see further growth in the amplitude of oscillation until we reach the maximum production rate from which the there is no more increase in the amplitude any more. From figure 4.13 we see that the parameter k which is the non-dimensional maximum rate of production we see that as there is any increase in k the is more growth in the amplitude of oscillation.

Figure 4.14 is another direct numerical investigation of the distribution of

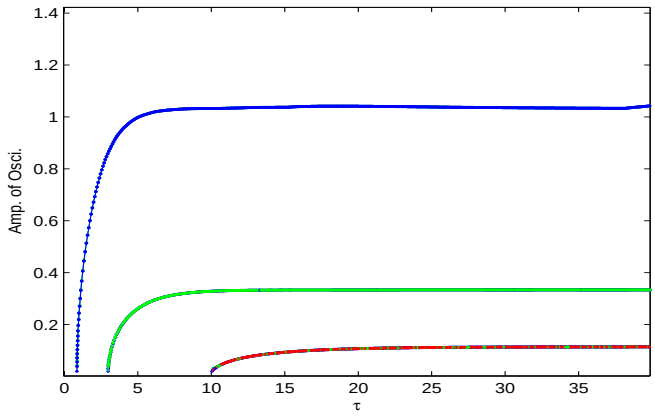


Figure 4.12: Plot of oscillation amplitude against delay time, τ. A numerical continuation plot using the DDE-Biftool to show the Hopf bifurcation and the direction of the bifurcation using τ as the bifurcation parameter and a fixed $n = 10$ and $k = 1.2$ (blue), $k = 0.95$ (green) and $k = 0.9$ (red).

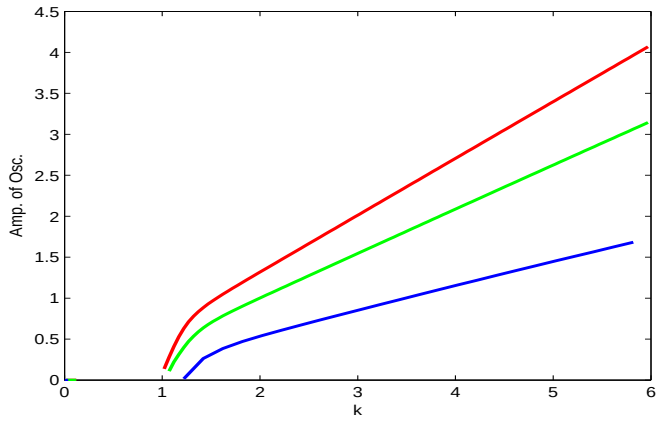
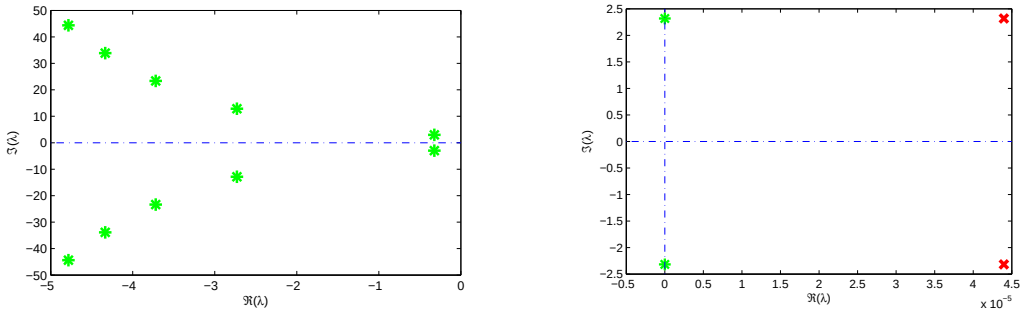


Figure 4.13: Plot of oscillation amplitude against k. A numerical plot showing the Hopf bifurcation and the direction of the bifurcation using k as the bifurcation parameter and a fixed $n = 20$ and $\tau = 0.4$ (blue), $\tau = 0.8$ (green) and $\tau = 1.2$ (red).



(a) (b)

Figure 4.14: The distribution of eigenvalues for varying τ and fixed $k = 1.2$, and $n = 10$. The green asterisk shows eigenvalues with negative real part while the red asterisk are those with positive real part.

eigenvalues of the Hopf bifurcation point with the delay as the bifurcating parameter. In figure 4.14a we have only negative real parts to the equilibrium points of the model but as we add a value of 0.1 in the form a step size, we get figure 4.14b. In figure 4.14b we see the red start which shows that we have unstable steady state, this is how the periodic solutions evolve.

From the phase plot in figure 4.15 we see that as we increase the delay we move from a spiral to periodic oscillation. Combining all the results we have thus far we can see consistency in both our analysis and the numerical simulation.

4.4 Conclusion

In conclusion the differential-delay equation has been analysed for both the linear part of the linearised equation and extended to the nonlinear part. We have shown that the inclusion of a delay parameter to a first order ordinary differential equation can express different types of states not displayed in the

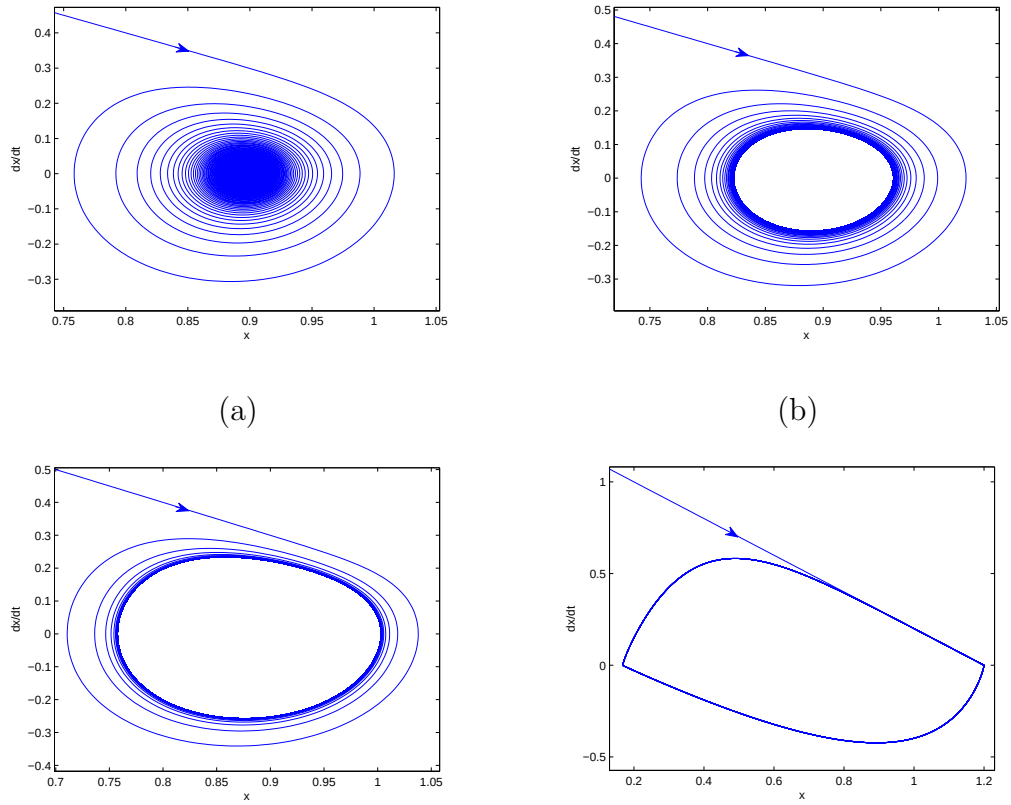


Figure 4.15: A phase portraits of dx/dt plotted against $x(t)$ for different time delays τ, for $k = 1.2$ and $n = 10$ fixed. (a) $\tau = 0.8$, (b) $\tau = 0.9$, (c) $\tau = 1$ and (d) $\tau = 9$.

first order ordinary differential equation. For a first order ordinary differential equation periodic oscillations are not displayed but the first order differential-delay equation has proved that this is a possibility. The multiple time scale was applied to investigate the behaviour of the critical point close to the Hopf bifurcation point. The nature of its stability was derived for the modelled equation (3.1). Hence for the given differential-delay equation the method

of multiple timescale can be directly applied to it without a center manifold reduction.

Chapter 5

The inclusion of a transcription factor in a negative autoregulation

The importance of negative autogenous regulation (NAR) can be seen from several studies such as the Hes1 and the circadian network systems studied by Monk in [65] and Bessho et al in [66] respectively. Various systems with negative autogenous regulation have been modelled and their complexities vary depending what the researches hopes to achieve. Xu et al in [67] investigated a complex model system of mRNA involving NAR with ordinary differential equations while Rosenfeld in [18] with a system of ordinary differential equation which included a NAR explicitly calculated the levels of mRNA by including its transcription factors. The following is a typical system of ODEs involving NAR for an mRNA with its transcription factor

$$\begin{aligned}\frac{\mathrm{d}}{\mathrm{dt}}Y_1(t) &= -\mu_1 Y_1(t) + \beta\frac{1}{1+(Y_2(t)/P_0)^n},\\ \frac{\mathrm{d}}{\mathrm{dt}}Y_2(t) &= -\mu_2 Y_2(t) + aY_1(t),\end{aligned} \tag{5.1}$$

where $Y_1(t)$ represents the concentration of mRNA, $Y_2(t)$ the transcription factor, μ_1 and μ_2 are the rate of decay respectively, a is the rate of production of the transcription factor and β is the maximum transcription rate. P_0 is the reference concentration constant of the transcription factor and n is the Hill's coefficient. Let $s = \mu_1 t$ such that $Y_1(t) = X_1(s)$ and $Y_2(t) = X_2(s)$ we note that for a, $\mu_2 \gg \mu_1$ such that

$$Y_2 \sim \frac{a}{\mu_2}Y_1, \tag{5.2}$$

then equation (5.1) corresponds to a rescaled model (4.1) studied chapter 4 where $P_0 = 1$ and $\beta = k\mu_1$. This rescaling would also apply in equation (5.3) and (5.4) where $\tau = \tau_a + \tau_b$. Some studies involving NAR have shown periodic oscillation.

Besshoe [66] experimentally studied the periodic repression by the Basic helix-loop-helix (bHLH) factor Hes7 where he showed that lack of functional Hes7 protein persistently up-regulates Hes7 transcription. He also showed that when the Hes7 protein is stabilized the transcription of Hes7. The Hes7 negative feedback served as the molecular basis for the segmentation clock. Monk [65] showed that in cultured mammalian cells, oscillation of mRNA are expressed with the transcription factors Hes1, where transcriptional delays are introduced into the model. The model (5.1) had a number of limitations, the first being that the ODE model did not generate oscillations as observed from several experimental simulations, this lack of periodic solution can be proved using the Bendixson's criterion. The second is that the ODE model in equation

(5.1) has the assumption that the mRNA and the transcription factor both initiate change at the same time t. Taking the time lag into account Monk [65], presented the following model (5.3) with a transcription time delay

$$\begin{aligned} \frac{\mathrm{d}}{\mathrm{dt}}Y_1(t) &= -\mu_1 Y_1(t) + \beta \frac{1}{1+(Y_2(t-\tau_a)/P_0)^n}, \\ \frac{\mathrm{d}}{\mathrm{dt}}Y_2(t) &= -\mu_2 Y_2(t) + aY_1(t), \end{aligned} \tag{5.3}$$

where τ_a is the lag time due to the transcription. Xiao in [27] proposed a model with both transcriptional and translational delays

$$\begin{aligned} \frac{\mathrm{d}}{\mathrm{dt}}Y_1(t) &= -\mu_1 Y_1(t) + \beta \frac{1}{1+(Y_2(t-\tau_a)/P_0)^n}, \\ \frac{\mathrm{d}}{\mathrm{dt}}Y_2(t) &= -\mu_2 Y_2(t) + aY_1(t-\tau_b), \end{aligned} \tag{5.4}$$

with τ_b as the translation delay. Both authors models produced good results and periodic oscillations were generated when certain conditions are met. The fact that we have introduced the second delayed parameter τ_2 does not change the fact that models (5.3) and (5.4) can reduce to the model (4.1) studied in chapter 4. Other authors who investigated the role both transcriptional and translational time delay in a two gene activator-inhibitor is Parmar et al [68]. In this chapter we will show that Xiao's model can be reduced to Monk's model where both delays in Xiao's model is represented by its sum in Monk's model. We also show that as the delay passes through some critical values a Hopf bifurcation is produced. We will show the direction of the Hopf bifurcation using the perturbation method of multiple time scales. By applying the method of multiple time scales we analyse the parameters close to the bifurcation point.

5.0.1 Stability Analysis

We shall be adopting the model studied by Xiao [27] which includes the translation delay τ_2, to the model studied by Monk [65]. In this section we investigate the model (5.4) with different rates of decay for the transcription factor and the mRNA and in subsequent section we apply the result derived to a system which has the same rate of decay. This makes our system the same as that studied by Verdugo et al in [43] and gives a basis to compare our results with those derived using other methods by other authors. For this model we assume $\mu_1, \mu_2, a, \beta > 0$ and $\tau_1, \tau_2 \geq 0$. Rescaling system (5.4) with $y_1 = Y_1/a$,$y_2 = Y_2/a\beta$, $p_0 = P_0/a\beta$ and τ_1, τ_2 as different lag times, this gives

$$\begin{aligned} \frac{\mathrm{d}}{\mathrm{dt}} y_1(t) &= -\mu_1 y_1(t) + \frac{1}{1 + (y_2(t-\tau_a)/p_0)^n}, \\ \frac{\mathrm{d}}{\mathrm{dt}} y_2(t) &= -\mu_2 y_2(t) + y_1(t-\tau_b). \end{aligned} \tag{5.5}$$

Let (y_1^*, y_2^*) be the steady state of the modelled system (5.5) this gives,

$$\mu_1 y_1^* = \frac{1}{1 + (y_2^*/p_0)^n}, \tag{5.6}$$

and

$$y_1^* = \mu_2 y_2^*, \tag{5.7}$$

from which we obtain

$$y_2^{*n+1} + p_0^n y_2^* - \frac{{p_0}^n}{\mu_1 \mu_2} = 0. \tag{5.8}$$

Let

$$Q(y_2^*) = y_2^{*n+1} + p_0^n y_2^* - \frac{{p_0}^n}{\mu_1 \mu_2}, \tag{5.9}$$

this gives,

$$
\begin{aligned}
Q(0) &= -\frac{{p_0}^n}{\mu_1\mu_2} \;<\; 0, \\
\frac{d}{dy_2^*}Q(y_2^*) &= (n+1)\, y_2^{*n} + p_0^n \;>0 \qquad \text{for any } y_2^* \;>0.
\end{aligned}
\tag{5.10}
$$

Let $q_1 \;=\; y_2^{*n+1} + p_0^n y_2^*$ and $q_2 \;=\; {p_0}^n/\mu_1\mu_2$, where $y_2^* \;>\; 0$ it implies that q_1 and q_2 intersect at least once and from equation (5.10) q_1 is a monotone increasing function. From equations (5.5) - (5.10) at the steady state there is a unique $y_2^* \;>\; 0$ which satisfies

$$
F(y_2^*) = \mu_1\mu_2\, y_2^*, \tag{5.11}
$$

where $F(y_2) \;=\; 1/(1 + (y_2(t-\tau_a)/p_0)^n)$. This implies that the equilibrium point (y_1^*, y_2^*) of equation (5.5) is unique. To analyse the steady state we perturb the system about its equilibrium point, let $x_1 = y_1 - y_1^*$, $x_2 = y_2 - y_2^*$.

$$
\begin{aligned}
\frac{\mathrm{d}}{\mathrm{dt}}x_1(t) &= -\mu_1(x_1(t) + y_1^*) + \frac{1}{1 + ((x_2(t-\tau_a) + y_1^*/p_0)^n}, \\
\frac{\mathrm{d}}{\mathrm{dt}}x_2(t) &= -\mu_2 x_2(t) + x_1(t-\tau_b).
\end{aligned}
\tag{5.12}
$$

The analysis of the linear part of this model would give us possible clues to how the solution to the model behaves. Applying the Taylor expansion to equation (5.12) to linearise it in the neighbourhood of the equilibrium point, we get

$$
\begin{aligned}
\frac{\mathrm{d}}{\mathrm{dt}}x_1(t) &= -\mu_1 x_1(t) + [-K x_2(t-\tau_a) + L x_2^2(t-\tau_a) + H x_2^3(t-\tau_a) + \mathrm{O}(x^4)], \\
\frac{\mathrm{d}}{\mathrm{dt}}x_2(t) &= -\mu_2 x_2(t) + x_1(t-\tau_b).
\end{aligned}
\tag{5.13}
$$

where

$$\begin{aligned}
\gamma &= \left(\frac{y_2^*}{p_0}\right)^n, \\
K &= \left(\frac{n\gamma}{y_2^*(1+\gamma)^2}\right), \\
L &= \frac{n\gamma(n\gamma - n + \gamma + 1)}{2(\gamma+1)^3 y_2^{*2}}, \\
H &= \frac{n\gamma(6n\gamma(1+\gamma)(n-1) - (n-1)(n-2)(1+\gamma)^2 - 6\,(n\gamma)^2)}{6\,(\gamma+1)^4\, y_2^{*3}}.
\end{aligned} \tag{5.14}$$

A compact form of equation (5.13) is

$$\begin{aligned}
\frac{\mathrm{d}^2}{\mathrm{dt}^2}x(t) + (\mu_1+\mu_2)\frac{\mathrm{d}}{\mathrm{dt}}x(t) + \mu_1\mu_2 x(t) + Kx(t-\tau) - Lx^2(t-\tau) \\
- Hx^3(t-\tau) + \mathrm{O}(x^4) = 0,
\end{aligned} \tag{5.15}$$

with $\tau = \tau_a + \tau_b$. which makes equation (5.4) equivalent to the model studied by Monk if Taylor expanded in the same way. Equation (5.15) with the $O(x^4)$ terms neglected will now be our focus in the rest of this chapter. The linearisation of equation (5.15) is

$$\frac{\mathrm{d}^2}{\mathrm{dt}^2}x(t) + (\mu_1+\mu_2)\frac{\mathrm{d}}{\mathrm{dt}}x(t) + \mu_1\mu_2 x(t) + Kx(t-\tau) = 0. \tag{5.16}$$

Let the roots of equation (5.16) be $x = \exp(\lambda\, t)$ where $\lambda \in \mathbb{C}$, the corresponding characteristic equation is

$$\Delta(\lambda) \equiv \lambda^2 + \lambda(\mu_1+\mu_2) + (\mu_1\mu_2) + Ke^{-\lambda\tau} = 0. \tag{5.17}$$

When the delay is $\tau = 0$ the roots of equation (5.17) is reduced to

$$\lambda_{1,2} = -\frac{(\mu_1+\mu_2) \pm \sqrt{(\mu_1-\mu_2)^2 - 4K}}{2}. \tag{5.18}$$

From equation (5.18) the real part of the roots of the equation are negative which gives the steady states as asymtotically stable. Let μ_{1H} be the Hopf

bifurcation parameter and let $\lambda = \alpha + i\omega$ where $\alpha, \omega \in \mathbb{R}^+$ for $\tau > 0$, if the stability of the system changes the real part of the roots must also change sign. Let the roots of equation (5.16) be purely imaginary i.e $\alpha = 0$, $\lambda = i\omega$ where $\omega > 0$ and let μ_{1H} and ω_H are the relevant quantity of μ_1 and ω_H at the Hopf bifurcation point, this gives

$$-\omega_H^2 + i\omega_H(\mu_{1H} + \mu_2) + (\mu_{1H}\mu_2) + Ke^{-i\omega_H\tau} = 0, \tag{5.19}$$

by equating the real parts and the imaginary parts we obtain

$$\begin{aligned} K\cos(\omega_H\tau) &= \omega_H^2 - \mu_2\mu_{1H}, \\ K\sin(\omega_H\tau) &= (\mu_2 + \mu_{1H})\omega_H. \end{aligned} \tag{5.20}$$

The value of ω would be

$$\omega_H = \frac{1}{2}\sqrt{-2\,(\mu_{1H}{}^2 + \mu_2{}^2) + 2\sqrt{(\mu_{1H}{}^2 - \mu_2{}^2)^2 + 4\,K^2}}, \tag{5.21}$$

and the value of τ is given as,

$$\tau_j = \frac{1}{\omega_{\mathrm{H}}}\left(\arccos\frac{\omega_{\mathrm{H}}^2 - \mu_2\mu_{1\mathrm{H}}}{K} + 2\,j\,\pi\right), \tag{5.22}$$

where τ_j is the Hopf bifurcation point and $j = 0, 1, 2, \cdots$. The primary Hopf bifurcation point is at $j = 0$ and the rest are secondary bifurcations. From equations (5.13) - (5.15) τ is the summation of τ_a and τ_b it implies that for a fixed value of either of the delayed parameter the other delay can be used for the corresponding value of the Hopf bifurcation point as shown in equation (5.23).

$$\begin{aligned} \tau_a &= -\tau_b + \frac{1}{\omega_{\mathrm{H}}}\left(\arccos\frac{\omega_{\mathrm{H}}^2 - \mu_2\mu_{1\mathrm{H}}}{K} + 2\,j\,\pi\right), \\ \tau_b &= -\tau_a + \frac{1}{\omega_{\mathrm{H}}}\left(\arccos\frac{\omega_{\mathrm{H}}^2 - \mu_2\mu_{1\mathrm{H}}}{K} + 2\,j\,\pi\right). \end{aligned} \tag{5.23}$$

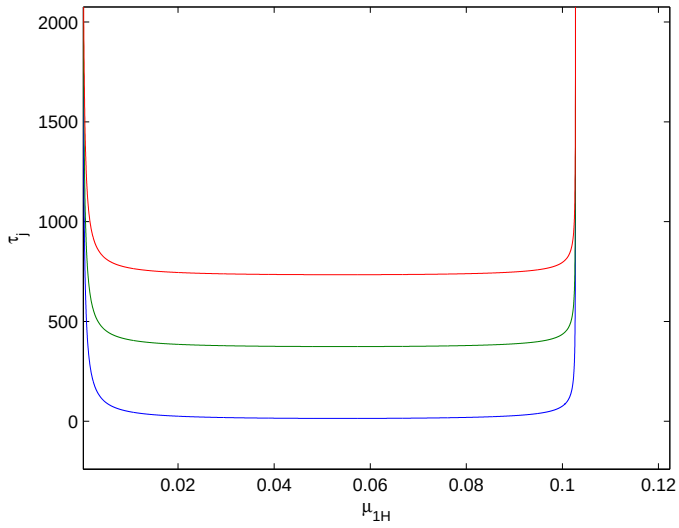


Figure 5.1: A plot of equation (5.21) showing the delay as we vary the decay for $j = 0$ (blue), $j = 1$ (green) and $j = 2$ (red).

From equations (5.23) we see that if either of the delay parameter is zero the corresponding value of the Hopf bifurcation point would still have to exceed a certain critical value. The property both delays could be captured in the summation or representation of the delays by just one of them. From figure 5.1 for each value of the bifurcating parameter μ_{1H} there is a corresponding critical delay which borders the stability switch from a stable solution to a periodic solution in the model. The primary critical delay in our system τ_0 is given by the solid blue line. Periodic Oscillations are displayed above the blue curve while below this curve periodic oscillation are not sustained. From the curve we can see that if we take delay as the Hopf bifurcation parameter then there are three possible corresponding values of μ_{1H}. First we can have a point where there is no value of μ_{1H} that gives rise to a periodic solution, we can have a point where only one value of μ_{1H} would give a periodic solution and

thirdly we can have a point that gives two values of μ_{1H}. To show that our result of the possible Hopf bifurcation we shall show that our result satisfies the transversality condition. Let us assume the real and the imaginary part of the root of the equation is a function of the delay, that is $\lambda(\tau) = \alpha(\tau) + i\omega(\tau)$, then we will analyse the transversality condition for our model with respect to this delay. Substituting and differentiating $\lambda(\tau)$ equation from (5.17) we have

$$\frac{\mathrm{d}}{\mathrm{d}\tau}\lambda\left(\tau\right) = -\frac{K\lambda\left(\tau\right)\mathrm{e}^{-\lambda(\tau)\tau}}{K\tau\,\mathrm{e}^{-\lambda(\tau)\tau} - 2\,\lambda\left(\tau\right) - \mu_1 - \mu_2}. \tag{5.24}$$

For a periodic solution to occur the real part of $\lambda(\tau)$ should be zero, hence we substitute $\alpha(\tau) = 0$ into equation (5.24) with equation (5.19) being replaced for the exponential term we have

$$\Re\left(\frac{\mathrm{d}}{\mathrm{d}\tau}\lambda\left(\tau\right)\right) = \frac{\omega^2(\mu_1^2 + \mu_2^2 + 2\omega^2)}{(\mu_1 + \mu_2 + \tau(\mu_1\mu_2 - \omega^2))^2 + (2\omega + \tau\omega(\mu_1 + \mu_1))^2} > 0. \tag{5.25}$$

The fact that the value is not zero satisfies the transversality condition for the existence of a periodic solution for our model. For both the transversality condition and the Hopf bifurcation theorem the assumption that $\alpha(\tau) = 0$ was applied this shows the existence of a periodic solution exists. Now we draw some facts about our analysis and the distribution of the eigenvalues thus far, if $\mu_1\mu_2 > K$ then all roots have negative real parts and the steady states (y_1^*, y_2^*) are asymptotically stable for all values of τ. Also if $0 \leq \tau < \tau_0$ then the steady state is also asymptotically stable. For $\tau = \tau_0$ we obtain a Hopf bifurcation at (y_1^*, y_2^*) which has imaginary roots for the model and at $\tau > \tau_0$ the solution obtained are periodic oscillation.

We have seen that Hopf bifurcation exist for equation (5.4) now we will analyse the type of periodic solution that occurs at this Hopf bifurcation point in the next section.

5.1 Weakly Nonlinear Analysis

To analyse the periodic solution of the system close to a Hopf bifurcation point, we apply the perturbation method based on multiple timescale analysis and harmonic balancing. For this system let $t = O(1)$ be the fast time and for the slow time $T = \epsilon^2 t = O(1)$. The fast scale is derived from the linear part of equation (5.15) while the slow scale from the nonlinearities that causes drift in the orbit as it accumulates over time.

The addition of nonlinear terms to equation (5.15) can change the behaviour of the system (5.5). To investigate the possible behaviour arising from these nonlinear terms we include these nonlinear terms systematically by rescaling them. Let $L = l$ and $H = h$ and $x = O(\epsilon)$ with $0 < \epsilon \ll 1$.
At $\mu_1 = \mu_{1H}$ we know from section 4.0.3 that we are at the Hopf bifurcation point with a little perturbation δ then $\mu_1 = \mu_{1\mathrm{H}} + \delta$. Let $\mu_1 = \mu_{1\mathrm{H}} + \epsilon^2\Delta$ such that $\delta = \epsilon^2\,\Delta$, we introduce Δ to determine the direction we are analysing close to the Hopf bifurcation point. The inclusion of these rescaled nonlinear terms to the linear equation changes the equation to a weakly nonlinear equation. Now the system (5.15) with rescaled non linear terms give

$$\begin{aligned}\frac{\mathrm{d}^2}{\mathrm{dt}^2}x(t) + (\mu_2 + \mu_{1H} + \epsilon^2\Delta)\frac{\mathrm{d}}{\mathrm{dt}}x(t) + \mu_2(\mu_{1H} + \epsilon^2\Delta)x(t) + Kx(t-\tau_0) \\ - \epsilon l x^2(t-\tau_0) - \epsilon^2 h x^3(t-\tau_0) + O(\epsilon^4) = 0.\end{aligned} \tag{5.26}$$

If $\Delta = 0$ then equation (5.26) reduces to (5.15) at the bifurcation point. From the perturbation method we expand $x(t)$ in two timescales as

$$x(t) = x_0(t,T) + \epsilon x_1(t,T) + \epsilon^2 x_2(t,T) + \mathrm{O}(\epsilon^3), \tag{5.27}$$

and we also express $x(t-\tau_0)$ in two timescales as

$$x(t-\tau_0) = x_0(t-\tau_0,T) + x_1(t-\tau_0,T)\epsilon - \left(\frac{\partial}{\partial T}x_0(t-\tau_0,T)\tau_0 - x_2(t-\tau_0,T)\right)\epsilon^2 + O\left(\epsilon^3\right). \tag{5.28}$$

Let the differential operator for the derivative be

$$\begin{aligned} \frac{\mathrm{d}}{\mathrm{d}t} &= \frac{\partial}{\partial t} + \epsilon^2\frac{\partial}{\partial T} \\ \frac{\mathrm{d}^2}{\mathrm{d}t^2} &= \frac{\partial^2}{\partial t^2} + 2\epsilon^2\frac{\partial^2}{\partial t\partial T} + \mathrm{O}(\epsilon^3). \end{aligned} \tag{5.29}$$

Substituting equation (5.27) - (5.29) into the equation (5.26) and matching the powers of the epsilon terms gives;

at $O(\epsilon^0)$:

$$\frac{\partial^2}{\partial t^2}x_0(t,T) + (\mu_{1\mathrm{H}}+\mu_2)\frac{\partial}{\partial t}x_0(t,T) + \mu_{1\mathrm{H}}\mu_2 x_0(t,T) + kx_0(t-\tau_0,T) = 0, \tag{5.30}$$

at $O(\epsilon^1)$:

$$\begin{aligned} &\frac{\partial^2}{\partial t^2}x_1(t,T) + (\mu_{1H}+\mu_2)\frac{\partial}{\partial t}x_1(t,T) + \mu_{1H}\mu_2 x_1(t,T) + kx_1(t-\tau_0,T) \\ &\quad = l\left(x_0(t-\tau_0,T)\right)^2, \end{aligned} \tag{5.31}$$

at $O(\epsilon^2)$:

$$\begin{aligned} &\frac{\partial^2}{\partial t^2}x_2(t,T) + (\mu_{1H}+\mu_2)\frac{\partial}{\partial t}x_2(t,T) + \mu_{1H}\mu_2 x_2(t,T) + kx_2(t-\tau_0,T) \\ &\quad = -(\mu_{1H}+\mu_2)\frac{\partial}{\partial T}x_0(t,T) + k\left(\frac{\partial}{\partial T}x_0(t-\tau_0,T)\right)\tau \\ &\qquad - 2\frac{\partial^2}{\partial t\partial T}x_0(t,T) + h\left(x_0(t-\tau_0,T)\right)^3 - \Delta\left(\frac{\partial}{\partial t}x_0(t,T)\right) \\ &\qquad + 2lx_0(t-\tau_0,T)x_1(t-\tau_0,T) + \mu_{1H}\Delta x_0(t,T). \end{aligned} \tag{5.32}$$

From ϵ^0, equation (5.30), is a linear differential-delay equation which has an equivalent structure with equation (5.16) which was studied in section (4.0.3)

hence let us assume the solution of $x_0(t,T)$ to be similar to that of equation (5.16) that is

$$x_0\left(t,T\right)=A\left(T\right)\cos\left(\omega\,t+\Phi\ \left(T\right)\right), \tag{5.33}$$

where $A_2(T)$ is the amplitude and $\Phi_2(T)$ the phase constant, both the amplitude and the phase constants are functions of the slow timescale. Equation (5.33) has no secular terms present, thus we proceed to substitute the value of $x_0(t,T)$ into equation (5.31) and this gives,

$$x_1\left(t,T\right)=C_{21}\left(T\right)\cos\left(2(\omega\,t+\Phi\ \left(T\right))\right)+E_{21}\left(T\right)\sin\left(2(\omega\,t+\Phi\ \left(T\right))\right)+F_{21}(T). \tag{5.34}$$

Where the coefficients are

$$\begin{aligned}
C_{21}&=-\frac{lA^2\left(T\right)\left(\left(4\,\omega^2-\mu_1\mu_2\right)\cos\left(2\,\omega\,\tau\right)+2\left(\omega\,\mu_1+\omega\,\mu_2\right)\sin\left(2\,\omega\,\tau\right)+k\right)}{2\left(C_{20}+4\omega^2\left(\omega^2+\mu_1^2+\mu_2^2\right)+\mu_1^2\mu_2^2+k^2\right)}\\
E_{21}&=\frac{lA^2\left(T\right)\left(2\left(\omega\,\mu_1+\omega\,\mu_2\right)\cos\left(2\,\omega\,\tau\right)-\left(4\,\omega^2-\mu_1\mu_2\right)\sin\left(2\,\omega\,\tau\right)\right)}{2\left(C_{20}+4\omega^2\left(\omega^2+\mu_1^2+\mu_2^2\right)+\mu_1^2\mu_2^2+k^2\right)}\\
F_{21}&=\frac{lA^2\left(T\right)}{2\left(\mu_1\mu_2+k\right)},
\end{aligned} \tag{5.35}$$

With

$$C_{20}=-4\,k\left(\left(2\,\omega^2-\frac{\mu_1\mu_2}{2}\right)\cos\left(2\,\omega\,\tau\right)+\omega\left(\mu_1+\mu_2\right)\sin\left(2\,\omega\,\tau\right)\right). \tag{5.36}$$

Just as in equation (5.34) there are no secular terms. The process is repeated again by substituting the values of $x_0(t,T)$ and $x_1(t,T)$ into equation (5.32) and solving for $x_2(t,T)$ at $O(\epsilon^2)$. The RHS of equation (5.32) gives

$$\begin{aligned}
&G_{22}\left(T\right)\cos\left(\omega\,t+\Phi\ \left(T\right)\right)+H_{22}\left(T\right)\sin\left(\omega\,t+\Phi\ \left(T\right)\right)\\
&+C_{22}\left(T\right)\cos\left(3\omega\,t+3\Phi\ \left(T\right)\right)+E_{22}\left(T\right)\sin\left(3\omega\,t+3\Phi\ \left(T\right)\right),
\end{aligned} \tag{5.37}$$

where the coefficients of equation (5.37) are as follows

$$\begin{aligned}
G_{22} &= \left(k\cos\left(\omega\,\tau\right)\tau - 2\,\mu\right)\frac{\mathrm{d}}{\mathrm{d}T}A\left(T\right) + \left(k\tau\,A\left(T\right)\sin\left(\omega\,\tau\right) + 2\,\omega\,A\left(T\right)\right)\frac{\mathrm{d}}{\mathrm{d}T}\Phi\left(T\right) \\
&\quad + \left(\left(C_{21} + \frac{3\,h}{4\,l} + 2\,F_{21}\right)\cos\left(\omega\,\tau\right) - E_{21}\sin\left(\omega\,\tau\right)\right) l\,A\left(T\right)^3 - 2\,\mu\,\Delta\,A\left(T\right) \\
H_{22} &= \left(k\cos\left(\omega\,\tau\right)\tau - 2\,\mu\right)\frac{\mathrm{d}}{\mathrm{d}T}A\left(T\right) + \left(k\tau\,A\left(T\right)\sin\left(\omega\,\tau\right) + 2\,\omega\,A\left(T\right)\right)\frac{\mathrm{d}}{\mathrm{d}T}\Phi\left(T\right) \\
&\quad + \left(\left(C_{21} + \frac{3\,h}{4\,l} + 2\,F_{21}\right)\sin\left(\omega\,\tau\right) + E_{21}\cos\left(\omega\,\tau\right)\right) l\,A\left(T\right)^3 - 2\,\mu\,\Delta\,A\left(T\right) \\
C_{22} &= \left(\left(C_{21} + \frac{1\,h}{4\,l}\right)\sin\left(3\,\omega\,\tau\right) + E_{21}\cos\left(3\,\omega\,\tau\right)\right) l\,A\left(T\right)^3 \\
E_{22} &= \left(\left(C_{21} + \frac{1\,h}{4\,l}\right)\cos\left(3\,\omega\,\tau\right) - E_{21}\sin\left(3\,\omega\,\tau\right)\right) l\,A\left(T\right)^3
\end{aligned} \tag{5.38}$$

In equation (5.37) secular terms are seen. These secular terms can change the periodic solution in different possible ways hence we eliminate these secular term from equation (5.37) by equating the coefficients cosine and sine terms to zero

$$G_{22} = 0 \qquad H_{22} = 0. \tag{5.39}$$

The equation (5.32) will now be

$$\begin{aligned}
&\frac{\partial^2}{\partial t^2}x_2\left(t,T\right) + \left(\mu_{1\mathrm{H}} + \mu_2\right)\frac{\partial}{\partial t}x_2\left(t,T\right) + \mu_{1\mathrm{H}}\mu_2 x_2\left(t,T\right) + k x_2\left(t-\tau_0,T\right) \\
&\qquad = C_{22}\left(T\right)\cos\left(3\omega\,t + 3\Phi\ \left(T\right)\right) + E_{22}\left(T\right)\sin\left(3\omega\,t + 3\Phi\ \left(T\right)\right).
\end{aligned} \tag{5.40}$$

Substituting into equation (5.27) the approximate solution of $x(t)$ is:

$$\begin{aligned}
x(t) &= A\left(\epsilon^2 t\right)\cos\left(\omega\,t + \Phi\ \left(\epsilon^2 t\right)\right) + \epsilon\,\left(C_{21}\left(\epsilon^2 t\right)\cos\left(2\,\omega\,t + 2\Phi\ \left(\epsilon^2 t\right)\right)\right. \\
&\quad \left. + E_{21}\left(\epsilon^2 t\right)\sin\left(2\,\omega\,t + 2\Phi\ \left(\epsilon^2 t\right)\right) + F_{21}\left(\epsilon^2 t\right)\right) \\
&\quad + \epsilon^2\left(C^*_{22}\left(\epsilon^2 t\right)\cos\left(3\,\omega\,t + 3\Phi\ \left(\epsilon^2 t\right)\right) + E^*_{22}\left(\epsilon^2 t\right)\sin\left(3\,\omega\,t + 3\Phi\ \left(\epsilon^2 t\right)\right)\right).
\end{aligned} \tag{5.41}$$

where $C_{22}^{*}\left(\epsilon^{2}t\right)\cos\left(3\,\omega\,t+3\Phi\ \left(\epsilon^{2}t\right)\right)+E_{22}^{*}\left(\epsilon^{2}t\right)\sin\left(3\,\omega\,t+3\Phi\ \left(\epsilon^{2}t\right)\right)$ is the solution to $x_{2}(t,T)$. From the coefficients of the secular terms derived from equation (5.37), two equations are obtained one for the amplitude and the other for the phase, see equations (5.42) and (5.43). With these equations we can solve for the rate of growth or decay in the amplitude and phase.

$$\frac{\mathrm{d}}{\mathrm{dT}}A\left(T\right)=\kappa\ A\left(T\right)\left(A\left(T\right)^{2}-\rho\,\Delta\right), \tag{5.42}$$

and

$$\frac{\mathrm{d}}{\mathrm{dT}}\Phi\left(T\right)=\alpha\,A\left(T\right)^{2}+\beta\,\Delta. \tag{5.43}$$

The coefficients in equations (5.42) and (5.43) are

$$\begin{aligned}
P_{0}&=4\ \left(-2\,k\tau\,\mu_{1}-2\,k\tau\,\mu_{2}\right)\cos\left(\omega\,\tau\right)+k^{2}\tau^{2}+4\,k\sin\left(\omega\,\tau\right)\omega\,\tau\\
&\quad+4\,\omega^{2}+{\mu_{1}}^{2}+2\,\mu_{1}\mu_{2}+{\mu_{2}}^{2},\\
P_{1}&=-\left(8\,l\omega\,E_{21}-4\,lC_{21}\mu_{1}-4\,lC_{21}\mu_{2}-8\,lF_{21}\mu_{1}-8\,lF_{21}\mu_{2}\right.\\
&\quad\left.-3\,h\mu_{1}-3\,h\mu_{2}\right)\cos\left(\omega\,\tau\right)\\
&\quad-\left(8\,l\omega\,C_{21}+16\,l\omega\,F_{21}+4\,lE_{21}\mu_{1}+4\,lE_{21}\mu_{2}+6\,h\omega\right)\sin\left(\omega\,\tau\right)\\
&\quad-8\,F_{21}kl\tau-4\,klC_{21}\tau-3\,hk\tau,\\
P_{2}&=\left(4\,k\sin\left(\omega\,\tau\right)\omega\,\tau-4\,k\cos\left(\omega\,\tau\right)\tau\,\mu_{2}+8\,\omega^{2}+4\,\mu_{1}\mu_{2}+4\,{\mu_{2}}^{2}\right)\Delta,\\
q_{1}&=-\left(8\,l\omega\,C_{21}+16\,l\omega\,F_{21}+4\,lE_{21}\mu_{1}+4\,lE_{21}\mu_{2}+6\,h\omega\right)\cos\left(\omega\,\tau\right)\\
&\quad-\left(-8\,l\omega\,E_{21}+4\,lC_{21}\mu_{1}+4\,lC_{21}\mu_{2}+8\,lF_{21}\mu_{1}+8\,lF_{21}\mu_{2}\right.\\
&\quad\left.+3\,h\mu_{1}+3\,h\mu_{2}\right)\sin\left(\omega\,\tau\right)\\
&\quad+4\,klE_{21}\tau,\\
q_{2}&=-\left(-4\,k\sin\left(\omega\,\tau\right)\tau\,\mu_{2}-4\,k\cos\left(\omega\,\tau\right)\omega\,\tau+4\,\omega\,\mu_{1}-4\,\omega\,\mu_{2}\right)\Delta.
\end{aligned} \tag{5.44}$$

If the rate of change in the amplitude is zero then from equation (5.42) we have

$$A(T)^2 = \rho\,\Delta, \tag{5.45}$$

which is the steady state solution of the amplitude for the period of oscillation. From equation (5.45) we substitute the value of $A(T)$ into equation (5.43) and solve for the phase $\Phi(T)$, this gives

$$\Phi(T) = (\alpha\,\varrho\, + \beta)\Delta\, T\, +\, \Phi_0, \tag{5.46}$$

where Φ_0 is the constant of integration. The of the phase shift is linear when the solution of equation (5.26) is a periodic oscillation. If the rate of decay or growth is not zero, then the value of $A(T)$ from (5.42) is

$$A\,(T) = \frac{\sqrt{P_2\,\Delta}}{\sqrt{(A(0)\mathrm{e}^{-2N\,T}\,\Delta\,P_2 +\, P_1}}, \tag{5.47}$$

where

$$N = \frac{\Delta\,\kappa\,P_2}{P_0}, \tag{5.48}$$

with $T = \epsilon^2 t$ and $A(0)$ as the constant of integration. For this value of $A(T)$ we also solve for the Phase $\Phi(T)$

$$\Phi(T) = \frac{\alpha\,P_2\,\Delta\,\ln\left(\Delta\,A_0 P_2\,\mathrm{e}^{-2\,N\,T} + P_1\right)}{2\,N P_1} + (\alpha\varrho + \beta)\,\Delta\,T\, + \Phi_0, \tag{5.49}$$

where A_0 and Φ_0 are the constants of integration. Substituting the values of $A(T)$ and $\Phi(T)$ into equation (5.33) gives

$$x\,(t) = \frac{\sqrt{P_2\,\Delta}}{\sqrt{(A_0\mathrm{e}^{-2N\,T}\,\Delta\,P_2 +\, P_1}}\,\cos\left(\omega\,t\, + \Phi(T)\right). \tag{5.50}$$

From equations (5.50) the limit of the amplitude of the oscillation for Δ being positive shows that as $t \to \infty$, $A(T) \to 0$ and as $t \to -\infty$, $A(T) \to \sqrt{\rho\,\Delta}$

which is equivalent to the amplitude of the oscillation when the rate of change of the secular term is zero, $(dA(T)/dT = 0)$. If Δ is negative we have a reverse case.

Hence the periodic oscillation is derived when the rate of the change of the secular term is zero. With the value of $A(T)$ obtained we can now substitute and solve for $\Phi(T)$ in equation (5.43).

5.1.1 Numerical simulation of the model

In this section we compare the analytical results we have obtained in previous sections of this chapter with the numerics and for simplicity we will let $\mu_1 = \mu_2 = \mu$. In subsequent sections we apply the same assumption that $\mu_1 = \mu_2 = \mu$ as this helps us compare results with those of other authors.

We will simulate the example studied by Aneal et al [43]. All parameter in the numerical simulation are as described in section 3.1. Let decay rate of x_1 and x_2 be $\mu_{\text{H}} = 0.03$, the Hill coefficient $n = 5$, the transcription delay $\tau_1 = 3$, the translational delay $\tau_2 = 1$ and the reference concentration be $p_0 = 100$. From the given parameters the steady state derived is $y_1^*, y_2^* = (4.377, 145.9)$ and $k = 3.909\text{x}10^{-3}$, $l = 6.278\text{x}10^{-5}$, $h = -6.4101\text{x}10^{-7}$, $\tau_0 = 18.247$, $\omega = 5.485\text{x}10^{-2}$.

Figures 5.2 and 5.3 shows the Hopf bifurcation point using DDE Biftool software for τ_1 and τ_2 as the bifurcation parameters respectively.

From equation (5.22) and (5.23), keeping τ_2 fixed and taking τ_{1H} as the bifurcation parameter, we see that the Hopf bifurcation takes place when the sum of both the fixed and varying delay is 18.247 see figures 5.2. Likewise if we choose τ_2 as the bifurcation parameter and τ_1 as the fixed delay the Hopf bifurcation would take place only when the sum of both delays is 18.247 see

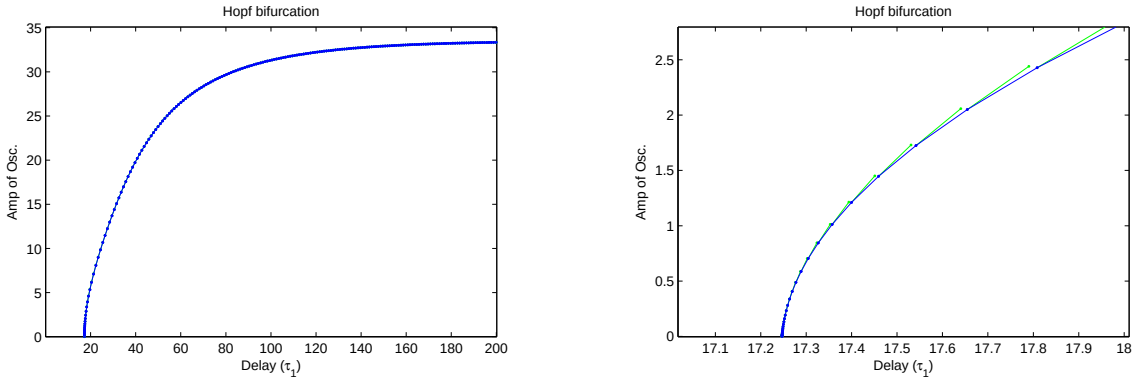


Figure 5.2: A bifurcation plot of equation (5.12) with τ_1 as the varying parameter and fixed paramter $\tau_2 = 1$, $p_0 = 100$, and $n = 5$.

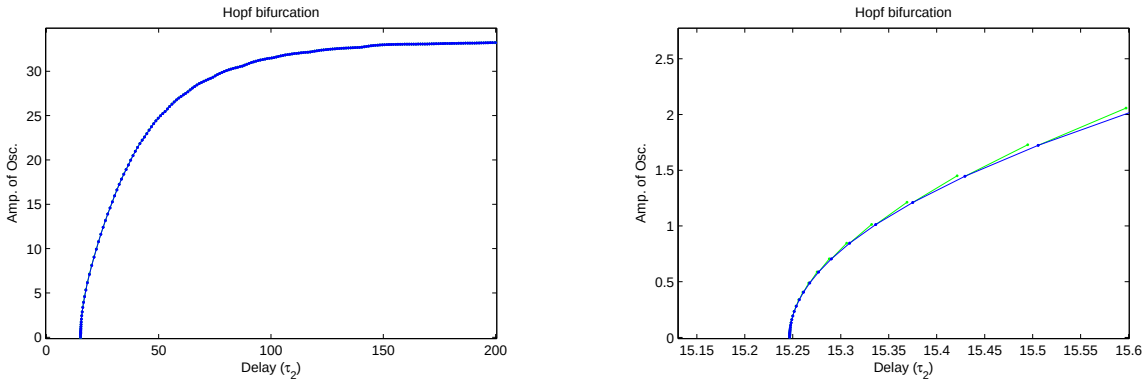


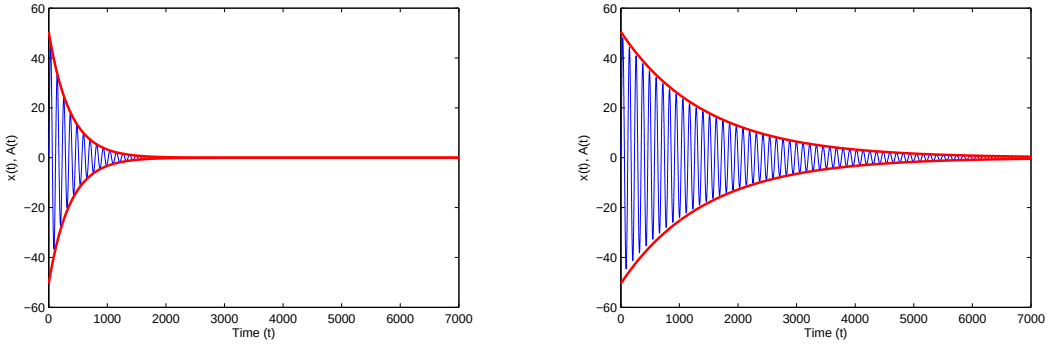
Figure 5.3: A bifurcation plot of equation (5.12) with τ_1 as the varying parameter and fixed paramter $\tau_2 = 3$, $p_0 = 100$, and $n = 5$.

figure 5.3.

Hence the continuation plot validates our analysis that the sum of τ_1 and τ_2 gives the Hopf bifurcation point τ_0. This shows that significant change in either the transcriptional or translational delay would have an impact on the negative autoregulation network.

Now we plot the result derived from section 5.1 equations (5.42) and (5.43) and compare it to numerical simulations applied to derive the limit of the amplitude and the phase of the oscillation close to the Hopf bifurcation point. For this

purpose we will continue with the numerical example under consideration.

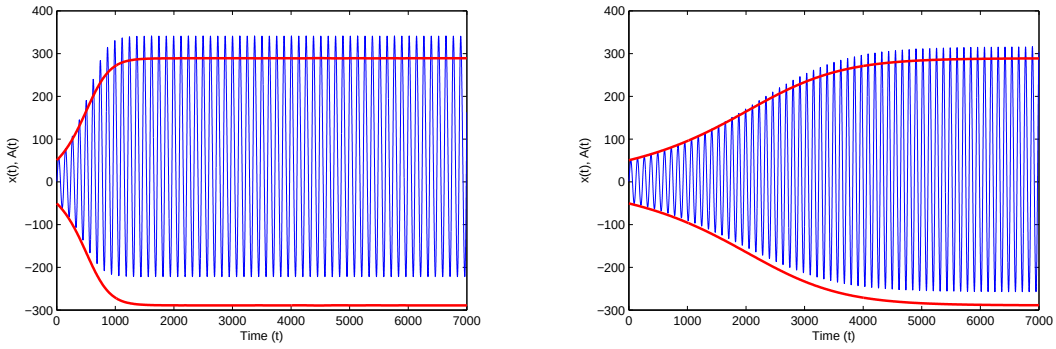


(a) (b)

Figure 5.4: Comparison between the multiple timescale (red) from equation (5.42) with initial condition $A(0) = 48.5$ and Direct numerical plot (blue) from equation (5.26) with initial condition $x(0) = 110\sin(-13)$. The multiple time scale gives the envelope, with (a) $\epsilon = 0.1$ and $\Delta = 0.4$ and (b) $\epsilon = 0.05$ and $\Delta = 0.4$.

keeping figures 5.4a and 5.4b side by side one would assume the are the same plots but this is not the case. Figure 5.4a is the multiple time scale plot derived from the analysis carried out in section 5.1 while figure 5.4b is the direct numerical plot. In figure 5.4 we have included the envelope derived from equation (5.42) and this matches the amplitude of the damped oscillation. The analytic solution and the direct numeric solution are indistinguishable, figure 5.4 shows that an increase in the rate of decay of would result in the damped oscillation. The amplitude of the periodic oscillatory solution is perfectly picked out by the method of multiple timescale.

Now we look at how a decrease in the decay rate will affect the dynamics of the solution.

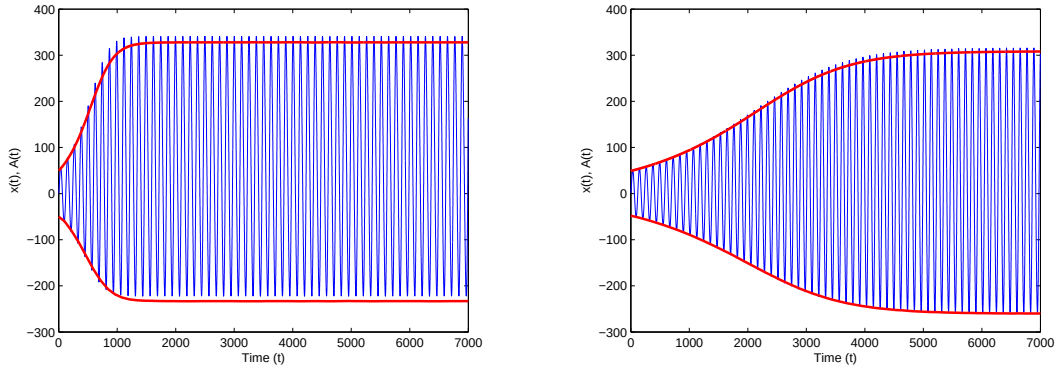


(a) (b)

Figure 5.5: Comparison between the multiple time scale from equation (5.42) with initial condition $A(0) = 48.5$ and direct numerical plot from equation (5.26) with initial condition $x(0) = 110\sin(-13)$. The multiple time scale gives the envelope, with (a) $\epsilon = 0.1$ and $\Delta = -0.4$ and (b) $\epsilon = 0.05$ and $\Delta = -0.4$.

Figure 5.5 we see the effect of the nonlinear term in play. For the same value of Δ and different values of ϵ we see that though there is a difference the closer we are to the Hopf bifurcation the greater the accuracy of the matched asymptotic to the weakly nonlinear numerics. Figure 5.6 is another way in which better results can be derived from the method of multiple timescale. The inclusion of the first correcting term in figure **??** for the same values as figure 5.5 gives better results.

Again from figure 5.5 we see a growth in the periodic solutions and this oscillations do not grow indefinitely but grow to a limit amplitude as predicted in equation (A.24) of the analysis. On the positive axis (upper half plane) of the amplitude the oscillation of the direct numerics and that of the multiple timescales is indistinguishable but the negative axis (lower axis) of the amplitude does not perfectly match. This is because the method of multiple



(a) (b)

Figure 5.6: Comparison between the multiple time scale from equation (5.42) with the first correcting term having initial condition $A(0) = 48.5$ and direct numerical plot from equation (5.26) with initial condition $x(0) = 110\sin(-13)$. The multiple time scale gives the envelope, with (a) $\epsilon = 0.1$ and $\Delta = -0.4$ and (b) $\epsilon = 0.05$ and $\Delta = -0.4$.

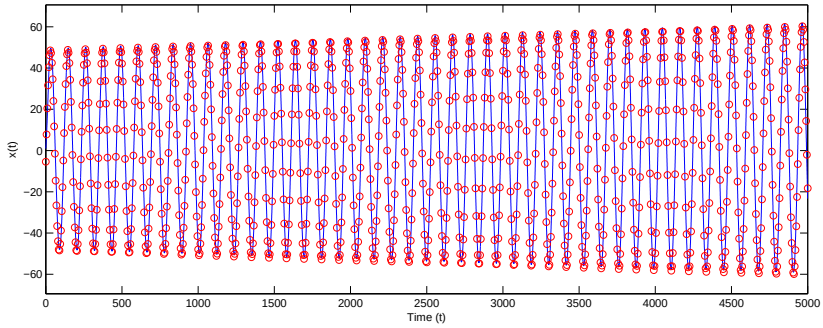


Figure 5.7: Multiple time scale plots (red circle) from equations (5.42) and (5.43) with $A(0) = 48.5$ and the direct numerics (blue solid line)from equation (5.26) with initial condition $x(0) = 110\sin(-13)$, for $\epsilon = 0.05$ and $\Delta = -0.04$.

timescales is symmetric but the system under study is non-symmetric. The solution derived from equation (5.42) for both the amplitude and the phase we see that this matches perfectly with the direct numerics of the model. With

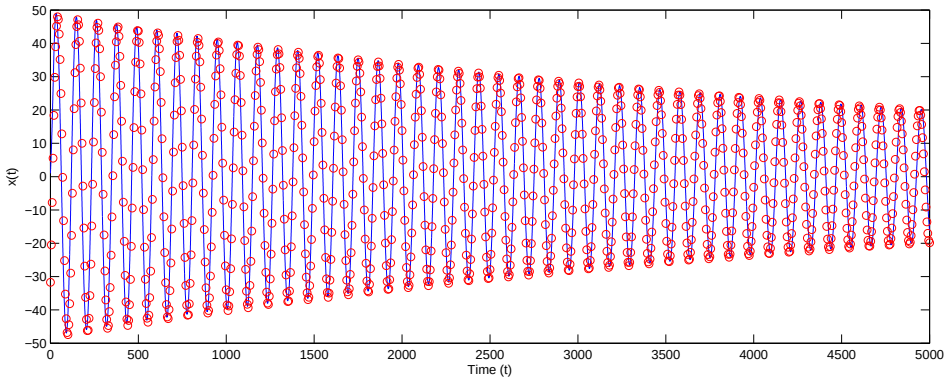


Figure 5.8: Multiple time scale plots (red circle) from equations (5.42) and (5.43) with $A(0) = 48.5$ and the direct numerics (blue solid line)from equation (5.26) with initial condition $x(0) = 110\sin(-13)$, for $\epsilon = 0.05$ and $\Delta = 0.1$.

figures 5.5 - 5.8 we do have very good results from the multiple time scale analysis for both sides of the Hopf bifurcation. We have seen these properties pictorially now let us substitute the values derived analytically into the equation (5.42) and draw conclusion on the amplitude A(T) derived, we obtain

$$\frac{d}{dT}A\left(T\right) = -0.6360\,A\left(T\right)\Delta - \left(3.3636\,h + 826.2443\,l^2\right)A\left(T\right)^3. \qquad (5.51)$$

At steady state if the values of $l > 0$ and $h > 0$, then equation (5.51) will have three possible roots and $A = 0$ will be one of the roots. As $t \to \infty$ for $\Delta < 0$, $A = 0$ is an unstable steady state while the other two will be stable. If $\Delta > 0$ then $A = 0$ will be a stable steady state while the other two roots will be unstable, which gives a supercritical bifurcation. But if $l < 0$ and $h < 0$ then we will have a subcritical bifurcation. Our model shows a supercritical bifurcation corresponding to our analysis of the limit of the amplitude of the oscillation of the system. If $\Delta > 0$ we approach a stable state at zero and if $\Delta < 0$ then there is a decrease in μ_{H} and we approach the periodic oscillation for $t \to \infty$.

Not only does the method of multiple scales help us to analyse the nature of our Hopf bifurcation but also give the limit of our oscillation. It also simplifies the nonlinear DDE model. It is worth noting that to satisfy equation (5.45) the initial value of $A(0) < \sqrt{\rho\,\Delta}$.

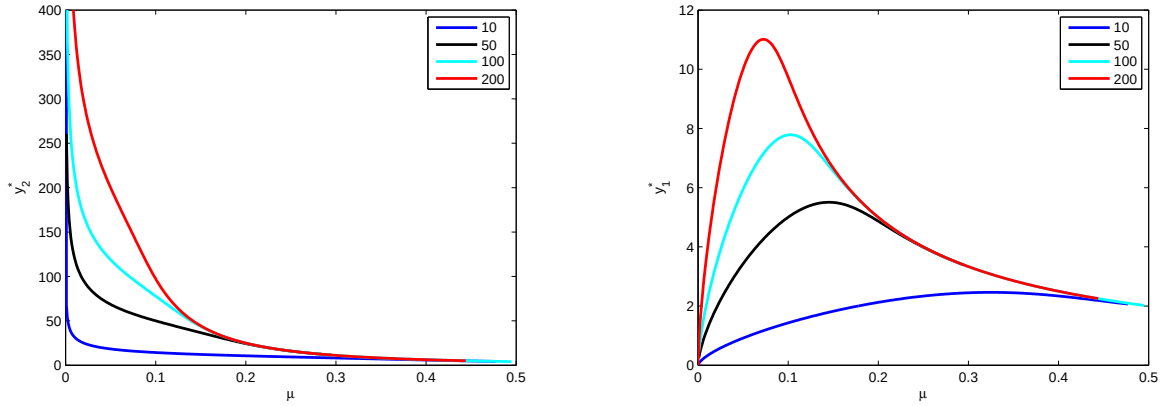
Numerical Simulation

To further justify that the method of multiple time scale gives accurate result we would in this section we simulate using the variables applied by Verdugo et al [43] to compare their plots with those we derived. The weakly nonlinear analysis for the delay can be found in appendix A.2. For simplicity let $\mu_1 = \mu_2 = \mu$ having values of $\mu = 0.03$ and for other parameters let $P_0 = 100$ and the Hill coefficient, $n = 5$.

Form the linear part of equation (5.15) we get the same values $(y_1^*, y_2^*) = (4.3774, 145.91)$ for the steady states. For the values of the parameters K, L and H we have $3.9089\,\mathrm{x}\,10^{-3}$, $6.2778\,\mathrm{x}\,10^{-5}$ and $-6.4101\,\mathrm{x}\,10^{-7}$ respectively. If these values are substituted into equation (A.3) we derive the value of $\omega = 5.4854\,\mathrm{x}\,10^{-2}$ and the Hopf bifurcation as $\tau_H = 18.2469$ which again is exactly the values derived by Verdugo et al.

Figures 5.9 and 5.10 are all the same as that derived by Verdugo et al [43] which shows that our analysis using the method of multiple timescales is accurate.

From figure 5.9a we see that as μ increases the steady state of protein factor decays rapidly then slowly irrespective of the value of the reference concentration, P_0. In figure 5.9b there is an increase in the steady state of the mRNA before it declines. We see that the rapid fall in the protein factor corresponds to that sharp rise in the mRNA and the slow decline in the protein factor



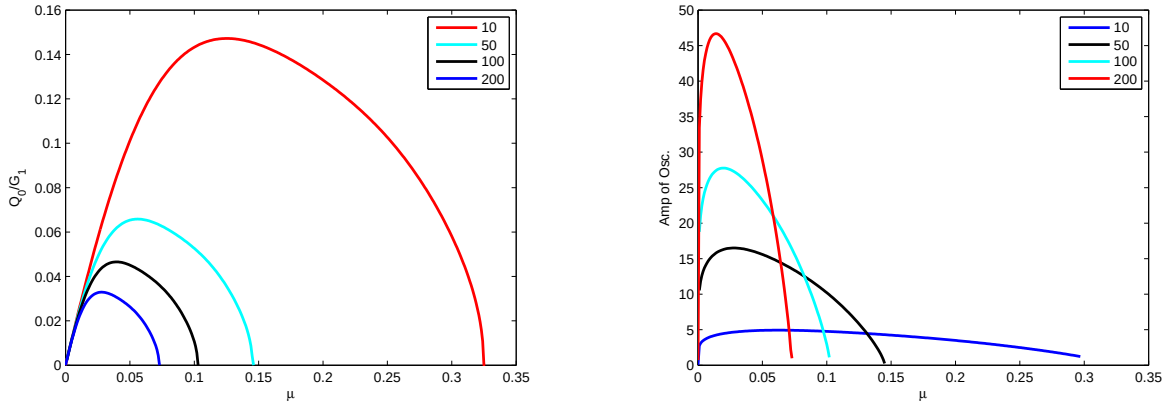
(a) (b)

Figure 5.9: (a) A Plot of the protein factor concentration y_2^* at steady state against the rate of decay μ for fixed values of $n = 5$, $\tau = 18.247$ and $p_0 = 10, 50, 100$ and 200 from equation (5.5). (b) A Plot of the mRNA concentration y_1^* at steady state against the rate of decay μ for fixed values of $n = 5$, $\tau = 18.247$ and $p_0 = 10, 50, 100$ and 200 from equation (5.5).

occurs after the maximum value of the mRNA has been reached and a decline begins. This fast rise is triggered during mRNA transcription, being a negative feedback it represses its own production when maximum production is reached. An increase in the rate of decay μ reduces concentration on mRNA which gives the figure 5.9b the gradual decline. In figure 5.10a we show the shift in the frequency for the delay as it moves away from the Hopf bifurcation point. This value is derived with the method of multiple timescales and gives the same figure as [43].

Figure 5.10b shows the plot of the amplitude for different values of the reference concentration. We see that for higher values of reference concentration there is an increase in the corresponding value amplitude.

Hence the multiple timescale analysis also achieves the same result as that



(a) (b)

Figure 5.10: (a) A plot of frequency change against the rate decay μ from the Hopf bifurcation point for fixed values of $n = 5$, $\tau = 18.247$ and $p_0 = 10$, 50, 100 and 200 from equation (A.22). (b) A Plot of the amplitude equation (A.23) of the protein factor against the rate of decay for fixed values of $n = 5$, $\tau = 18.247$ and $p_0 = 10$, 50, 100 and 200.

those in [43] and we can use this method to study each parameter and its effect on the model.

From figure 5.10b we see a rise and a fall in the amplitude with the highest amplitude corresponding to the highest reference concentration, p_0. The reference coefficient p_0 defines the concentration of mRNA needed to significantly activate its expression hence the greater the reference concentration the greater the concentration on mRNA needed. In figure 5.11 we observe that for some values of the delay one might have two corresponding values of μ. Direct numerical plots of the mRNA and protein factor are shown in the following figures

Since figure 5.11 shows the possibility of double Hopf bifurcation point, we

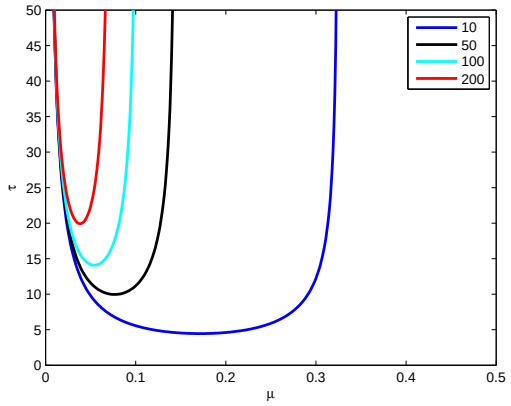


Figure 5.11: A Plot of the delay τ against μ from equation (5.5) for fixed values of $n = 5$, and $p_0 = 10$, 50, 100 and 200.

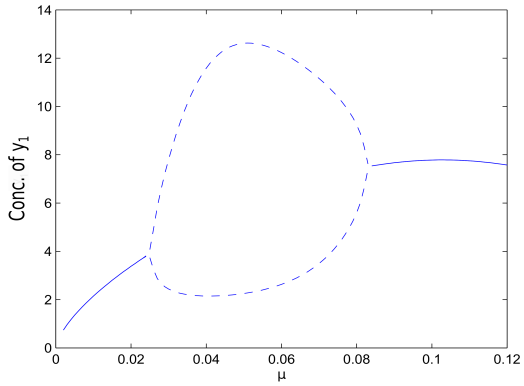


Figure 5.12: A Plot of the mRNA concentration as a function of the rate of decay μ with values of $n = 5$, $\tau = 18.247$ and $p_0 = 100$ fixed. The dash blues lines are amplitude of oscillation while the solid blue lines are steady state of equation (5.5).

plot the bifurcation diagram to observe how this occurs in our model. Both figures 5.12 and 5.13 show a supercritical Hopf bifurcation and a subcritical Hopf bifurcation. For $\mu < 0.4$ we get the supercritical Hopf bifurcation and when $\mu > 0.4$ the subcritical Hopf bifurcation. We see from the plots that

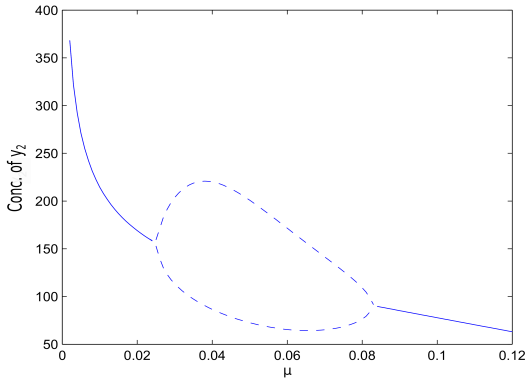


Figure 5.13: A Plot of the protein factor concentration as a function of the rate of decay μ with values of $n = 5$, $\tau = 18.247$ and $p_0 = 100$ fixed. The dash blues lines are amplitude of oscillation while the solid blue lines are steady state of equation (5.5).

when there is an increase in the mRNA the transcription factor decreases but this does not change the periodic oscillation of both the transcription factor and the mRNA.

5.2 Conclusion

As we have seen the method of multiple time scale is a very useful tool for analysing the properties of certain dynamical systems close to the Hopf bifurcation point. Next for this particular example, we reproduced the results derive by [43] and derived analytical solution to the weakly non-linear (5.4). Hence we have studied this second order negative autoregulation system and seen many properties being displayed in such a model (5.4) from asymptotically stable steady states to periodic solutions. If this simple network can produce such a varying property then that might be the reason why it is one

of the more abundant network motifs [2].

In all these models one would generally ask how large can the delay be? In the next chapter we could start by looking at the large delays for the logistic model.

Chapter 6

Large delay in a logistic differential-delay equation

6.1 Large Delays

In the previous chapters we studied the behaviour close to the Hopf bifurcation point for a number of differential-delay equations. We now revisit the logistic model and study this model for large values of the delay, τ. When the delay tends to infinity the physical implication might be able to give more useful information on extinction and other biological effects on population dynamics. We will apply both numerical and analytical methods to derive useful approximations to the solution of this model's analytical approximation for the solution. These approximations will then be compared to the solution from other authors to examine the how accurate our solutions are. To do this we rescale equation (2.10) which gives

$$\frac{d}{dt}p(t) = \tau\ \left(-p(t) + f(r, p(t-1))\right), \tag{6.1}$$

where $f(r, p(t-1)$=$r\, p(t-1)(1-p(t-1))$. The transformation to equation

(6.1) makes the model more flexible to work with and does not change the structure of the model. Since we will be studying the effect of the delayed parameter as $\tau \to \infty$, let $\varsigma = 1/\tau$ which implies that as $\tau \to \infty$, $\varsigma \to 0$. Substituting into equation (6.1) we get

$$\varsigma \frac{d}{dt} p(t) = -p(t) + f(r, p(t-1)). \tag{6.2}$$

Figure 6.1 shows the plot of equations (2.10) and (6.2) for $\tau = 100$ and $r = 3.1$, we see that both plots are the same but on a different time scale because we rescaled equation (6.2).

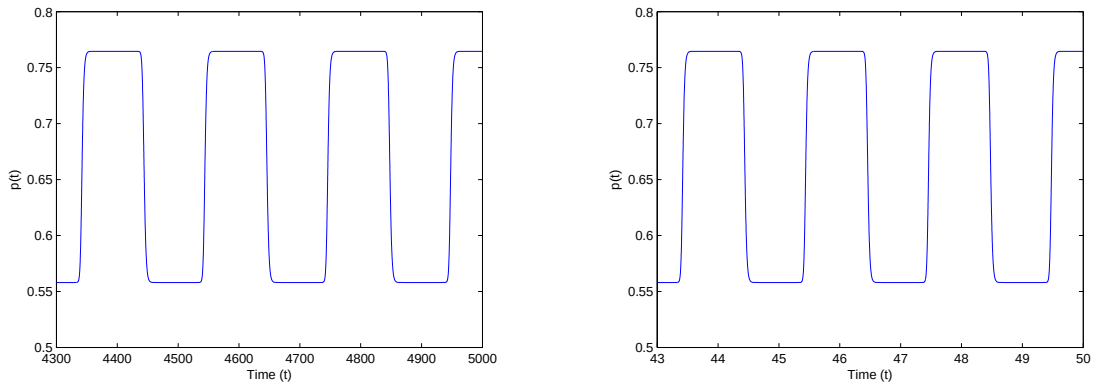


Figure 6.1: (a) Plot of equation (6.1) for $r = 3.1$ and $\tau = 100$. (b) Plot of equation(6.2) which is the rescaled form of (a).

In figure 6.1 we plotted the results for a delay of 100 and $r = 3.1$, we see that the plots show figures that are not like sine waves but rather produce square-like wave. This behaviour is not what was predicted by the weakly non-linear analysis carried out in chapter 2 for which sinusoidal waves are obtained. Since $\tau = 100$ was picked at random, let us pick different set of arbitrary values of $\tau = 6.3$, 20 and 60 and run a direct numerical plot of equation (6.2) to get a clearer picture of what transpired. From figure 6.2 the plot shows a growth in amplitude for τ to a certain amplitude, after this amplitude is reached any

further increase in the delay parameter results in a flat plateau, which increases as $\tau \to \infty$. Thus there are sinusoidal wave as observed until the amplitude is reached then we have a transition from sine wave to a square-like wave for any further increase in the delayed parameter.

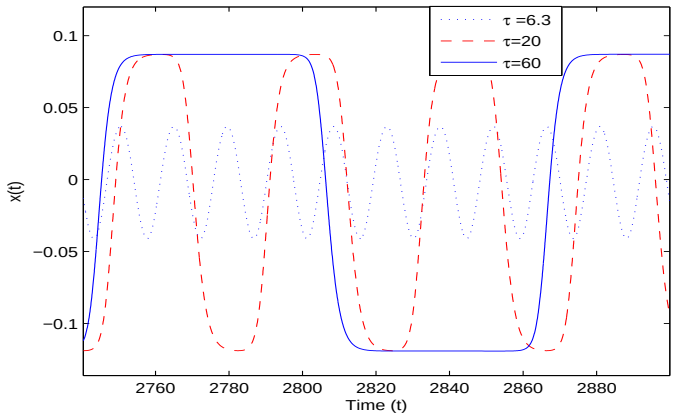


Figure 6.2: A plot of equation (6.1) for different values of delay, τ.

As the delay parameter increases the period also increases unlike the amplitude that reaches its maximum. The transition layers that connect these plateaux get steeper as $\tau \to \infty$ giving it a discontinuous look. The solution to equation (6.2) would take into account these plateaux and the transition layers which for $\varsigma \to 0$ corresponds to the maximum amplitude and a continuous growth of period oscillation for the corresponding value of the delay. This type of behaviour seen in figure 6.2 is known as relaxation oscillation where there is a fast phase and a slow phase displayed in the same model. Because it spends most of its time in the slow phase it is also called the slowly oscillating periodic solution (SOPS). The slow phase is the represented by the plateaux while the fast phase is the transition layer. This property is common in singularly-perturbed differential equations. Since $\tau \to \infty$ implies $\varsigma \ll 1$, equation (6.2) takes the form of a singularly-perturbed differential-delay equation. If the

equation (6.2) was an ordinary differential equation this would be approached using matched asymptotic expansion. The same technique would be applicable this our singularly differential-delay equation. This approach was applied by Wattis (2016), where he applied the asymptotic approximation to study the transition layers of this logistic equation. We shall compare our results with his.

We see that equation (6.2) collapse into logistic map when the delayed parameter gets as large as infinity, that is when $\varsigma = 0$, the logistic map

$$p_n = r\, p_{n-1}\,(1 - p_{n-1}), \tag{6.3}$$

with $p_n = p(t)$ and $p_{n-1} = p(t-1)$. The logistic map has the same fixed points as studied in chapter 2, that is 0 and $1 - 1/r$.

In chapter 2 we studied the steady states and showed that at $r_H = 3$ there is a Hopf bifurcation. At this point the steady states are unstable at $\varsigma = 0$ this map undergoes a period doubling bifurcation from which this map gives a period two fixed point.

These two fixed points are

$$p_{\pm} = \frac{r + 1 \pm \sqrt{(r+1)(r-3)}}{2\, r}. \tag{6.4}$$

This period two fixed point occurs for values of $3 < r \leq 3 + \sqrt{6}$. As the value of r increases further this fixed points become unstable and change to a period four fixed point emerges and if this continues we get period 8 and so on until we get a chaotic pattern. But we shall remain on the period two fixed point of the map and its corresponding differential-delay equation.

As we perturb equation (6.1) at steady state as $p = 1 - 1/r + x$ as done in

chapter 2 we had

$$\varsigma \frac{d}{dt}x(t) = -x(t) + (2-r)\,x(t-1) + r\,x^2(t-1), \tag{6.5}$$

from which we got equation (2.33) for the linear analysis for large delay, this is shown below

$$r_H \approx 3 + \frac{(k_1\,\pi\,\varsigma)^2}{2} + O(\varsigma^3) \tag{6.6}$$

where $k_1 = 2\,n + 1$ for $n = 0, 1, 2, 3, \cdots$. For most of the models we have analysed we have seen that for large delay the period of oscillation has a value of $2\tau + a'$, where a' is some constant. Can the relation between $r - \tau$ give more insight to the nonlinear model?

Since our equation (6.5) takes the form of a singular differential-delay equation, we shall adopt the method of matched asymptotic to study the dynamics of this equation.

6.2 Slow phase for the amplitude of the oscillation

After periodic doubling we can represent equation (6.5) would give us the solution to the model equation and give reasons why the curve transit from a sinusoidal wave to a square wave. Applying the method of matched asymptotic expansions we solve for the outer and inner solution. Just as in [56] for equation (6.5) at $0 < r < 4$ $x \in [0, 1]$ is mapped to $f \in [0, 1]$. The outer solution accounts for the slow phase, which represents the plateau. The leading term is derived when $\varsigma = 0$ gives the following equation

$$\begin{aligned} x_1(t) &= (2-r)\, x_2(t-1) + r\, x_2^2(t-1) \\ x_2(t) &= (2-r)\, x_1(t-1) + r\, x_1^2(t-1). \end{aligned} \tag{6.7}$$

Equation (6.7) has solutions which are independent of time hence it is equivalent to the steady solution which is

$$x_{1,2} = \frac{-r+3 \pm \sqrt{(r-3)(r+1)}}{2\,r} \tag{6.8}$$

The amplitude of the square wave is the difference between the two solution in equation (6.8) which gives

$$Amp = \frac{\sqrt{(r-3)(r+1)}}{r}, \tag{6.9}$$

where Amp is the amplitude of the square wave. Let $x_\pm = x_{1,2}$ represent both plateaux of the square wave which is the outer solution of equation (6.5), hence we have

$$f(\,x_\pm) = x_\mp \qquad \tau \to \pm\infty \tag{6.10}$$

A comparison of the value derived analytically in equations (6.8) and (6.9) with a direct numerical from equation (6.5) is shown in figure 6.3 for the value of $r = 3.1$ and an increasing delay. The value of the amplitude derived from equation (6.9) is given as 0.2066 which is equivalent to the amplitude in the direct numerical plot shown in the first plot of figure 6.3. The direct numerical plots in figure 6.3 used to compare the analytical solution was derived using the DDEbiftool which works with matlab.

Combining this result derived for the amplitude with the result derived in chapter 2 of the weakly nonlinear analysis, using the method of multiple time scale for values of r close to r_H and delayed parameter not too large. That is values which give sinusoidal waves still occur. Figure 6.4 shows all these

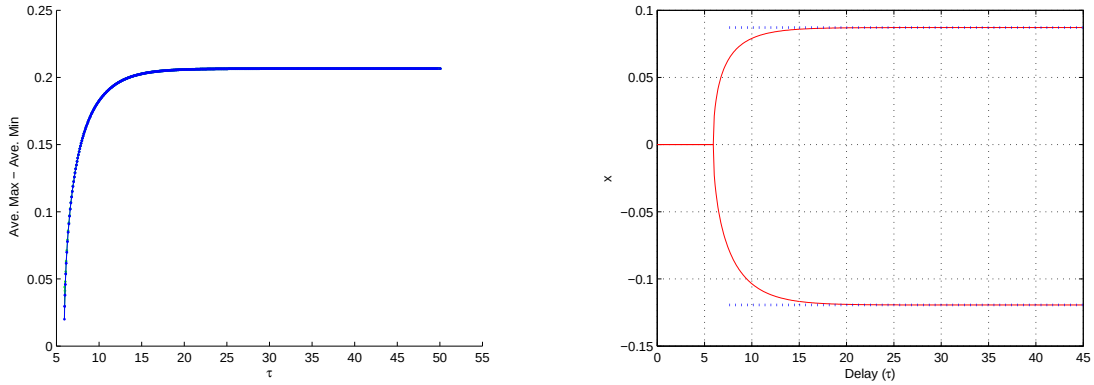


Figure 6.3: The plot of the amplitude of oscillation against the delay τ. (a) Amplitude of oscillation, (b) The direct numerical solution of equation (6.5) (red) and the large delay analysis from equation (6.8) (dotted blue) as $\tau \to \infty$ and $r = 3.1$.

plots and areas in which the analytic and the direct numerics agree. It shows that when the delayed parameter is close to the Hopf point the amplitude of oscillation is captured by the by the weakly non-linear analysis while for large delays the amplitude is captured using the outer solution of the matched asymptotic.

6.3 Fast phase-transition layer

Next we solve for the fast phase which is the transition layer that connects one plateau to another. From figure 6.2 we see that these transition gets steeper as $\varsigma \to 0$.

From the linear case analysed in chapter 2 equation (2.36) we saw that for large delay the period of oscillation tends to $2\tau + 2$. A good way to investigate if this result is the same for equation (6.5) is to solve this numerically. A direct numerical approach of solving for the transition layer would give the

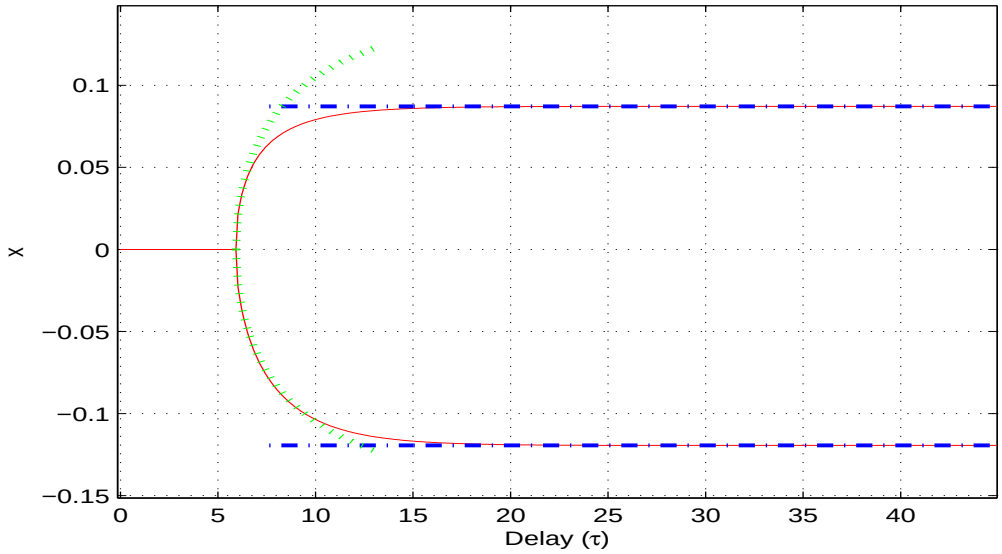


Figure 6.4: A total representation of the amplitude for equation (6.5), comparing direct numerics (red line), the analytical solution for delay parameter close to the bifurcation point (green dotted line) from equation (2.60a) and the analytical solution of large amplitude (blue dashed line) from equation (6.8). For $r = 3.1$, $\Delta = 2$ and $\epsilon = 0.1$.

exact value of the width between each transition layer. We then compare the period of oscillation with 2τ and deduce the general solution of the nonlinear equation. From figure 6.5 we see there is a slight difference between the linear and nonlinear period.

This difference is much clearer in figure 6.6 which shows that the period of oscillation tends to 2τ plus a constant a' and as $\varsigma \to 0$, the value of a' gets smaller as shown in the figure 6.6. From figure 6.6 we see that for values of $\varsigma \to 0$ the difference between the linear and the non-linear equation increases unlike the difference as the $\varsigma \to \infty$ where the difference is reduces very rapidly. In the other plots shown in figure 6.7 we see that as τ exceeds a certain value of τ the difference between the period and 2τ tends to a constant value. The

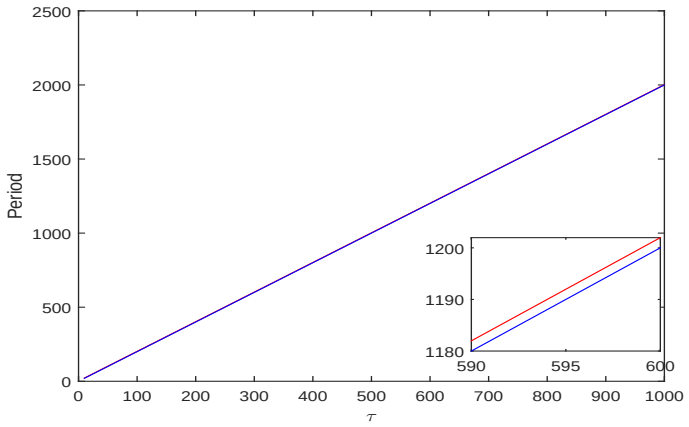


Figure 6.5: Plot of the period against delay, τ. Comparing the leading order term 2τ of period (blue line) and the direct numeric period (red line) of equation (6.5) with $r = 3.05$.

implication of this shows that as $\varsigma \to 0$ the period of oscillation tends to 2τ, implying that the transition layer tend to vertical lines. Thus making the sine wave a square wave.

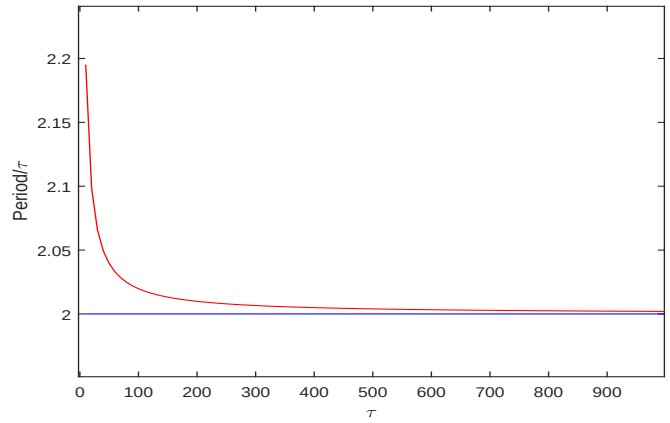


Figure 6.6: Plot of the period/τ as a function of the delay τ, from equation (6.5) for fixed $r = 3.05$.

We could further get the value of the difference in the period of oscillation

with respect to large delay as shown in figure 6.7 to further buttress this point. What is the value of " a' "? As stated in the beginning of this section one of our major goals is to derive the value of this constant a' which keeps occurring in addition to 2τ in periods with large delays. For a linear problem, to solve for the period of oscillation could be straight forward but for a nonlinear equation this might not necessarily be the case. The pictorial representation in the time plot showing the unknown parameter a' is shown in figure 6.8.

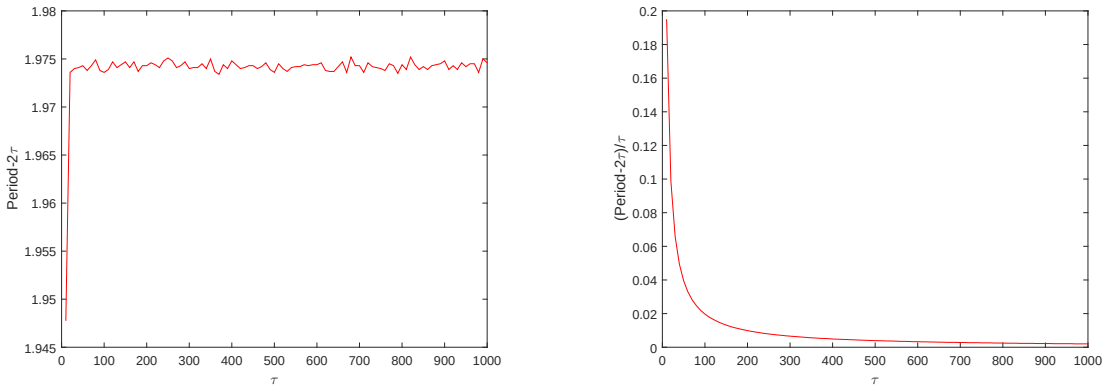


Figure 6.7: Left: plot of Period-2τ against delay, τ. Right: plot of (Period-2τ)$/\tau$ against delay, τ with $r = 3.05$, both periods of the figures on the left and right are from equation (6.5).

Since the period is $\approx 2\tau$, for simplicity let the correcting term a' be $2a$ such that half of the period is $\tau + a$. Let us assume that the reference point for the square wave is such that the distance between the transition layers are equal as shown in figure 6.8. From equation (6.5) we can represent the successive transition layer as $y(t)$ and $z(t)$ which are separated by a distance of $1 + a$. Let

$$y(t) = x(t); \quad z(t) = x(t - 1 - a), \tag{6.11}$$

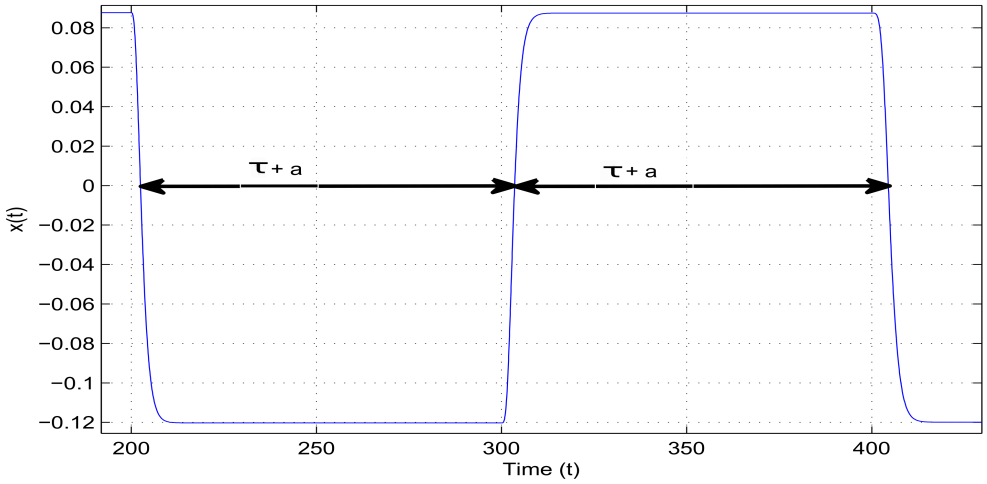


Figure 6.8: The square wave with a single period from equation (6.5).

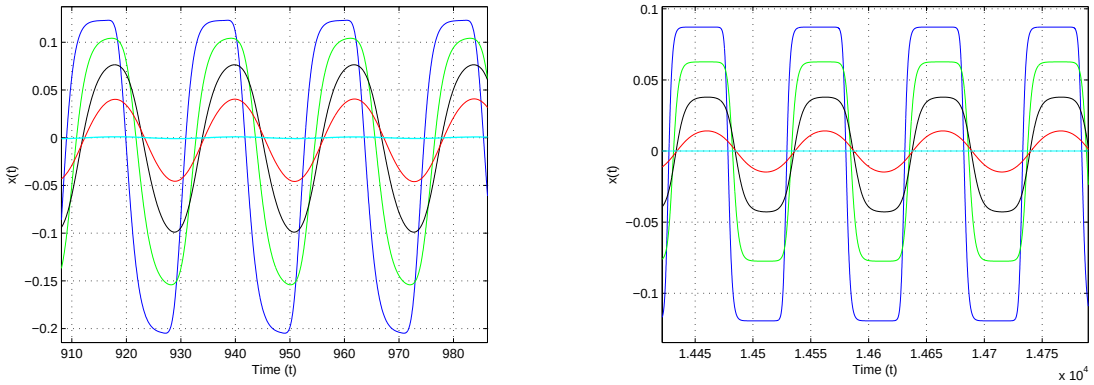
where $y(t)$ and $z(t)$ are successive transition layer see figure 6.8. Substituting equation (6.11) into (6.5) gives

$$\begin{aligned} \varsigma \frac{d}{dt} y(t) &= -y(t) + f(r, z(t+a)) \\ \varsigma \frac{d}{dt} z(t) &= -z(t) + f(r, y(t+a)). \end{aligned} \tag{6.12}$$

To derive an asymptotic solution for the fast phase which is the transition layer we have to solve for y, z the and the unknown variable a from two equations. The difficulty of solving for these three unknowns in two equation arises here because the model equation is a differential-delay equation.

We have looked at some direct numerics for a varying delayed parameter, before we go further into solving this equation we will also take a look at the effect of varying the second parameter r for a fixed delay. From figures 6.9, 6.10 and 6.11 we have taken the values of the delayed parameter as 10, 50, 100, 200 and 1000 for various values of r. There are several things to observe with these plots, first we can see that the amplitude keeps growing as the value of

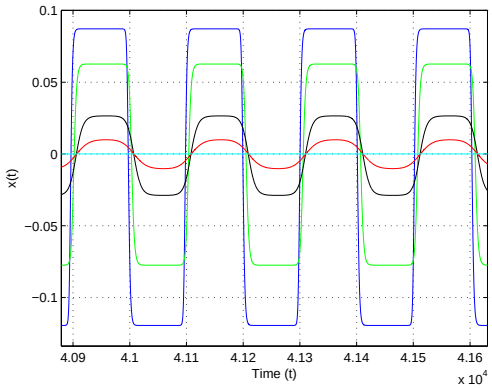
r increases unlike the when we varied the delayed parameter. We can also see that the period of oscillation has little or no increase as we increase the value of r which again is contrary to what transpired when the delay was increased. So we can say that the parameters r and τ does significantly affect the solution of our model in different ways.



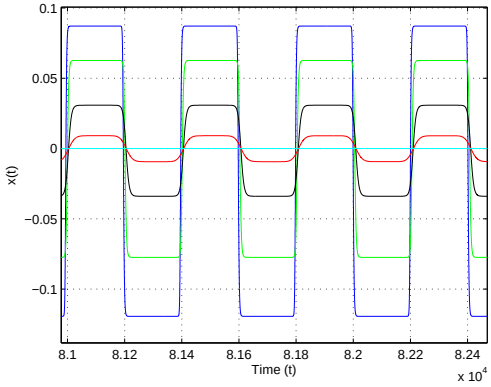
(a) For $\tau = 10$ and $r = 3.27$ (blue) $r = 3.17$ (green), $r = 3.095$ (black), $r = 3.055$ (red) and $r = 3.0$ cyan. $r_H = 3.0401$.

(b) For $\tau = 50$ and $r = 3.1$ (blue) $r = 3.045$ (green), $r = 3.015$ (black), $r = 3.0003$ (red) and $r = 2.8$ cyan. $r_H = 3.00189$.

Figure 6.9: The numerical plot of model (6.5) for varying values of r close to the Hopf bifurcation.



(a) For $\tau = 100$ and $r = 3.1$ (blue) $r = 3.045$ (green), $r = 3.007$ (black), $r = 3.00055$ (red) and $r = 2.8$ cyan. $r_H = 3.000483$.



For $\tau = 200$ and $r = 3.1$ (blue) $r = 3.045$ (green), $r = 3.0095$ (black), $r = 3.0002$ (red) and $r = 2.9$ cyan. $r_H = 3.000122$.

Figure 6.10: The numerical plot of model (6.5) for varying values of r close to the Hopf bifurcation.

Another important difference one would observe is that of the transition from sine wave to square when each of these parameter is varied as the other is fixed can be done by comparing figure 6.2 and figures 6.9 - 6.11. We see that the transition from sine-wave to square wave for a varied delay only takes place after the maximum amplitude has been achieved while for the varied r this transition is a continuum as r is increased. The red lines in figures 6.9 - 6.11 show sinusoidal waves patterns, above these red line square waves begin to emerge more evidently as r increases, and we have more sine waves as $r \to r_H$. r_H remains the Hopf bifurcation point of the model under study. After these sine waves we get decaying oscillation, which decay much rapidly $r < r_H$ decreases.

From our direct numerics we carefully inspect several values of r plotted to find where there is evidence of a flat surface and these values are marked for several

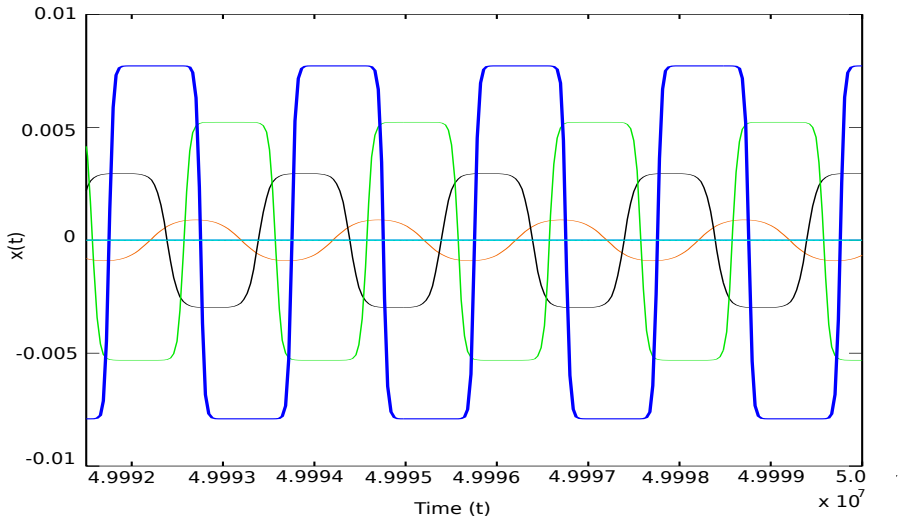


Figure 6.11: For $\tau = 1000$ and $r = 3.00055$ (blue) $r = 3.00025$ (green), $r = 3.00008$ (black), $r = 3.00001$ (red) and $r = 2.9$ cyan. $r_H = 3.00000493$. This is from equation (6.5).

delay values. These values of r marked are then plotted with its corresponding value of τ and the equation of this plots are we found to have the following transition scaling of

$$r \sim r_H + \frac{\beta}{\tau^2}, \tag{6.13}$$

where β is a positive constant which as it increase we see the transition from sine wave to square wave.

Hence for large fixed delay we have the square wave changing back into a sinusoidal wave as the values of $r \rightarrow r_H$. The period of oscillation tends to $2\tau + 2\,a$ for $r > r_H$, we will further investigate this shift. Again we will study this numerically by comparing the period of oscillation for the non-linear modelled equation with 2τ. From figure 6.12 we fix the value of the delay at 50 and varied r from 3 to 3.16, the two plots give the same details for the *period* against r and *period*/τ against r. A similar plot is derived for $\tau = 100$

in figure 6.14 and compared to the result for $\tau = 50$ in figure 6.12 and we see no major difference in structure but on the size of the period. In figure 6.13 and 6.15 shows the difference between the linear and non linear period as plotted and we see that both plots are exactly the same for $\tau = 50$ and $\tau = 100$.

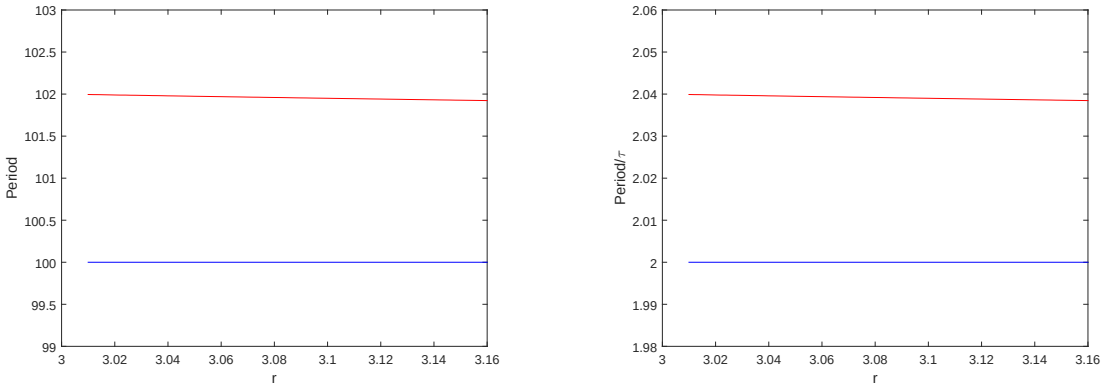


Figure 6.12: (a) A plot of the period against r from equation (6.5) (red line) in comparison with leading order term $2\,\tau$ from equation (2.36) (blue line). (b) A plot of the period/τ against r from equation (6.5) (red line) in comparison with leading order term $2\,\tau$ from equation (2.36) (blue line). For both figures $\tau = 50$.

From figures 6.12 and 6.15 we see that for a fixed delay as $r \to r_H$ the closer we get to 2 (that is $a \to 1$) and as we move away from the Hopf bifurcation point we move further away from the unknown constant being equivalent to 2. Since these are all points plotted by a continuous line we can solve for the slope of the line of best fit for the values plotted in figure 6.16.

From figures 6.16 applying the direct numerics we see a small decrease in period of oscillation when there is an increase in r. This clearly shows that the as $r \to r_H$ the difference in the period of oscillation tends to $2\tau + 2$. The equation from the line of best fit from figure 6.16 shows that for values close

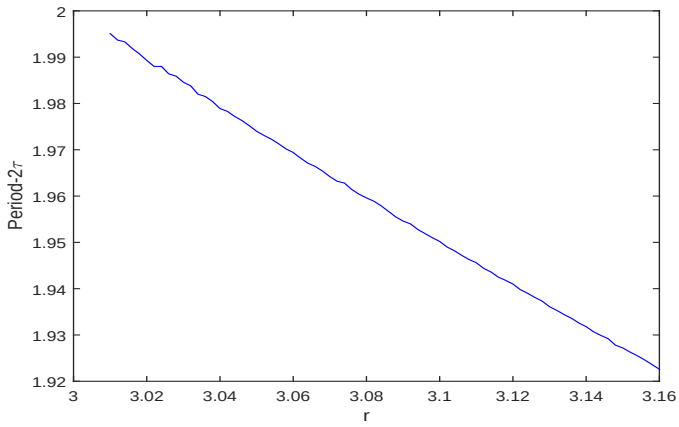


Figure 6.13: A plot of the difference between the period from (6.5) and $2\,\tau$ against r for fixed $\tau = 50$.

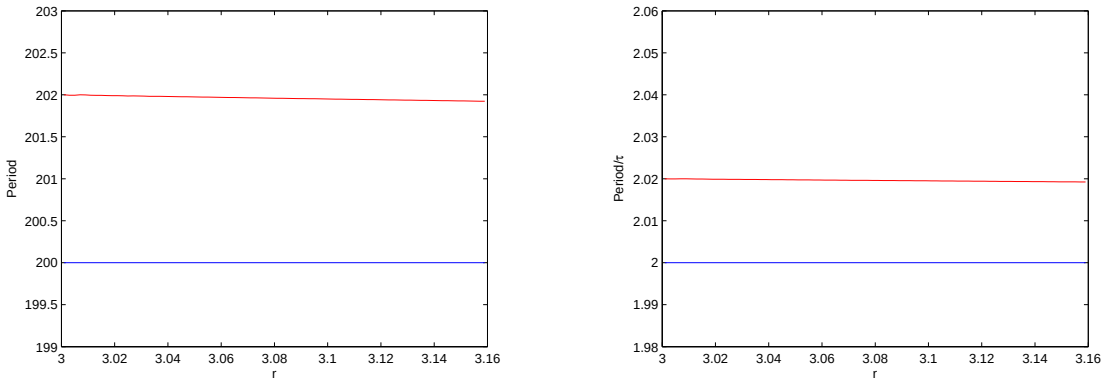


Figure 6.14: (a) A plot of the period against r from equation (6.5) (red line) in comparison with leading order term $2\,\tau$ from equation (2.36) (blue line). (b) A plot of the period/τ against r from equation (6.5) (red line) in comparison with leading order term $2\,\tau$ from equation (2.36) (blue line). For both figures $\tau = 100$.

to the Hopf bifurcation point for a delay having a value of $\tau = 50$ we obtain

$$Period \approx -0.53\,r + 102. \tag{6.14}$$

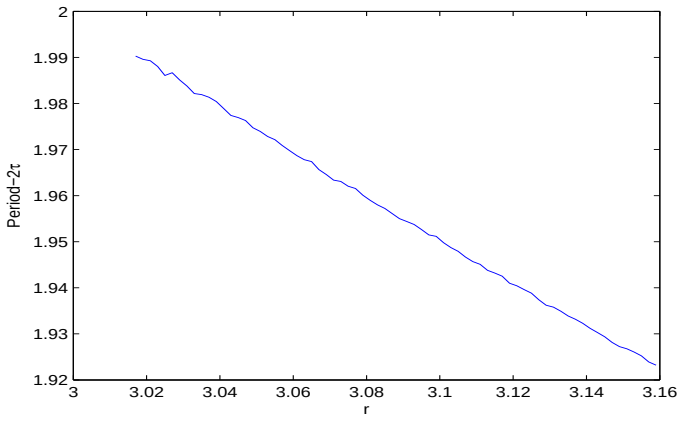


Figure 6.15: A plot of the difference between the period from (6.5) and 2τ against r for fixed $\tau = 100$.

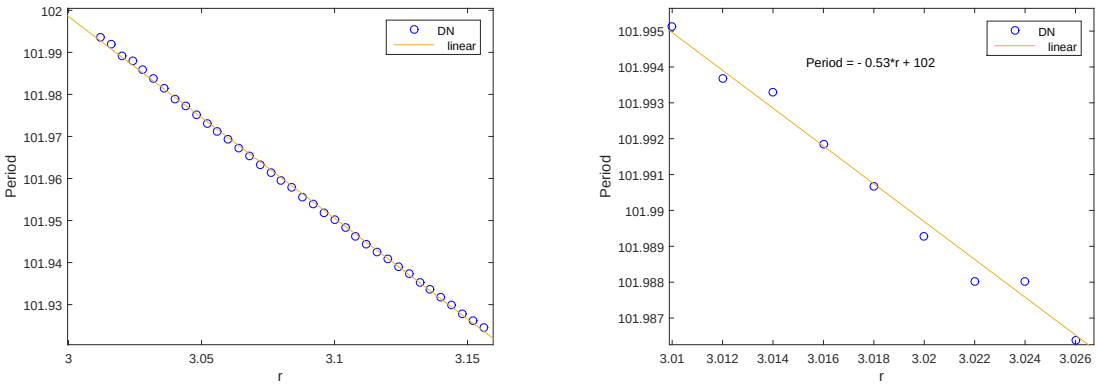


Figure 6.16: A plot of the period against r from equation (6.5). The 'blue o' is the value of the direct numerical plot while the red line is the linear line of best fit.

From the equation of the line of best fit for a fixed value of $\tau = 50$ and a varying r from 3 to 3.16 we get the intercept as 102 and the slope as -0.53. The only difference for $\tau = 100$ is the intercept which is 202. The question is can equation (6.14) be represented by both parameters r and τ? This equation gives us an approximate relation of the period of oscillation of the square wave

in terms of the two parameters, r and τ. The intercept of the slope can be represented as $2\tau + 2$ and since we begin from $r_H = 3$ we can represent the period of oscillation as

$$Period = 2\tau + 2 - 0.53\,(r - r_H) \tag{6.15}$$

Our result in equation (6.15) is the same as the result derived from Adhikari [69] who applied the Poincaré-Lindstedt. Adhakari applied the condition that the solution to the equation remain periodic instead of taking an asymptotic limit of $\tau \to \infty$. Equation (6.15)gives the values of the period of oscillation for large delay for a given r_H.

6.4 Conclusion

In conclusion we the value of the unknown parameter $2a = 2\varsigma - 0.53\,\varsigma\,(r - r_H)$. Comparing this value with the period of oscillation derive from the linear equation (2.36) in chapter 2 we see that for $r \to r_H$ the period of oscillation for the linear equation we have $2 + 2\varsigma - 2\varsigma^3 + O(\varsigma^4)$ while for the nonlinear equation we have $2 + 2\varsigma - 0.53\varsigma(r - r_H) + O(\varsigma^2)$ as $\varsigma \to 0$. The period for the linear equation is a function of ς while the period for the nonlinear equation is a function both parameter r and τ. Now that we have found the unknown parameter we can substitute into equation (6.12) and solve for the transition layers. We can compare the value of the period of oscillation derived here with that of other authors. Wattis [70] who analysed the shape of transition layers in this logistic differential-delay equation using strictly asymptotic techniques come to the same conclusion as we did. Other authour who had the same value as we did include [69], [71]. Secondly We have also identified the region in which this transition from a sine wave to a square wave occurs, but does this happen in all square differential- delay equation of this sort. In the next

chapter we shall be looking to analyse a more complex system in the same manner.

Chapter 7

Large delay in negative autogenous differential-delay model

In chapter 5 we analysed the negative autogenous regulation and gave the conditions for periodic oscillations to take place, these periodic oscillations take the form of sine waves. In section 4.1 we studied these parameters close to the Hopf bifurcation point. In this chapter we will investigate the effect of very large delay, that is $\tau \rightarrow \infty$ while we remain close to the Hopf bifurcation point as well. We will be analysing the original nonlinear equation as shown in equation (5.5). In the previous chapter we showed that the transcriptional delay τ_1 and the translational delay τ_2 can be represented by their sum. Hence we consider equation (5.5) in compact form as

$$\frac{d^2}{dt^2}\bar{x}(t) \; + \; (\mu_1 + \mu_2)\frac{d}{dt}\bar{x}(t) \; + \; (\mu_1\,\mu_2)\bar{x}(t) \; + f\left(\frac{\bar{x}(t-\tau)}{p_0}\right) = 0 \qquad (7.1)$$

where μ_1 is the bifurcation parameter and the parameter τ represents the sum of the translational and transcriptional delay. This model of negative autoge-

nous regulation has not been solved for large delay. In this chapter we will investigate the possible solution to this model and compare it to with numerical solution. Since the delay parameter tends to infinity, let the inverse of the delay be represented as $\varsigma = 1/\tau$ such that as $\tau \to \infty$ $\varsigma \to 0$. We rescaling equation (7.1) and represent it as a singular differential-delay equation, hence we now have a second order singular differential-delay equation. Let $t = t\tau$ such that in compact form this transforms equation (7.1) to

$$\varsigma^2 \frac{d^2}{dt^2}\bar{x}(t) + \varsigma(\mu_1 + \mu_2)\frac{d}{dt}\bar{x}(t) + (\mu_1\,\mu_2)\bar{x}(t) + f\left(\frac{\bar{x}(t-1)}{p_0}\right) = 0 \qquad (7.2)$$

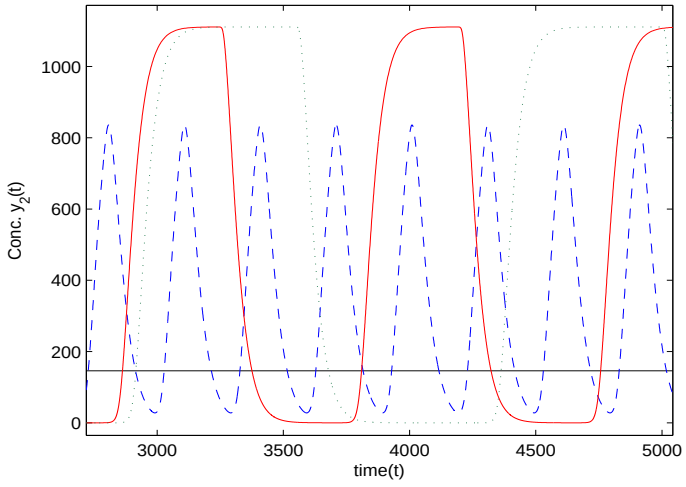


Figure 7.1: (a) A plot for $\mu_2 = \mu_1 = 0.03$ with arbitrary values of delay. For $\tau = 15$-black solid line, $\tau = 80$- blue dashed lines, $\tau = 400$- red solid line and $\tau = 650$- green dotted line.

Equation (7.2) does take on the form of a second order singular differential-delay equation. To study this model for large delay we shall be applying matched asymptotic. A plot of the system under study is shown in figure (7.1). We see square waves with steeper transition layer emerge as the delayed parameter $\varsigma \to 0$. This is similar to what occurred in chapter 6 for the

population model hence we will follow a similar trail and give more detailed solution to the negative autogenous regulatory model (NAR). Recall from the literature review that an autogenous regulation or autoregulation is when a gene or mRNA either promotes or represses itself. We shall continue with the analysis of a mRNA repressing itself through its transcription factor.

The property displayed by the model is called the relaxation oscillation in which we have a slow phase and a fast phase. The slow phase is represented by the plateaux and the transition layer is represented by the fast phase. In ordinary differential equation these type of equations are studied using matched asymptotic called the boundary layer theory. We will be applying this same technique since it gives us the ability to segment the model into slow and fast phases thus simplifying the system. We start the next section by solving for the slow phase

7.1 Slow phase of a periodic oscillation

As the $\varsigma \to 0$ we can see from figure 7.1 that there is a transition from the sine to square wave type of periodic oscillation. Figure 7.2 shows this square wave structure,
Substituting $\varsigma \to 0$ into equation (7.2), this gives

$$\varsigma^2 \frac{d^2}{dt^2}x(t) + \varsigma(\mu_1 + \mu_2)\frac{d}{dt}x(t) + (\mu_1\,\mu_2)x(t) + f\left(\frac{x(t-1)}{p_0}\right) = 0 \qquad (7.3)$$

The simplest form of dynamical system is a map. If this is represented by a map the model gives rise to oscillatory solutions of period approximately 2 unlike the logistic model the negative autogenous regulatory model does not give rise to oscillatory solutions of period 4, 8 and so on. For the slow phase of

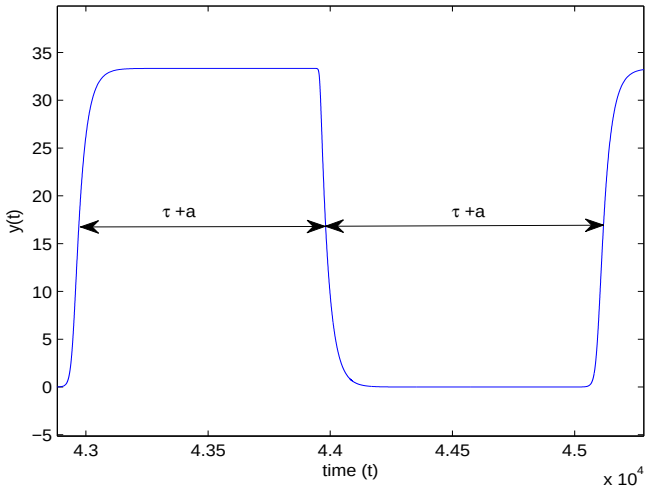


Figure 7.2: One period of oscillation with delay as $\tau = 1000$ and $\mu = 0.03$.

our singularly-perturbed differential-delay equation we make the assumption that $\varsigma = 0$. When this happens equation (7.3) collapses into a one dimensional map with period two-cycle, that is

$$\begin{aligned}(\mu_1\,\mu_2)x_1(t) &= f\left(\frac{x_2(t-1)}{p_0}\right),\\ (\mu_1\,\mu_2)x_2(t) &= f\left(\frac{x_1(t-1)}{p_0}\right).\end{aligned} \tag{7.4}$$

Equation (7.4) can be explicitly represented for the period 2 cycle from equation (7.3) as follows,

$$\begin{aligned}\mu_1\,\mu_2\,x_1 &= \frac{p_0^n}{p_0^n + x_2^n(t-1)},\\ \mu_1\,\mu_2\,x_2 &= \frac{p_0^n}{p_0^n + x_1^n(t-1)},\end{aligned} \tag{7.5}$$

where $x_1(t)$ and $x_2(t)$ represent the plateaux of the first oscillatory state, which is the two-cycle. At steady state, the solution to equation (7.5) depends on the value of n. If n is large then because of the order of the polynomial the solution has to be derived numerically but if the polynomial has an order < 3 then we

can easily solve for the roots of the polynomial. We shall be comparing the solutions from equation (7.5) with direct numerical simulations in section 7.2. From equation (7.5) at $\varsigma = 0$ we have our model reduced to a map, but what happens when values of $0 < \varsigma \ll 1$? From figure 7.1 we see transition from sine wave to a square wave as the $\tau \to \infty$ ($\varsigma \to 0$), these plateaux increased in length as the delay is increase while the transition layer gets steeper.
From equation (7.5) for given values of μ_1, μ_2, n and p_0 we would be able to solve for the slow sate which will represent the flat surface. We also need to solve for the fast transition layer and this would be analysed in the next section.

7.1.1 Fast phase

Now we move to the transition layers that connect these plateaux. These connections exhibit much faster dynamics than the plateaux. From figure 7.2 we can make the same argument as made in chapter 5 that any two consecutive transition layers are separated by a distance that is greater than $2\,\tau$ by some constant, which we call a'. From the previous chapter we saw that a' tends to 0 as $\varsigma \to 0$ because the steepness of the transition layer increases, we would have to solve for a' to be able to get the solution to the transition layers. But first we would like our model to capture this small shift a' to enable us to solve it. Later on in this chapter we will attempt to solve the period of oscillation using the technique derived by Adhikari [69] and Wattis [70] by letting equating the nonlinear term to take the form of the logistic differential-delay equation. At the end we shall compare the results obtained numerically and those derived from the logistic-like equation. We apply the same numerical simulation as in the previous chapter.

7.2 Numerical solution

Direct numerics is one of the best ways solving a lot of mathematical problems. A pictorial representation of this solution gives one the a visual representation of such a solution. The choice of making use of this method in this model guarantees high accuracy.

From figure 7.1 we see the transition from sinusoidal waves to square waves. When the amplitude of these sine waves gets to a certain level these plateaux emerge and, rather than increase in height, their width expands. We solved for the plateaus in our analysis, in the figure 7.3 the numerics show that the plateaus of this equation are correctly given by the outer solution for large delay.

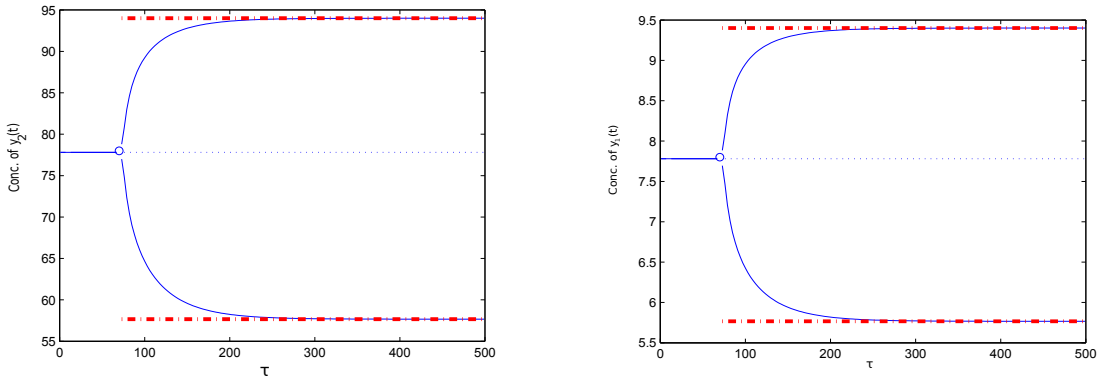


Figure 7.3: The bifurcation plot of the NAR, the blue lines are from the numerics while the red dash-dot lines are from the analysis carried out in section 7.1 for $\mu = 0.1$, $n = 10$ and $p_0 = 100$.

For a fixed value of $\mu = 0.1$ varying the value of the delayed parameter the analysis of section 7.1 equation (7.5) shows a lower plateau value of 5.7666 and the higher plateau at 9.4005 giving an amplitude of 3.5339. This amplitude numerically derived shows the same values and the amplitude is shown in figure 7.4. The outer solution of the matched asymptotic matches the numerical

solution, but as the value of n increase then even the outer solution would have to depend on some level of numerics for its solution.

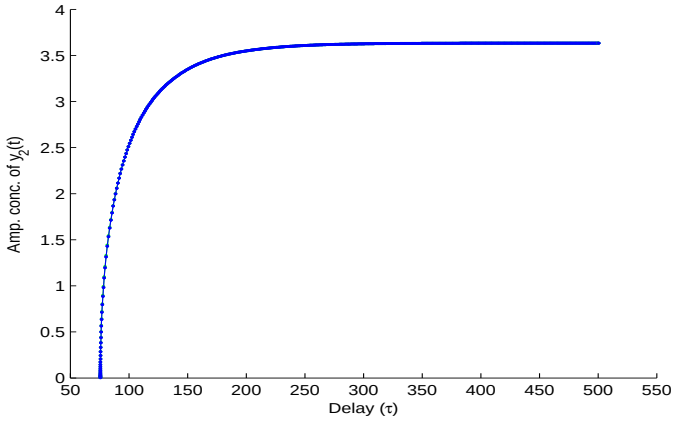


Figure 7.4: (a) Amplitude plot for a fixed $\mu = 0.1$ and the bifurcating parameter τ

Figures 7.3 and 7.4 are numerically plotted using the continuation package DDE biftool [64] and corresponds to the difference between the lower and upper limit of our analysis of the slow phase. Now that we have shown that the outer solution correctly matches equation (5.5) we try to do the same for with numerical comparison of the period of oscillation. In the numerics we compare the period of oscillation of the original model to the linear period of $2\,\tau$. A particular case with the delay as large as 1000 and the decay as 0.03, is shown in figure 7.2.

From figure 7.2 we see that the period of oscillation is just a bit larger than twice the value of the delay hence comparing the numerics of the original model equation (5.5) with $2\,\tau$ is appropriate. Let the additional shift be $'\tilde{a}'$, so the period P would be

$$P = 2\,\tau + \tilde{a}. \tag{7.6}$$

From the numerics we will solve for the value of the additional shift $'\tilde{a}'$. There are two parameters we begin by comparing the period of oscillation for a fixed delay having a value of 500 and μ acting as the varying parameter. From figure 7.5 we see that the period of oscillation formed as we vary μ is not linear for the original equation as obtained in chapter 6. We will analyse the curve generated in figure 7.5.

In figure 7.5 there are three points that draw our attention, the first is the small point on the red curve which has a negative slope. This point indicates the area where periodic oscillation does not take place, hence a stable steady state occurs at that point. The second region on the red line is the curve of the form $1/x$ which displays the region where oscillations occur and finally the region with a quick drop to zero which again represents a region without oscillation. These results indicate the model actually captures very good properties that

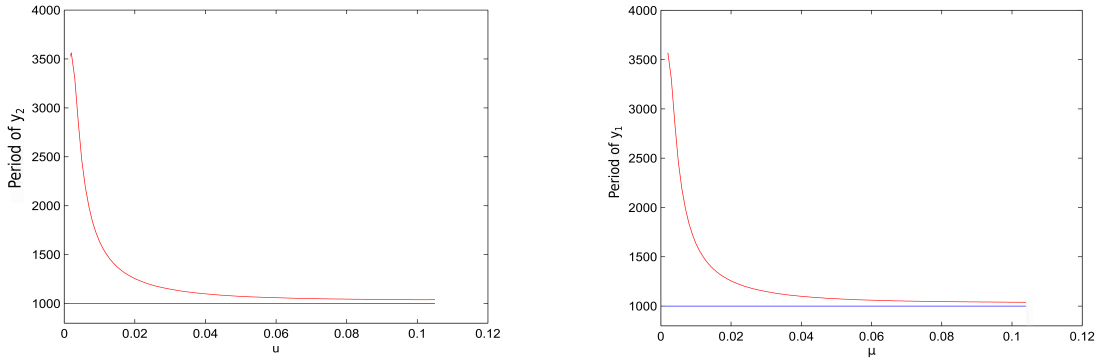


Figure 7.5: For a fixed delay $\tau = 500$, the period of oscillation is plotted against the decay with the red line as the nonlinear equation (5.5) and the blue as 2τ.

should be expected. In the first region where there is insufficient decay, there would be a burst in gene expression such that the resources would be over stretched in the long run and hence the expression of the gene dies out in a short time. In the second region there is some decay hence when there is excess resources the gene does very well and when the resources are exhausted the gene decays, this process continues except interrupted. And in the third region there is excessive decay hence the gene does not get to be expressed before it is taken out of the system. Hence the change from damped oscillation to periodic oscillation back to a non oscillating system can be explained by the fact that if more substance is taken out of a system before it can be expressed then that gene cannot express itself.

Figure 7.6 which is the difference between the period for the non linear and 2τ shows the point we are making with figure 7.5 in a better way, and since we can not have negative period of oscillation, we can say that the period goes to zero which shows that $\tilde{a}$ is independent of μ.

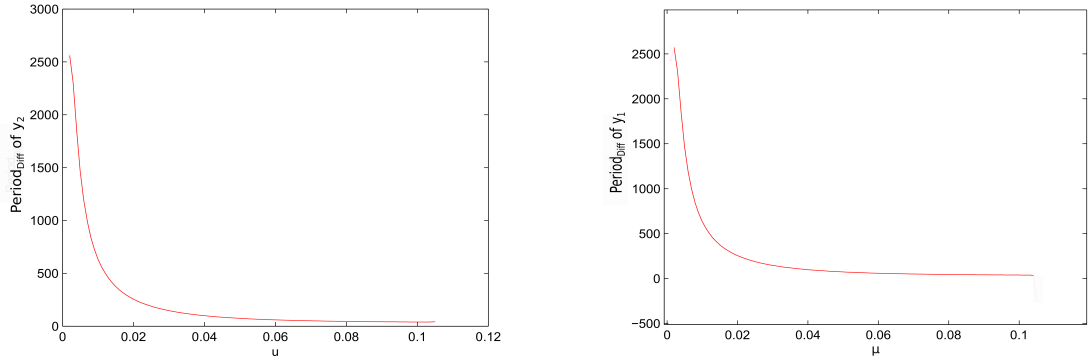


Figure 7.6: A direct numerical plot of equation (5.5) for the Period-2τ against the decay μ with a fixed delay $\tau = 500$.

The next set of numerics uses the delay τ as the varying parameter while the decay μ is kept fixed. Figure 7.7 shows the plot with τ as the varying parameter and we see that there is an obvious difference between the leading order term 2τ and the nonlinear numerics of equation (5.5). This implies that we have a certain shift $'a'$ added to the linear large period of oscillation 2τ.

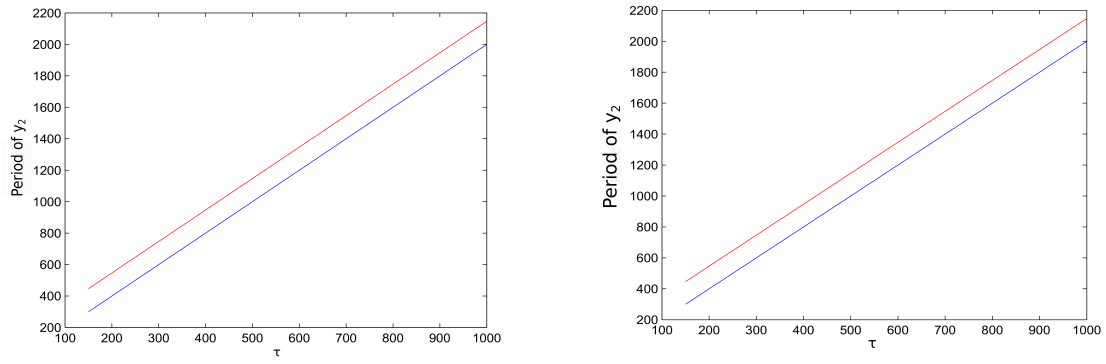


Figure 7.7: For a fixed decay $\mu = 0.1$, the period of oscillation is plotted against the delay. The blue line is 2τ and the red line is the nonlinear plot of equation (5.5).

We will plot the the difference of the linear $2\,\tau$ and the nonlinear equation to

deduce any type of information from it. Figure 7.8 which shows the difference in the period justifies this claim that the linear $2\,\tau$ should have an additional term to bridge this gap. In this plot of the difference between the linear and non-linear period, there are two regions of interest. At the initial stage the value of the period increases rapidly but after a certain value of the delay , τ the period of oscillation tend to cluster around a particular value. For $\mu = 0.1$ this cluster value of the periodic difference is 147.1 as shown in the figure 7.8.

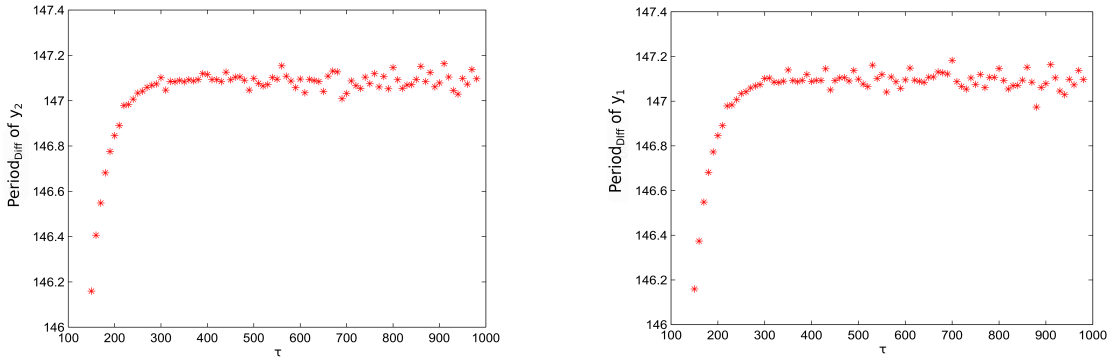


Figure 7.8: A plot of the Difference between the leading order term 2τ and nonlinear period of oscillation from equation (5.5) for a fixed $\mu = 0.1$ while varying τ.

If the periodic difference tends to some constant value, can the ratio of the non-linear period give us more details? A plot of the $period/\tau$ for a fixed delay shown in figure (7.9) shows that there would be decreasing curve of the form $1/x$ as the value of the delay increases. From this figure we have that the $period/\tau$ keeps on decreasing as $\tau \to \infty$, the ratio of the period tends towards 2.

A similar plot is shown for a fixed τ and a varying decay in the second plot of figure 7.9 which is steeper than the varying delay plot. In figure 7.8 we saw that when the rate of decay is 0.1 the period of oscillation tends to a value of 147.1 but is this true for all values of μ? Let us find out how the value of the decay affects this period by fixing different values of decay.

In figure 7.10 we see that as the value of μ increases the difference in the period of oscillation between the nonlinear equation (5.5) and 2τ also increases. This implies that the period of oscillation is not just a function of the delayed parameter but also the decay parameter. For the unknown shift $'a'$ which accounts for the transition layer, from our numerics so far we see that it is a function that depends on two parameters μ the decay rate and τ the time

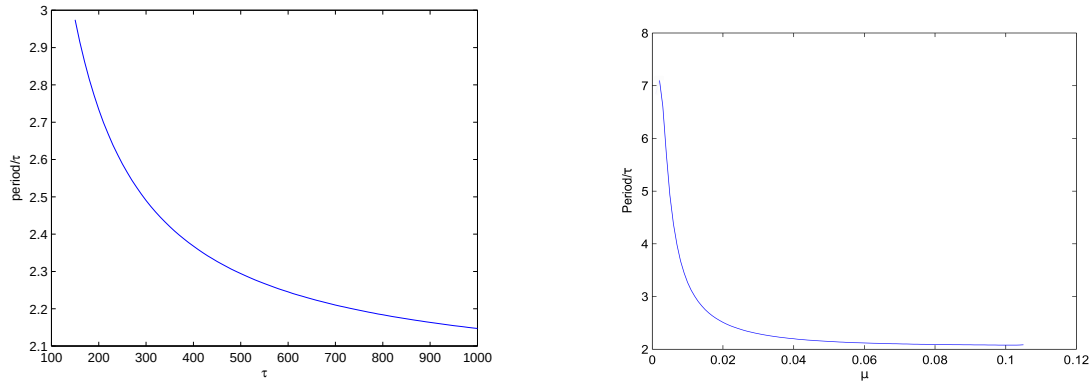


Figure 7.9: A plot of equation (5.5) of the *period*/τ plotted against μ for $\tau = 500$ is on the RHS and on the LHS it is plotted against the delay τ for $\mu = 0.1$.

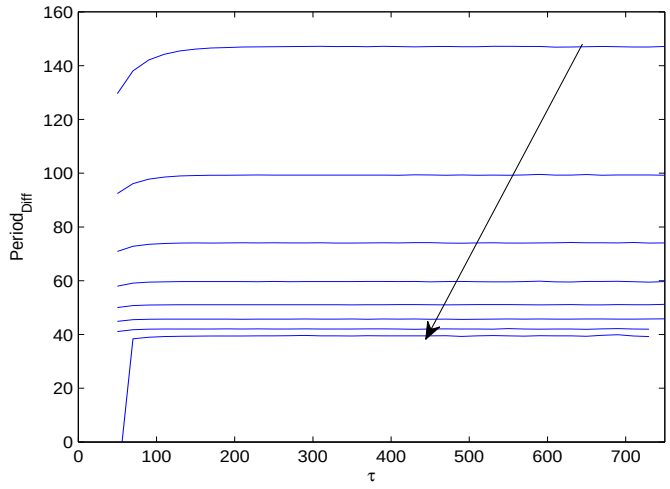


Figure 7.10: Plot of the difference between the nonlinear period minus 2τ against the delay τ for different fixed μ from 0.03 to 0.1. The arrow moves highest value of μ to the lowest.

delay. For simplicity we have taken both decay parameters to be the same but this might not be the case at all times.

$$Period = 2\,\tau + 147. \tag{7.7}$$

From our numerics, the equation (7.7) defines the period of the non-linear equation, hence from this equation we can determine the value of the unknown shift for large delay. From this equation one can derive the value of the period given the value of the delay and the decay.

7.2.1 Fast phase using a Taylor expanded non-linear terms

Now we move to the transition layers applying the same technique as Adhikari [69] and Wattis [70] by equating the nonlinear term to take the form of the logistic differential-delay equation. At the end we shall compare the results with the numerical derived in previous sections.

$$x_1(t) = x(t), \qquad x_2(t) = x(t-1-a), \tag{7.8}$$

where $a' = a/2$ and because this is $2\tau + 2a$ periodic it implies

$$\begin{aligned} x_1(t) &= x_2(t-1-a) = x_2(t+1+a), & x_1(t-1) &= x_2(t+a) \\ x_2(t) &= x_1(t-1-a) = x_1(t+1+a), & x_2(t-1) &= x_1(t+a) \end{aligned} \tag{7.9}$$

we now substitute these into equation (7.3) and we get two second order differential-delay equations from the single second order differential-delay equation as shown in equation (7.10)

$$\begin{aligned}
\varsigma^2\frac{d^2}{dt^2}x_1(t) \,+\, \varsigma(\mu_{1_H}+\mu_2)\frac{d}{dt}x_1(t) \,+\, (\mu_{1_H}\,\mu_2)x_1(t) \,&=\, K\,x_2(t+a) \,-\, L\,x_2^2(t+a)\\
\varsigma^2\frac{d^2}{dt^2}x_2(t) \,+\, \varsigma(\mu_{1_H}+\mu_2)\frac{d}{dt}x_2(t) \,+\, (\mu_{1_H}\,\mu_2)x_2(t) \,&=\, K\,x_1(t+a) \,-\, L\,x_1^2(t+a)
\end{aligned} \tag{7.10}$$

To analyse the fast transition layer it is important to represent its expansion as a stretch variable and not necessarily the original time variable. Let $t = \varsigma T$ and $a = \varsigma\alpha$ which imply that $\varsigma d/dt = d/dT$ and $X_1(T) = x_1(t)$ and $X_2(T) = x_2(t)$, substituting these rescaling into equation (7.10) we get

$$\begin{aligned}
\frac{d^2}{dT^2}X_1(T) \,+\, (\mu_{1_H}+\mu_2)\frac{d}{dT}X_1(T) \,+\, (\mu_{1_H}\,\mu_2)X_1(T)&\\
=\, K\,X_2(T+\alpha) \,-\, L\,X_2^2(T+\alpha)&\\
\frac{d^2}{dT^2}X_2(T) \,+\, (\mu_{1_H}+\mu_2)\frac{d}{dT}X_2(T) \,+\, (\mu_{1_H}\,\mu_2)X_2(T)&\\
=\, K\,X_1(T+\alpha) \,-\, L\,X_1^2(t+\alpha)&
\end{aligned} \tag{7.11}$$

By inspecting figure 7.1 we see that we basically have two types of transition layer, one with a positive slope and the other with a negative slope. Both of these slopes tend to be undefined since they become vertical as $\varsigma \,\to\, 0$ and hence making the period tend to 2τ as $\varsigma \,\to\, 0$. As in chapter 6 we would like to find the connecting transition layer from one plateau to another, let $X_1(T) \,=\, M + \,(A/2)\,Y(t)$ and $X_2(T) \,=\, M - \,(A/2)\,Z(t)$ where

$$M = \frac{K+\mu_1\,\mu_2}{2\,L}, \qquad\qquad A = \frac{\sqrt{(K+\mu_1\,\mu_2)\,(K-3\mu_1\,\mu_2)}}{L}, \tag{7.12}$$

such that $Y(T)$, $Z(T) \,\to\, \pm 1$ as $T \,\to\, \pm\infty$. Substituting into equation (7.11) we get

$$\begin{aligned}
\frac{d^2}{dT^2}Y(T) \;+\; (\mu_{1_H}+\mu_2)\frac{d}{dT}Y(T) \;+\; (\mu_{1_H}\,\mu_2)Y(T) \;=\; (\mu_{1_H}\,\mu_2)Z(T+\alpha) \\
+\; \frac{A\,L}{2}\,(Z^2(T+\alpha)-1), \\
\frac{d^2}{dT^2}Z(T) \;+\; (\mu_{1_H}+\mu_2)\frac{d}{dT}Z(T) \;+\; (\mu_{1_H}\,\mu_2)Z(T) \;=\; (\mu_{1_H}\,\mu_2)Y(T+\alpha) \\
-\; \frac{A\,L}{2}\,(Y^2(T+\alpha)-1),
\end{aligned} \tag{7.13}$$

where A is the amplitude of oscillation as described in equation (6.7). The point of focus is the limit as $K \to 3\mu_1\mu_2$ so that $A \ll 1$ as we investigate the inner solution of the boundary layer problem. Let $\delta = \sqrt{K-3\,\mu_1\,\mu_2}$ such that $\delta \ll 1$, we can further rescale equation (7.13) by letting $T = \delta s$, $\alpha = \delta v$ and $Y(T) = y(s)$, $Z(T) = z(s)$ and substituting into equation (7.13)

$$\begin{aligned}
\delta^2\frac{d^2}{ds^2}y(s) \;+\; \delta(\mu_{1_H}+\mu_2)\frac{d}{ds}y(s) \;+\; (\mu_{1_H}\,\mu_2)y(s) \;=\; (\mu_{1_H}\,\mu_2)z(s+u) \\
+\; \delta\;(z^2(s+u)-1)\,\frac{\sqrt{K+\mu_1\mu_2}}{2} \\
\delta^2\frac{d^2}{ds^2}z(s) \;+\; \delta(\mu_{1_H}+\mu_2)\frac{d}{ds}z(s) \;+\; (\mu_{1_H}\,\mu_2)z(s) \;=\; (\mu_{1_H}\,\mu_2)y(s+u) \\
-\; \delta\;(y^2(s+u)-1)\frac{\sqrt{K+\mu_1\mu_2}}{2},
\end{aligned} \tag{7.14}$$

Applying the asymptotic expansion let

$$\begin{aligned}
y(s) &= y_0(s)+\delta y_1(s)+\delta^2 y_2(s)+\delta^3 y_3(s)+O(y^4), \\
z(s) &= z_0(s)+\delta z_1(s)+\delta^2 z_2(s)+\delta^3 z_3(s)+O(z^4), \\
v &= v_0 \;+\; \delta v_1 \;+\; \delta^2 v_2 \;+\; \delta^3 v_3 \;+\; O(v^4),
\end{aligned} \tag{7.15}$$

and as $K \to 3\mu_1\mu_2$ we have

$$\sqrt{K+\mu_1\,\mu_2} = \sqrt{\mu_1\mu_2}\left(2+\frac{\delta^2}{4\mu_1\mu_2} \;-\; \frac{\delta^4}{(8\mu_1\mu_2)^2}+\frac{\delta^6}{(8\mu_1\mu_2)^3}+O\left(\delta^7\right)\right). \tag{7.16}$$

Simplifying and substituting equations (7.15)-(7.16) into equation (7.14) we get the following by collecting the coefficients of the power in order of δ which is equal on the left and right hand side of equations gives

$O(1)$

$$\begin{aligned} y_0(s) &= z_0(s) \\ z_0(s) &= y_0(s) \end{aligned} \tag{7.17}$$

$O(\delta)$

$$\begin{aligned} \left(\frac{\mathrm{d}}{\mathrm{d}s} y_0(s)\right)(\mu_1+\mu_2) + \mu_1\mu_2 y_1(s) &= \left(z_1(s) + \left(\frac{\mathrm{d}}{\mathrm{d}s} z_0(s)\right) v_0\right)\mu_1\mu_2 \\ &\quad + \sqrt{\mu_1\mu_2}\left(\left(z_0(s)\right)^2 - 1\right) \\ \left(\frac{\mathrm{d}}{\mathrm{d}s} z_0(s)\right)(\mu_1+\mu_2) + \mu_1\mu_2 z_1(s) &= \left(y_1(s) + \left(\frac{\mathrm{d}}{\mathrm{d}s} y_0(s)\right) v_0\right)\mu_1\mu_2 \\ &\quad - \sqrt{\mu_1\mu_2}\left(\left(y_0(s)\right)^2 - 1\right) \end{aligned} \tag{7.18}$$

$O(\delta^2)$

$$\begin{aligned} L(y_0) &= \left(z_2(s) + \left(\frac{\mathrm{d}}{\mathrm{d}s} z_0(s)\right) v_1 + \left(\frac{\mathrm{d}}{\mathrm{d}s} z_1(s)\right) v_0 + \left(\frac{\mathrm{d}^2}{\mathrm{d}s^2} z_0(s)\right)\frac{{v_0}^2}{2}\right)\mu_1\mu_2 \\ &\quad + 2\sqrt{\mu_1\mu_2} z_0(s)\left(z_1(s) + \left(\frac{\mathrm{d}}{\mathrm{d}s} z_0(s)\right) v_0\right) \\ L(z_0) &= \left(y_2(s) + \left(\frac{\mathrm{d}}{\mathrm{d}s} y_0(s)\right) v_1 + \left(\frac{\mathrm{d}}{\mathrm{d}s} y_1(s)\right) v_0 + \left(\frac{\mathrm{d}^2}{\mathrm{d}s^2} y_0(s)\right)\frac{{v_0}^2}{2}\right)\mu_1\mu_2 \\ &\quad - 2\sqrt{\mu_1\mu_2} y_0(s)\left(y_1(s) + \left(\frac{\mathrm{d}}{\mathrm{d}s} y_0(s)\right) v_0\right) \end{aligned} \tag{7.19}$$

$O(\delta^3)$

$$
\begin{aligned}
L(y_1) &= \left(z_3(s) + \left(\frac{\mathrm{d}}{\mathrm{d}s} z_0(s)\right) v_2 + \left(\frac{\mathrm{d}}{\mathrm{d}s} z_1(s)\right) v_1 + \left(\frac{\mathrm{d}}{\mathrm{d}s} z_2(s)\right) v_0 + \left(\frac{\mathrm{d}^2}{\mathrm{d}s^2} z_0(s)\right) v_0 v_1 + \left(\frac{\mathrm{d}^2}{\mathrm{d}s^2} z_1(s)\right) \frac{{v_0}^2}{2}\right. \\
&\quad + \left(\frac{\mathrm{d}^3}{\mathrm{d}s^3} z_0(s)\right) \frac{{v_0}^3}{6}\Bigg) \mu_1\mu_2 + \sqrt{\mu_1\mu_2}\left(2\, z_0(s)\left(z_2(s) + \left(\frac{\mathrm{d}}{\mathrm{d}s} z_0(s)\right) v_1 + \left(\frac{\mathrm{d}}{\mathrm{d}s} z_1(s)\right) v_0\right.\right. \\
&\quad \left.\left. + \left(\frac{\mathrm{d}^2}{\mathrm{d}s^2} z_0(s)\right) \frac{{v_0}^2}{2}\right) + \left(z_1(s) + \left(\frac{\mathrm{d}}{\mathrm{d}s} z_0(s)\right) v_0\right)^2\right) + \frac{\sqrt{\mu_1\mu_2}\left(\left(z_0(s)\right)^2 - 1\right)}{8\,\mu_1\mu_2} \\
L(z_1) &= \left(y_3(s) + \left(\frac{\mathrm{d}}{\mathrm{d}s} y_0(s)\right) v_2 + \left(\frac{\mathrm{d}}{\mathrm{d}s} y_1(s)\right) v_1 + \left(\frac{\mathrm{d}}{\mathrm{d}s} y_2(s)\right) v_0 + \left(\frac{\mathrm{d}^2}{\mathrm{d}s^2} y_0(s)\right) v_0 v_1 + \left(\frac{\mathrm{d}^2}{\mathrm{d}s^2} y_1(s)\right) \frac{{v_0}^2}{2}\right. \\
&\quad + \left(\frac{\mathrm{d}^3}{\mathrm{d}s^3} y_0(s)\right) \frac{{v_0}^3}{6}\Bigg) \mu_1\mu_2 - \sqrt{\mu_1\mu_2}\left(2\, y_0(s)\left(y_2(s) + \left(\frac{\mathrm{d}}{\mathrm{d}s} y_0(s)\right) v_1 + \left(\frac{\mathrm{d}}{\mathrm{d}s} y_1(s)\right) v_0\right.\right. \\
&\quad \left.\left. + \left(\frac{\mathrm{d}^2}{\mathrm{d}s^2} y_0(s)\right) \frac{{v_0}^2}{2}\right) + \left(y_1(s) + \left(\frac{\mathrm{d}}{\mathrm{d}s} y_0(s)\right) v_0\right)^2\right) - \frac{\sqrt{\mu_1\mu_2}\left(\left(y_0(s)\right)^2 - 1\right)}{8\mu_1\mu_2}
\end{aligned}
\tag{7.20}
$$

where

$$
\begin{aligned}
L(y_n) &= \frac{\mathrm{d}^2}{\mathrm{d}s^2} y_n(s) + \left(\frac{\mathrm{d}}{\mathrm{d}s} y_{n+1}(s)\right)(\mu_1 + \mu_2) + \mu_1\mu_2 y_{n+2}(s) \\
L(z_n) &= \frac{\mathrm{d}^2}{\mathrm{d}s^2} z_n(s) + \left(\frac{\mathrm{d}}{\mathrm{d}s} z_{n+1}(s)\right)(\mu_1 + \mu_2) + \mu_1\mu_2 z_{n+2}(s)
\end{aligned}
\tag{7.21}
$$

We will solve for $y(s)$ and $z(s)$ at each order of δ then substitute the result into the next order. From equation (7.17), that is at leading order term we get that $y_0(s) = z_0(s)$. We now substitute this into the next order of $O(\delta)$, we further simplify by solving for both equations in equation (7.18), this gives

$$
\begin{aligned}
\left(\mu_1\mu_2\, v_0 - (\mu_1 + \mu_2)\right) \frac{dz_0(s)}{ds} &= 0 \\
y_1 - z_1 &= \frac{1}{\sqrt{a\, b}}\left(1 - z_0^2\right)
\end{aligned}
\tag{7.22}
$$

We know that $d/ds(z_0(s)) \neq 0$ it implies that

$$
v_0 = \frac{\mu_1 + \mu_2}{\mu_1\, \mu_2}. \tag{7.23}
$$

Substituting the values $z_0 = y_0$ derived from equation (7.17) and $y_1(s)$ and v_0 from equations (7.22) and (7.23) into equation (7.19). This gives

$$
\begin{aligned}
y_2(s) = \; & z_2(s) + \frac{2\sqrt{\mu_1\,\mu_2}z_0(s)\,z_1(s) + (z_0(s))^3 - z_0(s)}{\mu_1\,\mu_2} \\
& \frac{\mathrm{d}^2}{\mathrm{d}s^2}z_0(s) + 2\,\frac{{\mu_1}^2{\mu_2}^2}{{\mu_1}^2+{\mu_2}^2}\left(\frac{\mathrm{d}}{\mathrm{d}s}z_0(s)\right)v_1 - 2\,\frac{\mu_1\,\mu_2\,z_0(s)\,(z_0^2(s)-1)}{{\mu_1}^2+{\mu_2}^2} = 0
\end{aligned}
\tag{7.24}
$$

If v_1 is zero then we can solve this second order differential equation. Hence solving equation (7.24) gives that

$$
z_0(s) = \tanh\left(\frac{\sqrt{\mu_1\,\mu_2}s}{\sqrt{{\mu_1}^2+{\mu_2}^2}}\right) \tag{7.25}
$$

using boundary condition that $z(s) \to 1$ as $s \to \infty$. After solving for $z_0(s)$ from the nonlinear second order differential equation, that is at $O(\delta^3)$ we substitute all values derived into equation (7.20) and algebraically reduce it. Summing both two equations derived after the algebraic reduction and we get

$$
\begin{aligned}
& \frac{\mathrm{d}^2}{\mathrm{d}s^2}z_1(s) + \frac{2\,\mu_1\mu_2}{{\mu_1}^2+{\mu_2}^2}z_1(s)\left(1-3\,z_0^2(s)\right) \\
& \quad = \frac{2\sqrt{\mu_1\mu_2}}{({\mu_1}^2+{\mu_2}^2)^{5/2}}(1-z_0^2(s))\left[2\left({\mu_1}^3+{\mu_2}^3\right)\left(z_0^2(s)-\frac{1}{3}\right)\right. \\
& \quad \left. -{\mu_1}^2{\mu_2}^2\left({\mu_1}^2+{\mu_2}^2\right)v_2\right]
\end{aligned}
\tag{7.26}
$$

which is a forced linear second order differential equation. From equation (7.26) we can solve for $z_1(s)$ and we will go through the process. Multiply through equation (7.26) by $d/ds(z_0(s))$ and this gives

$$
\begin{aligned}
& \frac{\mathrm{d}}{\mathrm{d}s}\left[\left(\frac{\mathrm{d}}{\mathrm{d}s}z_1(s)\,\frac{\mathrm{d}}{\mathrm{d}s}z_0(s)\right) + \frac{2\,\mu_1\mu_2}{{\mu_1}^2+{\mu_2}^2}z_1(s)\left(z_0(s) - z_0^3(s)\right)\right] \\
& \quad = \frac{2\sqrt{\mu_1\mu_2}}{({\mu_1}^2+{\mu_2}^2)^{5/2}}(1-z_0^2(s))\left[2\left({\mu_1}^3+{\mu_2}^3\right)\left(z_0^2(s)-\frac{1}{3}\right)\right. \\
& \quad \left. -{\mu_1}^2{\mu_2}^2\left({\mu_1}^2+{\mu_2}^2\right)v_2\right]\frac{\mathrm{d}}{\mathrm{d}s}z_0(s)
\end{aligned}
\tag{7.27}
$$

We now take the integral of equation (7.27) for the interval of time from $s = -\infty$ to $s = \varrho$

$$\frac{\mathrm{d}}{\mathrm{d}\varrho}z_1(\varrho)\,\frac{\mathrm{d}}{\mathrm{d}\varrho}z_0(\varrho)+\frac{2\,\mu_1\mu_2}{{\mu_1}^2+{\mu_2}^2}z_1(\varrho)\left(z_0(\varrho)-z_0^3(\varrho)\right)$$
$$=\int_{-\infty}^{\varrho}\left(\frac{2\sqrt{\mu_1\mu_2}}{\left({\mu_1}^2+{\mu_2}^2\right)^{5/2}}(1-z_0^2(s))\left[2\left({\mu_1}^3+{\mu_2}^3\right)\left(z_0^2(s)-\frac{1}{3}\right)\right.\right. \tag{7.28}$$
$$\left.\left.-{\mu_1}^2\mu_2^2\left({\mu_1}^2+{\mu_2}^2\right)v_2\right]\frac{\mathrm{d}}{\mathrm{d}s}z_0(s)\right)\mathrm{d}s$$

From the leading order term $z_0(s)=\tanh(\Lambda s)$ where $\Lambda=\left(\sqrt{ab}/\sqrt{a^2+b^2}\right)$ at $s=\varrho$ we have $z_0(\varrho)=1+O\left(\mathrm{e}^{-2\Lambda\varrho}\right)$. And for the rest of the terms in equation (7.28) we have $z_0(s)-z_0^3(s)=O\left(\mathrm{e}^{-2\Lambda\varrho}\right)$. For the right hand side of equation (7.28), let the integrand be Πv_2 such that we get

$$\begin{aligned}\int_{-\infty}^{\varrho}\Pi v_2\,\mathrm{d}s&=\int_{-\infty}^{\infty}\Pi v_2\,\mathrm{d}s-\int_{\varrho}^{\infty}\Pi v_2\,\mathrm{d}s\\&=\int_{-\infty}^{\infty}\Pi v_2\,\mathrm{d}s+O\left(\mathrm{e}^{-4\Lambda\varrho}\right)\end{aligned} \tag{7.29}$$

If multiply through equation (7.26) by $\exp(-2\Lambda s)$ the order of the equation for the terms of the leading order solution is

$$\frac{\mathrm{d}}{\mathrm{d}\varrho}z_1(\varrho)\ \mathrm{O}(1)+\ z_1(\varrho)\ \mathrm{O}(1)=\ \mathrm{e}^{-2\Lambda\varrho}\int_{-\infty}^{\infty}\Pi v_2\,\mathrm{d}s+O\left(\mathrm{e}^{-2\Lambda\varrho}\right) \tag{7.30}$$

Since this system is periodic it implies that the energy in the system is conserved for this to happen we need the left hand side of equation (7.30) to be equal to the right hand side of the equation. In solving for a homoclinic orbit that satisfies similar conditions Jordan and Smith [34] assumed the integral on the right hand side to be equal to zero. We follow a similar line reason, that is if the integral is zero, then the right hand side is $\mathrm{O}(\mathrm{e}^{-2\Lambda\varrho})$. For our assumption to hold, the order of $z_1(s)$ right hand side of the equation should be $O\left(\mathrm{e}^{-2\Lambda\varrho}\right)$. This is the condition that when satisfied we have a system with a conserved energy. This means that our assumption is valid and is a necessary condition for the heteroclinic orbit at $\mathrm{O}(\delta^2)$.

Since the integral is zero we search for the value of v_2 from it, this gives

$$\begin{aligned} &- v_2 \frac{2\left(\mu_1\,\mu_2\right)^3}{\left({\mu_1}^2+{\mu_2}^2\right)^2}\int_{-\infty}^{\infty}\left(1-z_0^2\left(s\right)\right)^2\,\mathrm{d}s \\ &- \frac{2\mu_1\,\mu_2({\mu_1}^3+{\mu_2}^3)}{3\left({\mu_1}^2+{\mu_2}^2\right)^3}\int_{-\infty}^{\infty}\left(1-z_0^2\left(s\right)\right)^2\left(6\,z_0^2\left(s\right)-2\right)\,\mathrm{d}s=0. \end{aligned} \tag{7.31}$$

From equation (7.31) we compute the value of the unknown parameter v_2 which adds for the width of the transition layer during the fast phase this is given as

$$v_2 = -\frac{4\left({\mu_1}^3+{\mu_2}^3\right)}{15\,{\mu_1}^2{\mu_2}^2\left({\mu_1}^2+{\mu_2}^2\right)} \tag{7.32}$$

Now we solve for $z_1(s)$ and get the following

$$\begin{aligned} z_1\left(s\right) = C_0\,\mathrm{sech}^2\left(\Lambda\,s\right) + C_1\left(3\Lambda s\,\mathrm{sech}^2\left(\Lambda\,s\right)+3\,\tanh\left(\Lambda\,s\right)\right. \\ \left.+2\,\sinh\left(\Lambda\,s\right)\cosh\left(\Lambda\,s\right)\right) \end{aligned} \tag{7.33}$$

where C_0, C_1 are arbitrary constants. We can conclude this analysis by obtaining a particular solution to $x_1(s)$.

$$\begin{aligned} A\left(s\right) &= C_0 + \frac{\left(a^3+b^3\right)}{10\,\left(a^2+b^2\right)^{3/2}\sqrt{ab}}\left(8\,\ln\left(\mathrm{sech}\left(\Lambda\,s\right)\right)\right. \\ &\quad\left.+3\,\mathrm{sech}^2\left(\Lambda\,s\right)\left(\Lambda\,s\tanh\left(\Lambda\,s\right)\mathrm{sech}^2\left(\Lambda\,s\right)-\,\mathrm{sech}^2\left(\Lambda\,s\right)+\frac{1}{3}\right)\right) \\ B\left(s\right) &= C_1 - \frac{\left(a^3+b^3\right)\sinh\left(\Lambda\,s\right)}{10((a^2+b^2)^{3/2}\sqrt{ab}\left(\cosh\left(\Lambda\,s\right)\right)^5)} \end{aligned} \tag{7.34}$$

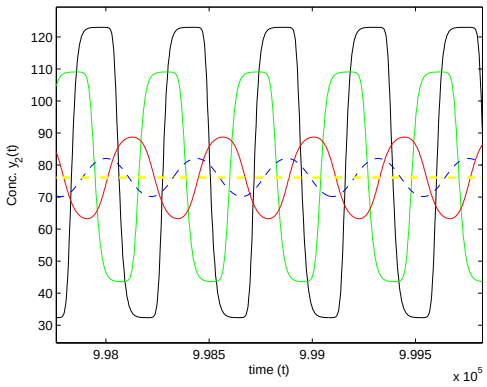
We observe from this analysis that the result derive is similar to the logistic modelled studied in chapter 5. In actual fact this is a rescaled result of the analysis carried out by Wattis [70]. We shall now carry out a similar numerical study just like we did in chapter 5 to see if our analysis is justified for this system.

It would also be important to compare our findings with the analytic developed in section 6.0 from equation (7.1). From the matched asymptotic we have the additional shift is given by,

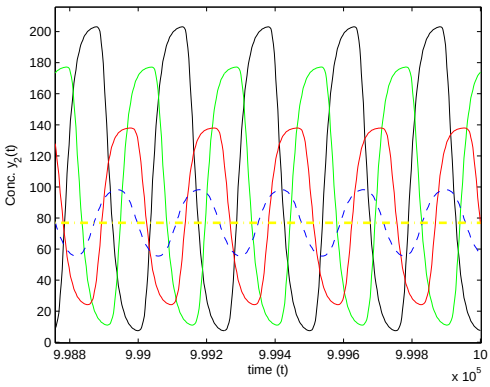
$$a = 2v_0 + 2v_1\,\delta^2 = 2\frac{\mu_1 + \mu_2}{\mu_1\,\mu_2} - \frac{8}{15}\frac{(\mu_1^3 + \mu_2^3)}{\mu_1\,\mu_2(\mu_1^2 + \mu_2^2)}\delta^2 \tag{7.35}$$

Comparing the value derived from equations (7.35) for $\mu = 0.03$ we got the value of $'\tilde{a}'$ as 127.1627 but from equation (7.7) we get a different value for $'\tilde{a}'$ which is 146.58. The difference derived from the direct numeric and the analytical value of $\tilde{a}$ could be from the fact that analytics does not account for the nonlinear terms of order three and above, see equation (7.11). Equation (7.7) is far more accurate than the value of $'a'$ derived from equation (7.35) which is different from what we got from equation (7.7). This proves that a reduced form of the model to take on a logistic for as suggested by Adhikari [69] does not hold in all cases.

Now that we have solved for the value of the shift $'a'$, the value of the period of oscillation of the square wave has also been derived. Equation (7.7) justifies our plot in figures 7.9 and 7.10 which shows the transition from sine wave to square wave. We saw in chapter 5 we saw that the condition for the Hopf bifurcation point using the rate of decay as the bifurcating parameter now we see that for point close to the Hopf bifurcation point and large delay there is a transition from sine wave to a square wave. The Hopf bifurcation point determines where the transition to a square wave occurs in the system.

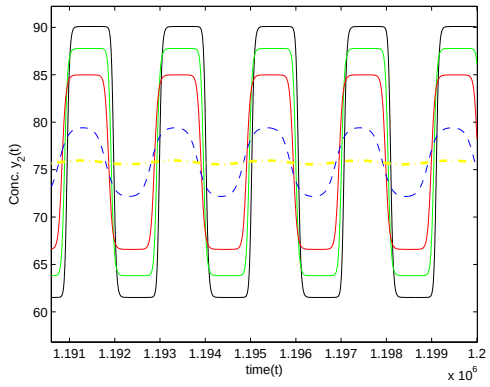


(a)For $\tau = 200$ and $\mu = 0.10235$ (yellow dash-dot), $\mu = 0.1020$ (blue dash), $\mu = 0.1011$ (red), $\mu = 0.095$ (green) and $\mu = 0.09$ (black).

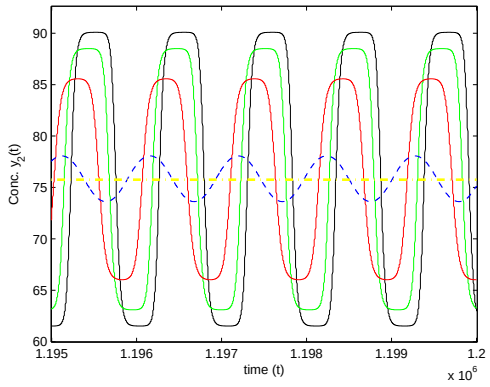


(b)For $\tau = 100$ and $\mu = 0.1012$ (yellow dash-dot), $\mu = 0.10$ (blue dash), $\mu = 0.085$ (red), $\mu = 0.0755$ (green) and $\mu = 0.09$ (black).

Figure 7.11: The numerical figures for a fixed large delay while varying the value of the decay. For $\tau = 200$, $\mu_H = 0.10224$ in figure (a) and for $\tau = 100$ $\mu_H = 0.10103$ in figure (b).



(a)For $\tau = 1000$ and $\mu = 0.10282$ (yellow dash-dot), $\mu = 0.10271$ (blue dash), $\mu = 0.10255$ (red), $\mu = 0.10235$ (green) and $\mu = 0.1022$ (black).



(b)For $\tau = 500$ and $\mu = 0.10278$ (yellow dash-dot), $\mu = 0.10262$ (blue), $\mu = 0.10190$ (red), $\mu = 0.10135$ (green) and $\mu = 0.101$ (black)

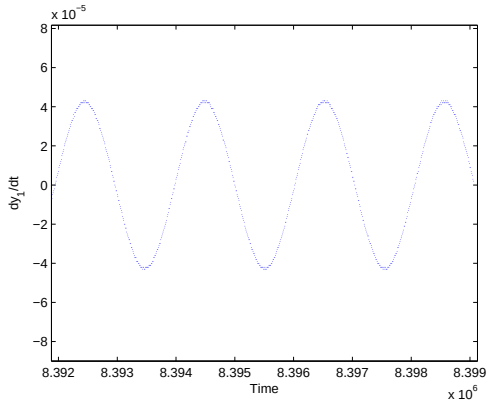
Figure 7.12: The numerical figures for a fixed large delay while varying the value of the decay. For $\tau = 1000$, $\mu_H = 0.10272$ in figure (a) and for $\tau = 500$ $\mu_H = 0.10265$ in figure (b).

Figures 7.11 and 7.12 capture the transition from sine wave to square wave for various values of delay τ, while decay is fixed. Another point that comes from the two figures is that for every value of the decay parameter there is a different amplitude, these amplitude increases as the value of the decay parameter decreases. This phenomenon is different from what was observed in the logistic differential-delay equation where we observed that the amplitude increased with an increase in the value of the varying parameter, see figures 6.9 - 6.11. Again from figures 7.11 and 7.12 we have that for every value decay there is a different value for the period of oscillation though the value of the delay is fixed. This corresponds to our earlier deduction that led to the derived equation (7.7).

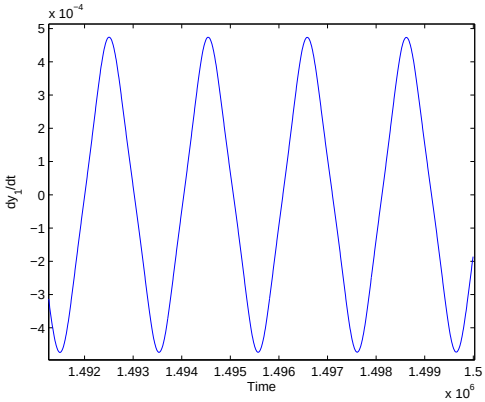
At what point does this system transit from sine wave to square wave? Though the transition is a continuum, is there a particular point where we begin to see this square wave? By the numerics carried out thus far especially figures 7.11 and 7.12 we observe from this negative autogenous regulation there is a transition from sine to square wave. We plotted several values for the rate of decay, μ such that we physical checked each on for flat surfaces. At each point where flat surface where observed such points where marked and plotted against the corresponding delay and range of such plots give the scale of

$$\mu \sim \mu_H - \frac{\beta}{\tau^2}, \tag{7.36}$$

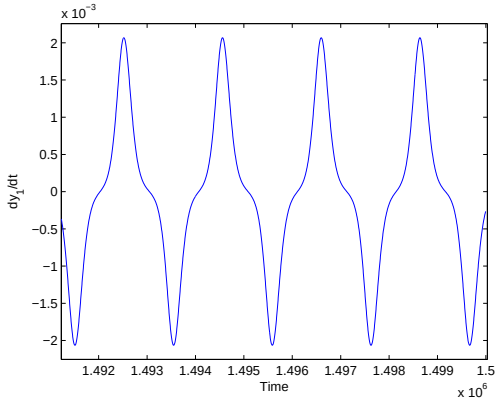
where β is a constant. There is a smooth, continuous and gradual transition from a sine wave to a square wave. Equation (7.36) is the point at which the change from a sine wave to a square wave is observed. Further decrease of the decay and we have a square wave while an increase in the decay would cause a sine wave to take place as shown in figures 7.11 and 7.12. We also plot the time derivative, see figure 7.13 to show how these curves change with time. This time derivative plot shows a transition from a cosine wave to a double spike-kind of wave as we move from sine to square wave.



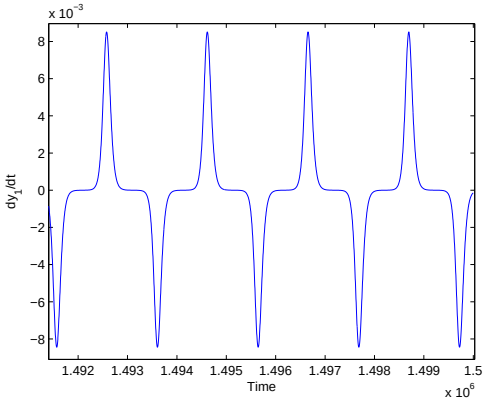
(a) The plot of the time derivative of the sine wave gives a cosine wave, $\mu = 0.102718$.



(b) The plot of the time derivative of the sine-square wave, $\mu = 0.102713$.



(c) The plot of the time derivative of the sine-square wave, $\mu = 0.10261$.

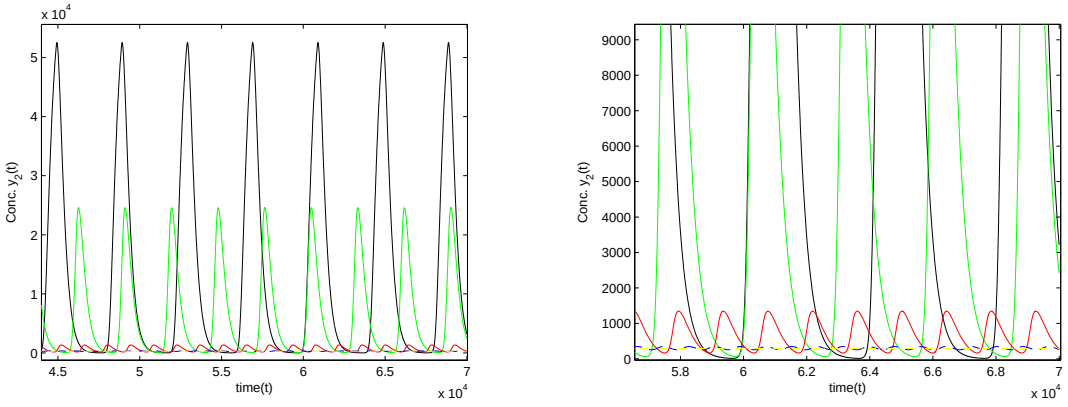


(d) The plot of the time derivative of the square wave, $\mu = 0.1022$.

Figure 7.13: The plot of time derivative of the sine wave to the square wave for a fixed delay of 1000.

For each value of the delay τ we have, there is a possibility of no Hopf bifurcation, one Hopf bifurcation or two possible Hopf bifurcation point, see

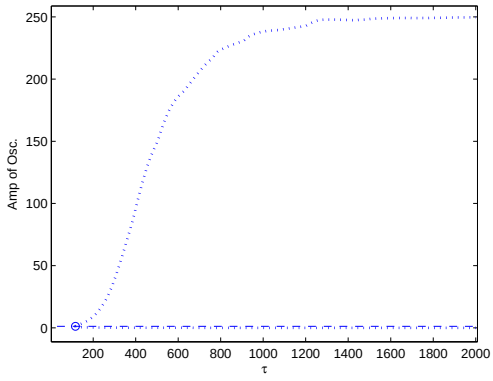
figure 5.1. The possibility of having two Hopf bifurcating point is also seen in figure 5.11 when we investigated the weakly nonlinear analysis. We have so far numerically studied one Hopf bifurcation point arising from a fixed decay. Now for a fixed delay we will look at the second Hopf bifurcation point which corresponds to a much smaller value of decay μ, in comparison to the first Hopf bifurcation studied earlier. Close to the second Hopf point we get sine wave for the given delayed parameter but as the delay is increased we do not get a square wave immediately, we see that there is only one plateau which is at the base as shown in figure 7.14. As it moves further away from the Hopf bifurcation point it begins to pick up properties of a square wave which is dominant with the second Hopf bifurcation point.



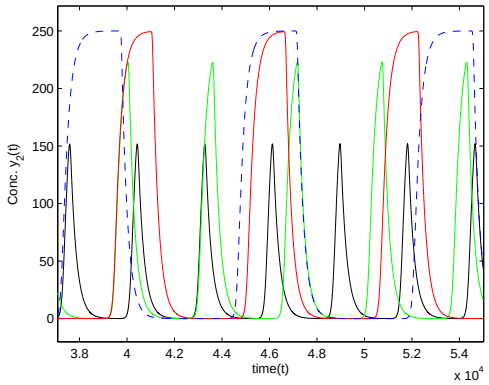
(a) (b)

Figure 7.14: A plot of $\mu_H = 0.004$ and $\tau = 1000$ (black), $\tau = 500$ (green), $\tau = 200$ (red), $\tau = 120$ (blue) and $\tau = 70$ (yellow dash-dotted line).

To get a better understanding of what is happening a bifurcation plot of this is shown in figure 7.15a and a time plot for arbitrary values of the delay parameter is shown figure 7.15b. The bifurcation plot does shows the bottom plateau emanating before the second plateau at the peak shows up at larger values of the delay. For selected values of the delay the time plot as shown in figure 7.15b corresponds to those values on the bifurcation plot.



(a) A bifurcation plot for a fixed decay having a value of 0.004 while the delay is being varied from 0 to 2000.

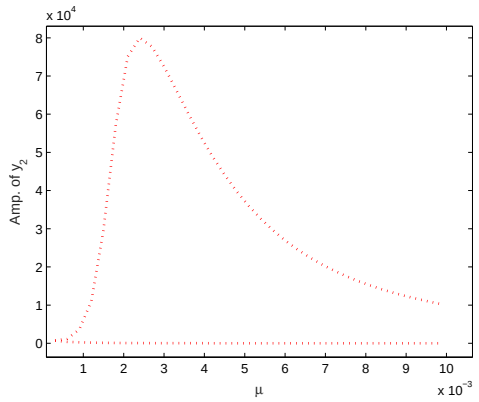


(b) A plot for a fixed decay value of 0.004 and the delay as 500 (black), 800 (green), 1800 (red) and 2700 (blue dashed).

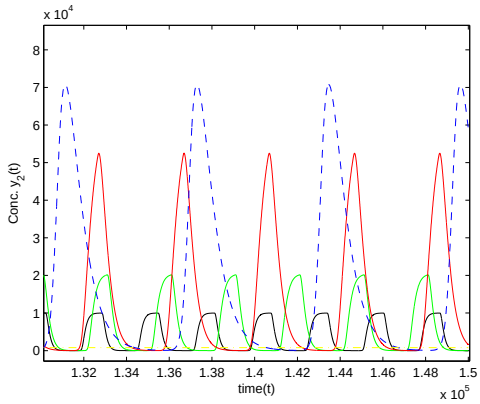
Figure 7.15: Possible structure of second Hopf point using delay as the bifurcating parameter.

To investigate this spike-kind of periodic behaviour further, we perform similar numerics with the decay as the varying parameter and the delay as the fixed parameter figure 7.16a and compare it with the time plot as shown in figure 7.16b. These spike-kind of periodic solution persist even for a fixed delay and a varying decay. This property is unlike the properties displayed for the first Hopf bifurcation point investigated earlier, see figure 7.1.

Next we investigate if the map close to this Hopf bifurcation point for large delay to get the solution of the amplitude if it tallies with the amplitude of



(a) A bifurcation plot for a fixed delay of 1000, we vary the decay rate at the first Hopf bifurcation, $\mu = 0.0004637$.



(b) A plot for $\tau = 1000$ and $\mu = 0.01$ (black), $\mu = 0.007$ (green), $\mu = 0.004$ (red), $\mu = 0.002$ (blue), and $\mu = 0.0002$ (yellow dashed).

Figure 7.16: A plots for a fixed delay.

the square wave. For values of $\mu = 0.004$, $n = 5$ and 100 equation (7.5) is

$$\begin{aligned} 0.004^2\, y_1(t) &= \frac{100^5}{100^5 + y_2^5(t-1)}, \\ 0.004^2\, y_2(t) &= \frac{100^5}{100^5 + y_1^5(t-1)}, \end{aligned} \tag{7.37}$$

From equation (7.37) gives three real and positive roots which give, $y_1 = 6.5536$ x 10^{-10}, 292.1735 and 62500 while $y_2 = 2.6214$ x 10^{-12}, 1.16869 and 250. We have plotted the values for y_2 in figure 7.17.

Comparing the analysis of the map and on the bifurcation plot shows that the amplitude derived from the map is a very good approximation for the amplitude of the square wave for this Hopf bifurcation point. For every decay there is a maximum and minimum value and this corresponds to the values derived for the map. It is only when this maximum and minimum values are reached that one begins to see the emergence of this plateau and this occurs

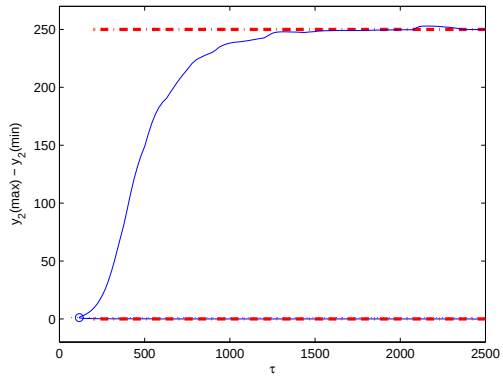


Figure 7.17: A bifurcation plot for $\mu_H = 0.004$ (blue) and the map (red). The circle is the Hopf bifurcation point, the dotted line in the unstable steady state.

for both Hopf bifurcations. In the second Hopf bifurcation the minimum is reached much earlier than the maximum unlike the first Hopf bifurcation were both are reached at approximately the same point. Since the minimum is reached much quicker in the second Hopf bifurcation we continue to see spikes from the minimum until the spikes reach the maximum before the flat surfaces are seen which form the square wave. The periodic oscillations from this Hopf bifurcation is different from those observed previously, does this influence the process of transiting from sine wave to square wave? We apply the same numerics to analyse the transition. Figures 7.18 - 7.20 we numerically show an approximate point where it is difficult to distinguish if the curve is a square wave or not. From these indecisive points which are the red lines in figures 7.18 - 7.20 we get the scaling that

$$\mu \sim \mu_H + \frac{\beta}{\tau}, \tag{7.38}$$

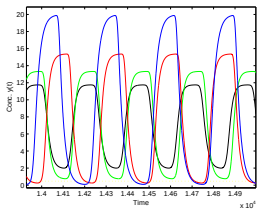
where β is a constant. Comparing equation (7.36) and (7.38), we see that the

scaling is different at each of the Hopf bifurcation point. The scaling from equation (7.36) is $\mu - \mu_H = O(\tau^{-2})$, this is the point of transition from sine wave to square wave for the first Hopf bifurcation while from equation (7.38) we have a scaling which is $\mu - \mu_H = O(\tau^{-1})$ as the point where the transition takes place.

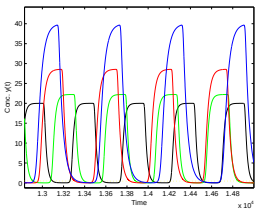
Another phenomenon of note is that at the second Hopf bifurcation point as the delay parameter gets larger the period of oscillation gets much greater than $2\,\tau$.

7.3 Conclusion

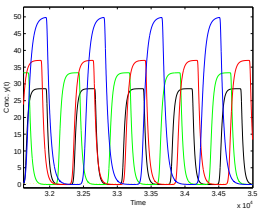
The model constructed for the negative autogenous regulation displays a wide range of characteristics in terms of structure. All of this properties only arise after a delay parameter has been imputed into this model. In a model without delay there are no periodic oscillation as shown in chapter 5. Now for a nonlinear differential equation the analytical solution might not be easily derived, again for an n^{th} order sigmoid nonlinearity we see that the complexity increases as n gets larger. If we are able to solve this analytically for an ODE it does not guarantee that we would be solvable analytically for a nonlinear DDE which can be much more complex than an ODE. We tried to solve this model using the matched asymptotic as done by previous authors the problem arise on how to represent the sigmoid curve in such a way that this method can used to be solve it. We also have seen that using the Taylor expansion and truncating at $O(x^3)$ is not the best for this model since it gives the nonlinear term a behaviour that could be chaotic and such a result is not a good representation of this model. Therefore the best possible way to understand the dynamics of this model is the use of numerics to solve for this model.



(a) For $\tau = 100$.

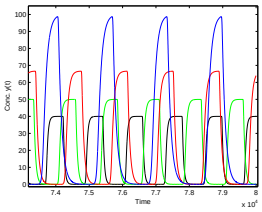


(b) For $\tau = 200$.

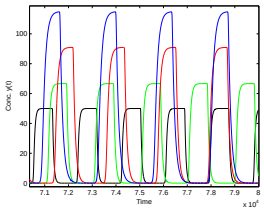


(c) For $\tau = 300$.

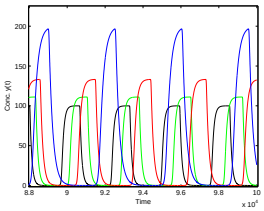
Figure 7.18: (a) $\mu = 0.085$-black, $\mu = 0.075$-green, $\mu = 0.065$-red, $\mu = 0.05$-blue, $\mu = 0.001$-yellow dash-dot. (b) $\mu = 0.05$-black, $\mu = 0.045$-green, $\mu = 0.035$-red, $\mu = 0.025$-blue, $\mu = 0.001$-yellow dash-dot. (c) $\mu = 0.035$-black, $\mu = 0.03$-green, $\mu = 0.027$-red, $\mu = 0.02$-blue, $\mu = 0.0005$-yellow dash-dot



(a) For $\tau = 500$.

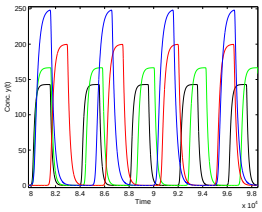


(b) For $\tau = 800$.

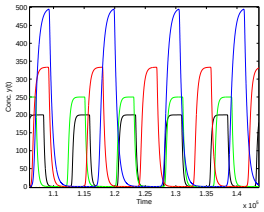


(c) For $\tau = 1000$.

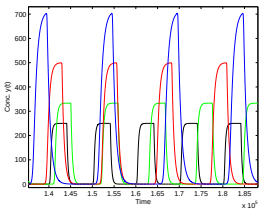
Figure 7.19: (a)$\mu = 0.025$-black, $\mu = 0.02$-green, $\mu = 0.015$-red, $\mu = 0.01$-blue, $\mu = 0.0003$-yellow dash-dot. (b)$\mu = 0.02$-black, $\mu = 0.015$-green, $\mu = 0.011$-red, $\mu = 0.008$-blue, $\mu = 0.0002$-yellow dash-dot. (c)$\mu = 0.01$-black, $\mu = 0.009$-green, $\mu = 0.0075$-red, $\mu = 0.05$-blue, $\mu = 0.0001$-yellow dash-dot.



(a) For $\tau = 1500$.



(b) For $\tau = 3000$.



(c) For $\tau = 4000$.

Figure 7.20: (a) $\mu = 0.007$-black, $\mu = 0.006$-green, $\mu = 0.005$-red, $\mu = 0.004$-blue, $\mu = 0.0001$-yellow dash-dot. (b) $\mu = 0.005$-black, $\mu = 0.004$-green, $\mu = 0.003$-red, $\mu = 0.002$-blue, $\mu = 0.0001$-yellow dash-dot. (c) $\mu = 0.004$-black, $\mu = 0.003$-green, $\mu = 0.002$-red, $\mu = 0.0014$-blue, $\mu = 0.0001$-yellow dash-dot

Chapter 8

Conclusion and further work

In this thesis, we have studied several modelled differential-delay equation applying the closed form approximation of the multiple timescale analysis to investigate the role of each parameter in the model. Starting from the first order differential equation to the higher order differential-delay equation we showed that time lags can produce periodic oscillation and other properties not seen in the ordinary differential equation.

The exact solution of such model would have been preferable but due to the nonlinearity and the shift to the infinite dimension these models had to be carefully studied. The numerical solutions to this model played a key role in comparing our analytical solutions. In some instances, the direct numerical method could be time consuming in comparison to the analytic solution but it still serves as one of the most reliable ways to solve non-linear differential equation. In each chapter of this thesis we have compared the analytical solutions derived with direct numerical solutions. To gain insight on how certain parameters influenced each model we plotted the bifurcation diagrams and also compared it to the bifurcation point derived analytically. It was seen that

the introduction of the delay(s) did not increase or decrease the number of steady states but in some cases change the type of steady state.

In chapter 1 a background study with literature review was carried out on each of the different models investigated. The methods that were applied to solving this Differential-delay equation were discussed and the overall structure of the thesis was put in perspective. The key model of the negative autoregulation (NAR) was introduced and other types of gene regulation were discussed as well.

In chapter 2 a first order differential delay equation for a population model was investigated and the techniques that would be used in subsequent chapters was applied to get the concept introduced at lower level with lower non-linearity. In this chapter, there is a single time lag.

The first two chapters gave an insight into the use of the differential delay equation, now chapter 3 we now applied these techniques to a first order differential delay equation having a negative feedback. The model was invested for a large Hill coefficient which two discontinuous differential equation where represented the differential-delay equation. In this chapter there is a single delay like in chapter one. We derived very high accuracy with this method in comparison with the direct numerical approach.

In chapter 5 we have a higher order differential delay equation but this time we had two time lags. The first time lag represented the transcriptional delay and the second represented the translational delay. We saw the Hopf bifurcation occurred when the sum of both delays was equivalent to the critical delay. Again the method of multiple time scale is used to analyse each of the param-

eters that is involved in the this model which. The method of multiple scales equally simplifies the nonlinear differential-delay equation to a form that can be studied easily.
In chapter 6 we examined the square wave arising from large delay in the population model. We saw that the period is just over twice the time lag. The square wave consist of two flat plateaux and transition layers connecting these plateaux. The direct numerics was applied and the result matched with results from other authors who applied the match asymptotic. Our result tallied with these authors in deriving the approximate solution to the square wave.

As in chapter 6 we examine the square wave that comes as a result of the large delay in the negative autogenous regulation in chapter 7. Several results derived and a lot of differences where observed in this model in comparison to the population model. In this chapter we derived an equation (7.36) that gives the transition point from a sine wave to a square wave. From chapter 6 and 7 we were able to show the value of the constant a' that occurs for square waves with large delays.

In future we would like to produce an analytical method that can be used to solve these type of models, this would play a significant role as it can be used to compare the only odd scaling of $\mu = \mu_H \pm \beta/\tau$ we derive out of all models considered. The study of bifurcation points, weakly non-linear analysis and the effect of large delay can be applied to investigate larger networks with negative feedback, or a combination of models with the negative autogenous regulatory network. Another aspect this opens up for research is the analysis of delay as a state variable, a discrete or continuous delayed parameter from a model without delay to a model with large delay.
In this thesis we have shown the different possible solutions that the negative

autogenous regulation can display, from a simple solution to a periodic solution either the spiky or regular sine wave and then to a square wave. We have also shown how these solution transit from one to another.

The introduction of time lag into a differential equation has been analysed and we have seen how these system have have produced sine and square wave, we applied mathematical techniques which such as asymptotic analysis and method of multiple timescales to investigate these models. A system which can transit from a stable steady state solution, a periodic oscillatory solution to a square wave solution can be applied in many networks that show one or more of this solution type and might be the reason why the negative autogenous regulation is one of the most dominant network motifs, see Alon [2].

Appendix A

appendix

A.1 Network Motifs

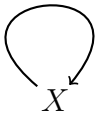


Figure A.1: Positive autoregulation.

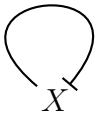


Figure A.2: Negative autoregulation.

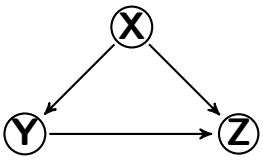


Figure A.3: Feed forward loop.

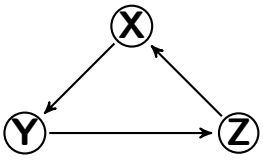


Figure A.4: Feed backward loop.

These diagrams can be found in the book by Alon [2] where more description of each network motif are made.



Figure A.5: Positive DFBL.



Figure A.6: Negative DFBL.

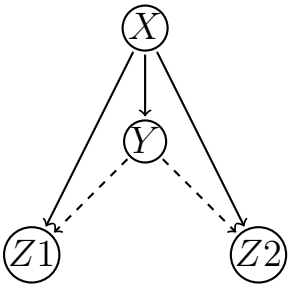


Figure A.7: Multi-output FFL.

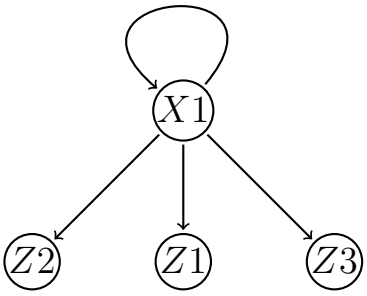


Figure A.8: SIM.

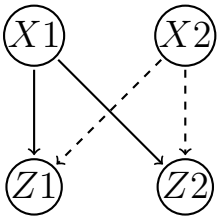


Figure A.9: BI-FAN.

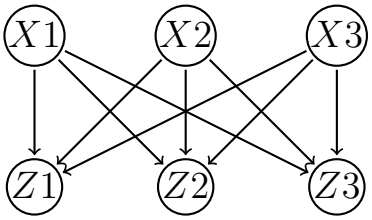


Figure A.10: DOR.

A.2 Delay as bifurcation parameter

In section 4.1 the system under study was analysed with the decay parameter as the bifurcation parameter. Various quantities such as K, L and H are dependent on the value of the decay parameters. Though this does not invalidate our results, in this section we will instead take the time delay as the bifurcating parameter. With this, we will investigate the Hopf bifurcation point and compare this with the results derived from section 4.1. To do this we start by rescaling the time t as $\tau\, t \ \rightarrow t$ such that $x(\tau\, t) \rightarrow x(t)$, this transforms equation (5.15) to

$$\frac{\mathrm{d}^2}{\mathrm{dt}^2}x\left(t\right)+\tau\ \left(\mu_1+\mu_2\right)\frac{\mathrm{d}}{\mathrm{dt}}x\left(t\right)+\tau^2\mu_1\mu_2x\left(t\right)+\tau^2K\,x\left(t-1\right)$$
$$=\ \tau^2Lx^2\left(t-1\right)+\ \tau^2Hx^3\left(t-1\right). \tag{A.1}$$

Following similar steps as in section 4.0, the root of the linear part of equation can also be shown to be a rescaling of the that for the equation (A.1) by $\omega\,\tau=\varpi$ which gives the following set of transcendental equations

$$\tau^2\,K\cos\left(\varpi\right)=-\mu_1\,\mu_2+\varpi^2,\qquad\qquad \tau^2\,K\sin\left(\varpi\right)=\left(\mu_1+\mu_2\right)\varpi\tau, \tag{A.2}$$

and for completion we further make the following algebraic calculations of equation (A.2) and we derive

$$\tau_{\mathrm{H}}\ =\ -\frac{{\mu_1}^2{\mu_2}^2-\varpi^2}{\left(\mu_1+\mu_2\right)\varpi}\tan\left(\varpi\right)\qquad\qquad \varpi=1/2\,\tau_{\mathrm{H}}\sqrt{-2\,{\mu_1}^2-2\,{\mu_2}^2+2\sqrt{\left({\mu_1}^2-{\mu_2}^2\right)^2+4\,k^2}} \tag{A.3}$$

where τ_{H} is the Hopf bifurcation point.

Now we apply the method of multiple time scales to equation (A.1), by converting the equation to a weakly nonlinear equation. Let $K=\epsilon\,k$, $L=\epsilon\,l$ and $H=\epsilon\,h$ and since we are investing the Hopf bifurcation point we have to perturb the Hopf bifurcation parameter.

Let $\tau=\tau_{\mathrm{H}}+\epsilon^2\Delta$ where Δ is the direction we are investigating at the Hopf bifurcation point and $0<\epsilon\leq1$. Following the substitution of the rescaled nonlinear terms into equation (A.1) we get the following,

$$\frac{\mathrm{d}^2}{\mathrm{dt}^2}x\left(t\right)+\left(\tau_{\mathrm{H}}+\epsilon^2\Delta\right)\ \left(\mu_1+\mu_2\right)\frac{\mathrm{d}}{\mathrm{dt}}x\left(t\right)+\left(\tau_{\mathrm{H}}+\epsilon^2\Delta\right)^2\mu_1\mu_2x\left(t\right)+\left(\tau_{\mathrm{H}}+\epsilon^2\Delta\right)^2k\,x\left(t-1\right)$$
$$=\epsilon(\tau_{\mathrm{H}}+\epsilon^2\Delta)^2lx^2\left(t-1\right)+\epsilon^2(\tau_{\mathrm{H}}+\epsilon^2\Delta)^2hx^3\left(t-1\right). \tag{A.4}$$

We now apply the the two time expansion such that $x(t) = x(t,T)$ where $t = t$ represents the fast timescale and $T = \epsilon^2 t$ represents the slow timescale. The slow timescale results from the secular terms. Using the multiple timescale we have

$$x(t) = x_0(t,T) + \epsilon x_1(t,T) + \epsilon^2 x_2(t,T) + \mathrm{O}(\epsilon^3), \tag{A.5}$$

and we can express $x(t-1)$ as

$$x(t-1) = x_0\left(t-1,T\right) + x_1\left(t-1,T\right)\epsilon - \left(\frac{\partial}{\partial T}x_0\left(t-1,T\right) - x_2\left(t-1,T\right)\right)\epsilon^2 + O\left(\epsilon^3\right). \tag{A.6}$$

Let

$$\begin{aligned} \frac{\mathrm{d}}{\mathrm{d}t} &= \frac{\partial}{\partial t} + \epsilon^2 \frac{\partial}{\partial T} \\ \frac{\mathrm{d}^2}{\mathrm{d}t^2} &= \frac{\partial^2}{\partial t^2} + 2\epsilon^2 \frac{\partial^2}{\partial t \partial T} + \mathrm{O}(\epsilon^3), \end{aligned} \tag{A.7}$$

We now substitute the equations (A.5) - (A.7) into equation (A.4) and match the powers of ϵ, this gives the following,

at $O(\epsilon^0)$

$$\frac{\partial^2}{\partial t^2}x_0\left(t,T\right) + \tau\left(\mu_1+\mu_2\right)\frac{\partial}{\partial t}x_0\left(t,T\right) + \tau^2\mu_1\mu_2 x_0\left(t,T\right) + \tau^2 k x_0\left(t-1,T\right) = 0, \tag{A.8}$$

at $O(\epsilon^1)$

$$\begin{aligned} &\frac{\partial^2}{\partial t^2}x_1\left(t,T\right) + \tau\left(\mu_1+\mu_2\right)\frac{\partial}{\partial t}x_1\left(t,T\right) + \tau^2\mu_1\mu_2 x_1\left(t,T\right) + \tau^2 k x_1\left(t-1,T\right) \\ &\qquad = \tau^2 l\left(x_0\left(t-1,T\right)\right)^2, \end{aligned} \tag{A.9}$$

at $O(\epsilon^2)$

$$\begin{aligned}
&\frac{\partial^2}{\partial t^2}x_2(t,T)+\tau\,(\mu_1+\mu_2)\,\frac{\partial}{\partial t}x_2(t,T)+\tau^2\mu_1\mu_2x_2(t,T)+\tau^2kx_2(t-1,T)\\
&\qquad=-2\,\frac{\partial^2}{\partial t\partial T}x_0(t,T)-\Delta\,(\mu_1+\mu_2)\,\frac{\partial}{\partial t}x_0(t,T)-\tau\,(\mu_1+\mu_2)\,\frac{\partial}{\partial T}x_0(t,T)\\
&\qquad\quad-2\,\tau\,\Delta\,\mu_1\mu_2x_0(t,T)+\tau^2kD_2(x_0)(t-1,T)-2\,\tau\,\Delta\,kx_0(t-1,T)\\
&\qquad\quad+2\,\tau^2lx_0(t-1,T)\,x_1(t-1,T)+\tau^2h\left(x_0(t-1,T)\right)^3.
\end{aligned}\tag{A.10}$$

Equation (A.8) is a linear differential-delay equation which can easily be solved. This equation is equivalent to the linear part of equation (A.1) studied at the beginning of this section and seen to be a rescaled form of equation (5.16. The analysis of equation (A.8) shows there is a Hopf bifurcation and hence the existence of a periodic solution. Let us assume the periodic the solution is

$$x_0(t,T)=A(T)\cos\left(\varpi\,t+\Phi(T)\right)\tag{A.11}$$

where $A(T)$ is the amplitude and $\Phi(T)$ is the phase both of which are functions of the slow timescale. From our assumption of the solution $x_0(t,T)$, we are inferring that there are no secular terms in $x(t,T)$ hence we proceed to solving the equation for $x_1(t,T)$ from equation (A.9). Substituting the value of $x_0(t,T)$ derived in equation (A.11) into equation (A.9), one obtains

$$x_1(t,T)=C(T)\cos\left(2\,\varpi\,t+2\,\Phi(T)\right)+E(T)\sin\left(2\,\varpi\,t+2\,\Phi(T)\right)+F(T)\tag{A.12}$$

where

$$\begin{aligned}
C(T)&=\frac{\tau^2\left(C_1\cos(2\,\varpi)-2\,C_2\sin(2\,\varpi)+k\tau^2\right)lA(T)^2}{2\left(\tau^2(2\,k\,C_2\cos(2\,\varpi)-4\,k\,C_2\sin(2\,\varpi)+4\,\varpi^2({\mu_1}^2+{\mu_2}^2)+\tau^2({\mu_1}^2{\mu_2}^2+k^2))+16\,\varpi^4\right)}\\
E(T)&=\frac{\tau^2\left(2\,C_2\cos(2\,\varpi)+C_1\sin(2\,\varpi)\right)lA(T)^2}{2\left(\tau^2(2\,k\,C_2\cos(2\,\varpi)-4\,k\,C_2\sin(2\,\varpi)+4\,\varpi^2({\mu_1}^2+{\mu_2}^2)+\tau^2({\mu_1}^2{\mu_2}^2+k^2))+16\,\varpi^4\right)}\\
F(T)&=\frac{A(T)^2\,l}{2(\mu_1\mu_2+k)}
\end{aligned}\tag{A.13}$$

and

$$C_1 = \tau^2 \mu_1 \mu_2 - 4\,\varpi^2 \qquad C_2 = \varpi\,\tau\,(\mu_1 + \mu_2)\,. \tag{A.14}$$

From equation (A.12) again there are no secular terms this process is carried out again and again until secular terms are obtained. Now we substitute the values of $x_0(t,T)$ and $x_1(t,T)$ from equation (A.11) and (A.12) into the RHS of equation (A.10). From this substitution the following equation is derived for the RHS equation (A.10)

$$\begin{aligned} &M(T)\cos(\varpi\,t + \Phi(T)) + N(T)\sin(\varpi\,t + \Phi(T)) \\ &\quad + P(T)\cos(3\,\varpi\,t + 3\,\Phi(T)) + R(T)\sin(3\,\varpi\,t + 3\,\Phi(T))\,. \end{aligned} \tag{A.15}$$

$$\begin{aligned} M = {} & \left(\cos(\varpi)\,k\tau^2 + (-\mu_1 - \mu_2)\,\tau\right)\frac{\mathrm{d}}{\mathrm{d}T}A(T) + A(T)\left(\sin(\varpi)\,k\tau^2 + 2\,\varpi\right)\frac{\mathrm{d}}{\mathrm{d}T}\Phi(T) \\ & + \left((3/4\,h + lC(T) + 2\,lF(T))\cos(\varpi) - l\sin(\varpi)\,E(T)\right)\tau^2\,(A(T))^3 \\ & + \left(-2\,\Delta\,\cos(\varpi)\,k - 2\,\Delta\,\mu_1\mu_2\right)\tau\,A(T) \end{aligned} \tag{A.16}$$

$$\begin{aligned} N = {} & \left(\sin(\varpi)\,k\tau^2 + 2\,\varpi\right)\frac{\mathrm{d}}{\mathrm{d}T}A(T) + \left(-\cos(\varpi)\,k\tau^2 + (\mu_1 + \mu_2)\,\tau\right)A(T)\,\frac{\mathrm{d}}{\mathrm{d}T}\Phi(T) \\ & + \left(E(T)\,l\cos(\varpi) + (3/4\,h + lC(T) + 2\,lF(T))\sin(\varpi)\right)\tau^2\,(A(T))^3 \\ & + \left(-2\,\tau\,\Delta\,k\sin(\varpi) + \Delta\,\mu_1\varpi + \Delta\,\mu_2\varpi\right)A(T) \end{aligned} \tag{A.17}$$

$$P(T) = \left(\left(C(T) + \frac{h}{4\,l}\right)\cos(3\,\omega\,\tau) - E(T)\sin(3\,\omega\,\tau)\right)l\,(A(T))^3 \tag{A.18}$$

$$R(T) = \left(E(T)\cos(3\,\omega\,\tau) + \left(C(T) + \frac{h}{4}\right)\sin(3\,\omega\,\tau)\right)l\,(A(T))^3 \tag{A.19}$$

From equation (A.15) secular terms emerge at this stage of the solution. We have to eliminate these secular terms from equation (A.15). These secular terms can change the behaviour of our solution. To eliminate the secular terms we equate of the coefficient of the sine and cosine terms to zero, $M\left(T\right)=0$ and $N\left(T\right)=0$. By equating these secular terms to zero two equations derived,

$$\frac{\mathrm{d}}{\mathrm{d}T}A\left(T\right)=-\frac{G_1}{G_2}\,A(T)\left(A(T)^2-\frac{G_3}{G_1}\Delta\right) \tag{A.20}$$

$$\frac{\mathrm{d}}{\mathrm{d}T}\Phi\left(T\right)=\frac{G_4}{G_2}\,A(T)^2+\frac{G5}{G_2}\Delta \tag{A.21}$$

where

$$\begin{aligned}
G_1 &= -((D_0\left(4\,l\;M+8\,l\,R+3\;h\right)-D_1\,4\,l\,N)=Q_1\tau+Q_0\\
G_2 &= D_0+D_2\\
G_3 &= D_0+D_3\\
G_4 &= (D_1\left(-4\,l\;M-8\,l\,R-3\;h\right)+D_0\,4\,l\,N)\\
G_5 &= -8\,k\tau\,D_1-8\,\sin\left(\varpi\right)k\tau^3\mu_1\mu_2-4\,\cos\left(\varpi\right)k\varpi\,\tau^2\left(\mu_1+\mu_2\right)+4\,\varpi\,\tau\,\left(\mu_1-\mu_2\right)^2\\
D_0 &= \cos\left(\varpi\right)\mu_1\tau+\cos\left(\varpi\right)\mu_2\tau-k\tau^2-2\,\sin\left(\varpi\right)\varpi\\
D_1 &= \sin\left(\varpi\right)\tau\,\mu_1+\sin\left(\varpi\right)\tau\,\mu_2+2\,\cos\left(\varpi\right)\varpi\\
D_2 &= -4(\tau^2(\mu_1+\mu_2)^2+4\,\varpi^2)\\
D_3 &= 4\varpi\left(\mu_1+\mu_2\right)\,\left(\sin\left(\varpi\right)k\,\tau^2+2\,\varpi\right)+8\,\tau^2\mu_1\mu_2(\mu_1+\mu_2-\cos\left(\varpi\right)k\tau)
\end{aligned} \tag{A.22}$$

Equation (A.20) controls the rate of change of the amplitude of the oscillation while equation (A.21) controls the rate of change of the phase. If the rate of change of the amplitude is zero we can have have periodic oscillations. If the rate of change of the amplitude is zero we obtain three values for the steady

state amplitude, A(T)=0 and a pair of constants as shown in the following equation

$$A\,(T)^2 = \frac{G_3}{G_1}\Delta. \tag{A.23}$$

At this state the amplitude of the periodic oscillation is at a steady state, as represented in equation (A.23). To ascertain if the steady state solution is supercritical or subcritical Hopf bifurcation we look at all possible solution of the amplitude. From equation (A.20) there are three possible solutions

$$A(T) = 0, \qquad A(T) = \pm\sqrt{\frac{G_3}{G_1}}. \tag{A.24}$$

If $\Delta > 0$ then there are three possible real roots see equation (A.24). For $A(T) = 0$ the root is unstable while the other pair of constants roots would be stable and represent the limit amplitude of the oscillation but if $\Delta < 0$ is there is only one real root which is $A(T) = 0$ and it is stable. From this it implies the Hopf bifurcation is supercritical.

Bibliography

[1] C. Li, L. Chen, and K. Aihara, "A systems biology perspective on signal processing in genetic network motifs," *Signal Processing Magazine, IEEE*, vol. 24, no. 2, pp. 136–147, 2007.

[2] U. Alon, *An introduction to systems biology: design principles of biological circuits*, vol. 10. Chapman & Hall/CRC, 2007.

[3] O. Sporns, D. R. Chialvo, M. Kaiser, and C. C. Hilgetag, "Organization, development and function of complex brain networks," *Trends in Cognitive Sciences*, vol. 8, no. 9, pp. 418–425, 2004.

[4] M. A. Olayioye, R. M. Neve, H. A. Lane, and N. E. Hynes, "The erbb signaling network: receptor heterodimerization in development and cancer," *The EMBO Journal*, vol. 19, no. 13, pp. 3159–3167, 2000.

[5] M. Tsodyks, K. Pawelzik, and H. Markram, "Neural networks with dynamic synapses," *Neural Computation*, vol. 10, no. 4, pp. 821–835, 1998.

[6] R. Segev, M. Benveniste, E. Hulata, N. Cohen, A. Palevski, E. Kapon, Y. Shapira, and E. Ben-Jacob, "Long term behavior of lithographically prepared in vitro neuronal networks," *Physical Review Letters*, vol. 88, no. 11, p. 118102, 2002.

[7] J.-D. J. Han, N. Bertin, T. Hao, D. S. Goldberg, G. F. Berriz, L. V. Zhang, D. Dupuy, A. J. Walhout, M. E. Cusick, F. P. Roth, *et al.*, "Evidence for dynamically organized modularity in the yeast protein–protein interaction network," *Nature*, vol. 430, no. 6995, pp. 88–93, 2004.

[8] J.-F. Rual, K. Venkatesan, T. Hao, T. Hirozane-Kishikawa, A. Dricot, N. Li, G. F. Berriz, F. D. Gibbons, M. Dreze, N. Ayivi-Guedehoussou, *et al.*, "Towards a proteome-scale map of the human protein–protein interaction network," *Nature*, vol. 437, no. 7062, pp. 1173–1178, 2005.

[9] A. Friedman and N. Perrimon, "Genetic screening for signal transduction in the era of network biology," *Cell*, vol. 128, no. 2, pp. 225–231, 2007.

[10] K. A. Janes and M. B. Yaffe, "Data-driven modelling of signal-transduction networks," *Nature Reviews Molecular Cell Biology*, vol. 7, no. 11, pp. 820–828, 2006.

[11] E. Ravasz, A. L. Somera, D. A. Mongru, Z. N. Oltvai, and A.-L. Barabási, "Hierarchical organization of modularity in metabolic networks," *Science*, vol. 297, no. 5586, pp. 1551–1555, 2002.

[12] R. Guimera and L. A. N. Amaral, "Functional cartography of complex metabolic networks," *Nature*, vol. 433, no. 7028, pp. 895–900, 2005.

[13] S. Gama-Castro, H. Salgado, M. Peralta-Gil, A. Santos-Zavaleta, L. Muñiz-Rascado, H. Solano-Lira, V. Jimenez-Jacinto, V. Weiss, J. S. García-Sotelo, A. López-Fuentes, L. Porrn-Sotelo, S. Alquicira-Hernndez, A. Medina-Rivera, I. Martnez-Flores, A.-H. K, R. Martnez-Adame, C. Bonavides-Martnez, J. Miranda-Ros, A. M. Huerta, A. Mendoza-Vargas, L. Collado-Torres, B. Taboada, L. Vega-Alvarado, M. Olvera,

L. Olvera, R. Grande, E. Morett, and J. Collado-Vides, "RegulonDB version 7.0: transcriptional regulation of Escherichia coli K-12 integrated within genetic sensory response units (Gensor Units),"

[14] J. C. J. Ray, J. J. Tabor, and O. A. Igoshin, "Non-transcriptional regulatory processes shape transcriptional network dynamics," *Nature Reviews Microbiology*, vol. 9, no. 11, pp. 817–828, 2011.

[15] R. Milo, S. Shen-Orr, S. Itzkovitz, N. Kashtan, D. Chklovskii, and U. Alon, "Network motifs: simple building blocks of complex networks," *Science Signaling*, vol. 298, no. 5594, p. 824, 2002.

[16] J. A. Grochow and M. Kellis, "Network motif discovery using subgraph enumeration and symmetry-breaking," in *Research in Computational Molecular Biology*, pp. 92–106, Springer, 2007.

[17] U. Alon, "Network motifs: theory and experimental approaches," *Nature Reviews Genetics*, vol. 8, no. 6, pp. 450–461, 2007.

[18] N. Rosenfeld, M. B. Elowitz, and U. Alon, "Negative autoregulation speeds the response times of transcription networks," *Journal of Mol. Biol.*, vol. 323, no. 5, pp. 785–793, 2002.

[19] S. Mangan and U. Alon, "Structure and function of the feed-forward loop network motif," *Proc. Natl Acad. Sci.*, vol. 100, no. 21, pp. 11980–11985, 2003.

[20] S. Mangan, A. Zaslaver, and U. Alon, "The coherent feedforward loop serves as a sign-sensitive delay element in transcription networks," *Journal of Mol. Biol.*, vol. 334, no. 2, pp. 197–204, 2003.

[21] S. Mangan, S. Itzkovitz, A. Zaslaver, and U. Alon, "The incoherent feed-forward loop accelerates the response-time of the gal system of escherichia coli," *Journal of Mol. Biol.*, vol. 356, no. 5, pp. 1073–1081, 2006.

[22] S. Widder, R. Solé, and J. Macía, "Evolvability of feed-forward loop architecture biases its abundance in transcription networks," *BMC Systems Biology*, vol. 6, no. 1, p. 7, 2012.

[23] A. Tiwari and O. A. Igoshin, "Coupling between feedback loops in autoregulatory networks affects bistability range, open-loop gain and switching times," *Physical Biology*, vol. 9, no. 5, p. 055003, 2012.

[24] D. Angeli, J. E. Ferrell, and E. D. Sontag, "Detection of multistability, bifurcations, and hysteresis in a large class of biological positive-feedback systems," *Proc. Natl Acad. Sci.*, vol. 101, no. 7, pp. 1822–1827, 2004.

[25] R. Thomas, D. Thieffry, and M. Kaufman, "Dynamical behaviour of biological regulatory networksi. biological role of feedback loops and practical use of the concept of the loop-characteristic state," *Bulletin of Mathematical Biology*, vol. 57, no. 2, pp. 247–276, 1995.

[26] R. Wang, Z. Jing, and L. Chen, "Modelling periodic oscillation in gene regulatory networks by cyclic feedback systems," *Bulletin of Mathematical Biology*, vol. 67, no. 2, pp. 339–367, 2005.

[27] M. Xiao and J. Cao, "Genetic oscillation deduced from hopf bifurcation in a genetic regulatory network with delays," *Mathematical Biosciences*, vol. 215, no. 1, pp. 55–63, 2008.

[28] K. Zhuang and H. Zhu, "Stability and bifurcation analysis in a model of hes1 self regulation with time delay," *Int. J. Comput. Math. Sci*, vol. 4, no. 4, pp. 188–190, 2010.

[29] J. Wei and C. Yu, "Hopf bifurcation analysis in a model of oscillatory gene expression with delay," *Proc. Roy. Soc. Edin.*, vol. 139, no. 4, p. 879, 2009.

[30] X. P. Wu and M. Eshete, "Bifurcation analysis for a model of gene expression with delays," *Communications in Nonlinear Science and Numerical Simulation*, vol. 16, no. 2, pp. 1073–1088, 2011.

[31] K. Zhuang and H. Zhu, "Periodic oscillations for a model of gene expression with delay," in *Biomedical Engineering and Informatics (BMEI), 2010 3rd International Conference*, vol. 6, pp. 2423–2425, IEEE, 2010.

[32] Q. Wang, B. Liu, and S. Yan, "Oscillatory dynamics induced by multi-delays in gene expression," *Advances in Complex Systems*, vol. 14, no. 03, pp. 451–469, 2011.

[33] S. H. Strogatz, *Nonlinear Dynamics and Chaos: with Applications to Physics, Biology and Chemistry*. Perseus publishing, 2001.

[34] D. W. Jordan and P. Smith, *Nonlinear Ordinary Differential Equations: An Introduction for Scientists and Engineers*. New York, 2007.

[35] H. Wang and H. Hu, "Remarks on the perturbation methods in solving the second-order delay differential equations," *Nonlinear Dynamics*, vol. 33, no. 4, pp. 379–398, 2003.

[36] H. Wang and H. Hu, "Bifurcation analysis of a delayed dynamic system via method of multiple scales and shooting technique," *International Journal of Bifurcation and Chaos*, vol. 15, no. 02, pp. 425–450, 2005.

[37] E. Hinch, *Perturbation methods*. Cambridge University Press, 1991.

[38] A. H. Nayfeh, *Perturbation methods*. John Wiley & Sons, 2008.

[39] S. Das and A. Chatterjee, "Multiple scales without center manifold reductions for delay differential equations near hopf bifurcations," *Nonlinear Dynamics*, vol. 30, no. 4, pp. 323–335, 2002.

[40] S. Das and A. Chatterjee, "Second order multiple scales for oscillators with large delay," *Nonlinear Dynamics*, vol. 39, no. 4, pp. 375–394, 2005.

[41] M. Peil, M. Jacquot, Y. K. Chembo, L. Larger, and T. Erneux, "Routes to chaos and multiple time scale dynamics in broadband bandpass nonlinear delay electro-optic oscillators," *Physical Review E*, vol. 79, no. 2, p. 026208, 2009.

[42] T. Erneux, "Multiple time scale analysis of delay differential equations modeling mechanical systems," in *ASME 2005 International Design Engineering Technical Conferences and Computers and Information in Engineering Conference*, pp. 883–889, American Society of Mechanical Engineers, 2005.

[43] A. Verdugo and R. Rand, "Hopf bifurcation in a DDE model of gene expression," *Communications in Nonlinear Science and Numerical Simulation*, vol. 13, no. 2, pp. 235–242, 2008.

[44] T. R. Malthus, *An essay on the principle of population*, vol. 1. Cosimo, Inc., 2013.

[45] J. D. Murray, "Mathematical Biology I: An introduction, vol. 17 of interdisciplinary applied mathematics," 2002.

[46] O. Arino, M. L. Hbid, and E. A. Dads, *Delay Differential Equations and Applications: Proceedings of the NATO Advanced Study Institute held in Marrakech, Morocco, 9-21 September 2002*, vol. 205. Springer Science & Business Media, 2007.

[47] K. Gopalsamy, I. Györi, and G. Ladas, "Oscillations of a class of delay equations with continuous and piecewise constant arguments," *Funkcial. Ekvac*, vol. 32, no. 3, pp. 395–406, 1989.

[48] M. Idlango, J. Gear, and J. Shepherd, "Survival to extinction in a slowly varying harvested logistic population model," *Applied Mathematics Letters*, vol. 26, no. 11, pp. 1035 – 1040, 2013.

[49] D. Ludwig, R. Hilborn, and C. Walters, "Uncertainty, resource exploitation, and conservation: lessons from history.," *Science(Washington)*, vol. 260, no. 5104, p. 17, 1993.

[50] W. B. Meyer and B. L. Turner, "Human population growth and global land-use/cover change," *Annual Review of Ecology and Systematics*, pp. 39–61, 1992.

[51] G. E. Hutchinson, *An introduction to population ecology.* Hew Haven Connecticut Yale University Press, 1978.

[52] Y. Muroya, "Persistence, contractivity and global stability in logistic equations with piecewise constant delays," *Journal of Mathematical Analysis and Applications*, vol. 270, no. 2, pp. 602–635, 2002.

[53] D. Ludwig, D. D. Jones, and C. S. Holling, "Qualitative analysis of insect outbreak systems: the spruce budworm and forest," *The Journal of Animal Ecology*, pp. 315–332, 1978.

[54] R. B. Banks, *Growth and diffusion phenomena: Mathematical frameworks and applications*, vol. 14. Springer Science & Business Media, 2013.

[55] C. E. Taylor and R. R. Sokal, "Oscillations in housefly population sizes due to time lags," *Ecology*, pp. 1060–1067, 1976.

[56] R. M. May, "Simple mathematical models with very complicated dynamics," *Nature*, vol. 261, no. 5560, pp. 459–467, 1976.

[57] M. C. Mackey and L. Glass, "Oscillation and chaos in physiological control systems," *Science*, vol. 197, no. 4300, pp. 287–289, 1977.

[58] L. Berezansky, E. Braverman, and L. Idels, "Delay differential equations with hill's type growth rate and linear harvesting," *Computers & Mathematics with Applications*, vol. 49, no. 4, pp. 549–563, 2005.

[59] M. C. Mackey, C. Ou, L. Pujo-Menjouet, and J. Wu, "Periodic oscillations of blood cell populations in chronic myelogenous leukemia," *SIAM Journal on Mathematical Analysis*, vol. 38, no. 1, pp. 166–187, 2006.

[60] L. Pujo-Menjouet, S. Bernard, and M. C. Mackey, "Long period oscillations in a g 0 model of hematopoietic stem cells," *SIAM Journal on Applied Dynamical Systems*, vol. 4, no. 2, pp. 312–332, 2005.

[61] B. D. Hassard, N. D. Kazarinoff, and Y.-H. Wan, *Theory and applications of Hopf bifurcation*, vol. 41. CUP Archive, 1981.

[62] P. Buono and R. Eftimie, "Lyapunov-schmidt and centre manifold reduction methods for nonlocal pdes modelling animal aggregations," 2015.

[63] A. H. Nayfeh, "Order reduction of retarded nonlinear systems–the method of multiple scales versus center-manifold reduction," *Nonlinear Dynamics*, vol. 51, no. 4, pp. 483–500, 2008.

[64] K. Engelborghs, T. Luzyanina, and D. Roose, "Numerical bifurcation analysis of delay differential equations using DDE-BIFTOOL," *ACM Transactions on Mathematical Software (TOMS)*, vol. 28, no. 1, pp. 1–21, 2002.

[65] N. A. Monk, "Oscillatory expression of Hes1, p53, and NF-κB driven by transcriptional time delays," *Current Biology*, vol. 13, no. 16, pp. 1409–1413, 2003.

[66] Y. Bessho, H. Hirata, Y. Masamizu, and R. Kageyama, "Periodic repression by the bHLH factor Hes7 is an essential mechanism for the somite segmentation clock," *Genes & Development*, vol. 17, no. 12, pp. 1451–1456, 2003.

[67] B.-L. Xu and Y. Tao, "External noise and feedback regulation: steady-state statistics of auto-regulatory genetic network," *Journal of Theoretical Biology*, vol. 243, no. 2, pp. 214–221, 2006.

[68] K. Parmar, K. Blyuss, Y. Kyrychko, and S. Hogan, "Time-delayed models of gene regulatory networks," *Computational and Mathematical Methods in Medicine*, vol. 2015, 2015.

[69] M. H. Adhikari, E. A. Coutsias, and J. K. McIver, "Periodic solutions of a singularly perturbed delay differential equation," *Physica D: Nonlinear Phenomena*, vol. 237, no. 24, pp. 3307–3321, 2008.

[70] J. A. D. Wattis, "Shape of transition layers in a logistic differential-delay equation," *submitted*, 2016.

[71] S.-N. Chow, J. Hale, and W. Huang, "From sine waves to square waves in delay equations," *Proceedings of the Royal Society of Edinburgh: Section A Mathematics*, vol. 120, no. 3-4, pp. 223–229, 1992.